uKNIT: Breaking Round-alignment for Cipher Design Featuring uKNIT-BC, an Ultra Low-Latency Block Cipher

Kai Hu[1,4], Mustafa Khairallah[2,3], Thomas Peyrin[3] and Quan Quan Tan[3]

[1] School of Cyber Science and Technology, Shandong University, Qingdao, Shandong, China kai.hu@sdu.edu.cn
[2] Dept. of Electrical and Information Technology, Lund University, Lund, Sweden mustafa.khairallah.1608@eit.lth.se
[3] Nanyang Technological University, Singapore thomas.peyrin@ntu.edu.sg, quanquan001@e.ntu.edu.sg
[4] Key Laboratory of Cryptologic Technology and Information Security, Ministry of Education, Shandong University, Jinan, China

Abstract. Automated cryptanalysis has seen a lot of attraction and success in the past decade, leading to new distinguishers or key-recovery attacks against various ciphers. We argue that the improved efficiency and usability of these new tools have been undervalued, especially for design processes. In this article, we break for the first time the classical iterative design paradigm for symmetric-key primitives, where constructions are built around the repetition of a round function. We propose instead a new design framework, so-called uKNIT, that allows a round-by-round optimization-led automated construction of the primitives where each round can be entirely different from the others (the security/performance trade-off actually benefiting from this non-alignment).

This new design framework being non-trivial to instantiate, we further propose a method for SPN ciphers using a genetic algorithm and leveraging advances in automated cryptanalysis: given a pool of good cipher candidates on x rounds, our algorithm automatically generates and selects $(x+1)$-round candidates by evaluating their security and performance. We emphasize that our design pipeline is also the first to propose a fully automated design process, with completely integrated implementation and security analysis.

We finally exemplify our new design strategy on the important use-case of low-latency cryptography, by proposing the uKNIT-BC block cipher, together with a complete security analysis and benchmarks. Compared to the state-of-the-art in low-latency ciphers (PRINCEv2), uKNIT-BC improves on all crucial security and performance directions at the same time, reducing latency by 10%, while increasing resistance against classical differential/linear cryptanalysis by more than 10%. It also reduces area by 17% and energy consumption by 44% when fixing the latency of both ciphers. As a contribution of independent interest, we discovered a generalization of the Superposition-Tweakey (STK) construction for key schedules, unlocking its application to bit-oriented ciphers. We also discuss the benefits of uKNIT to many other possible use-cases.

Keywords: uKNIT, low-latency, block cipher, primitive design.

1 Introduction

Designing symmetric-key cryptography algorithms has always been a delicate balance between achieving robust security and optimizing performances. Historically, both the design of cryptographic primitives and their subsequent cryptanalysis were predominantly manual processes, relying on human ingenuity and expertise. However, in the last decade, the community has witnessed remarkable advancements in automated cryptanalysis techniques. Tools based on Boolean satisfiability problem (SAT) [88,106,113,82], Mixed-Integer Linear Programming (MILP) [89,17,18,84], and Constraint Programming (CP) [63,51,42] solvers have become essential in the cryptanalyst's arsenal, automating substantial parts of the analysis, even including the key-recovery phase [97]. Their ease of use has allowed researchers to explore more complex and interesting search spaces in the analysis of ciphers.

While cryptanalysis has seen significant automation, cipher design has largely remained a task performed by humans. The core structure of most modern symmetric-key algorithms continues to be crafted by cryptographers, with automation typically limited to selecting internal components such as S-boxes, linear layer matrices, and rotation values (mostly via local brute-force searches). Despite the evident power of automated tools in cryptanalysis, their potential in the design phase remains relatively underexplored (one counter-example being the search for large `AES`-round-based permutations [71,92,98]). We believe that harnessing these tools for the design process could lead to the discovery of more secure and efficient cryptographic primitives.

In particular, symmetric-key cryptography is almost entirely characterized by the iterative function design paradigm, where the primitive is built by repeating a fixed round function with minor variations along the rounds (constants, counters, or rotation values). This design approach is exemplified in widely adopted standards like `AES`, `SHA-2` or `SHA-3`. Iterative functions were initially favored because they facilitated both compact implementations (using `for` loops) and ease of human-guided analysis/provable security. However, in many use cases, these two advantages are increasingly becoming less relevant. First, in many scenarios, such as in fast software or low-latency hardware, unrolled implementations do not pose significant challenges (they are actually favored in low-latency hardware). Secondly, automated tools now dominate cryptanalysis, rendering the human-friendly iterative structure less critical (these tools fundamentally do not assume nor care about such a structure).

In this paper, we explore whether *abandoning the classical iterative design paradigm could yield symmetric-key algorithms with better security/performance trade-offs*. A non-iterative design framework offers greater flexibility, potentially leading to more diverse and powerful cryptographic constructions. Maybe even more importantly, by creating primitives via incremental addition of rounds and allowing each to vary in structure, the designer might benefit from a locally guided, greedy approach to optimize security and performance simultaneously. This exploration could provide insights into alternative cipher designs that outperform their iterative counterparts. However, implementing such a framework presents its own set of challenges, and realizing its potential seems not straightforward.

A natural use case to test this new design strategy is low-latency cryptography, which essentially consists in providing secure cryptographic primitives performing with the lowest possible latency in hardware implementations (typically fully unrolled implementations in ASIC), while maintaining area and energy consumption to reasonable levels. This is notably different from the goal of lightweight cryptography (currently undergoing standardization by the NIST [111]), which does not originally aim to optimize latency. This research field has received much attention very recently due to its numerous critical applications: autonomous vehicles, cloud computing, and financial transactions, require secure, low-latency communication for rapid and essential decision-making. More specifically, low-latency ciphers are already used for RAM memory encryption/authentication [94] or to authenticate pointers for system security [15].

The first published cipher with low-latency as stated target is the block cipher `PRINCE` [35], later upgraded to `PRINCEv2` [39]. Other low-latency block ciphers have been proposed by the community [78,81,119,66], as well as low-latency tweakable block ciphers [14,4,5,40,15,6] and various other low-latency primitives such as PRFs [8,16,3,114,2]. Unfortunately, similarly to lightweight cryptography, the heavy constraints imposed on the performance led to several candidates presenting security issues or little security margin [58,86,37,20]. In fact, most low-latency primitives have reduced security claims compared to their functional sizes (e.g. `PRINCE` only guarantees security up to 2^{126-n} for 2^n data) or very small block sizes [15,40].

Creating a secure low-latency cipher is a complex task as it represents a dual-objective optimization problem: designers must strike a balance between security and latency. Typically, the approach cryptographers take is to focus on one objective first and then attempt to 'fit' the other. One can of course take the classical approach of relying on mathematical constructions to ensure a minimum level of security, such as guaranteeing adequate diffusion in the linear layer or a minimum algebraic degree for an S-box. Most low-latency constructions basically use low-latency sub-components (S-boxes, linear layers) in the hope that this will transfer to the global construction. Then, among the candidates with similar security properties, they select the one with the lowest latency. While this strategy could be sound, it may not yield the best security/latency ratio, mainly because when functions are composed, the interactions between different components become too complex to manage effectively. In addition, latency is very hard to predict [81] (in contrast to area and throughput in lightweight cryptography, which can be quite accurately modelled). Being able to build a cipher round per round, optimizing for latency and security at the same time, might partially solve these issues.

Our contributions. In this paper, we propose `uKNIT`, a new simple design paradigm for building symmetric-key primitives, leaving behind the classical iterative top-down constructions that prevailed thus far. `uKNIT` does not enforce each round to be the same, and more importantly allows to build the primitive one round at a time (*knitting* a cipher), optimizing for both security and performance. This optimization-guided search strategy explores a much larger space than previous designs and allows to locally adapt the cipher to meet the designer's global security/performance targets.

Exploring efficiently such a large design space is not trivial and presents many challenges. Our second contribution is a search technique based on a genetic algorithm for the large class of substitution-permutation network (SPN) primitives. This algorithm is generic and can be configured to many different security and performance goals, but for simplicity we describe it within the scenario of an attacker trying to maximize the resistance of his primitive against classical differential and linear cryptanalysis, while minimizing latency.

The third contribution is the application of this technique to the important and very practical use-case of low-latency cryptography, currently undergoing intense study by the community. More precisely, we propose `uKNIT-BC`, a novel 64-bit block 128-bit key ultra low-latency SPN block cipher. Our candidate largely improves over the current best-performing low-latency block cipher, `PRINCEv2` [39] on all crucial security and performance directions at the same time: reduction of the latency by 10%, while increasing resistance against classical differential/linear cryptanalysis by more than 10%. Besides, it shows area reduction of 10% to 20% and power consumption reduction of 8% to more than 50% at different comparison points normalized at different frequencies. To strengthen the confidence in the security of our design, we performed a very thorough analysis regarding many state-of-the-art attack techniques. This contribution not only validates the interest of exploring new primitives within the `uKNIT` framework, but also represents an important achievement in the field of low-latency cryptography by itself.

We emphasize that 64-bit cipher for low-latency is one clear example that we chose to explore in detail in this paper, but we believe our search strategy will lead to more efficient primitives for many other sizes (128-bit and more), many other areas and use cases (lightweight cryptography, fast software encryption, etc.). We discuss some of them in Section 8.

As an additional contribution, our design process is supported by an entirely automated security and hardware performance evaluation pipeline. At each step of the search, automated cryptanalysis tools conduct complex security analysis of the pre-candidates, while hardware implementations and benchmarks are automatically produced for a more accurate evaluation of their latency (previous works did not predict latency, or only estimated it via modeling). To the best of our knowledge, this is the first time a cryptographic scheme is being built from such a fully automated security/performance evaluation pipeline.

Finally, as a last contribution of independent interest, we describe a novel method to build strong key schedules, generalizing over the Superposition-Tweakey (STK) construction, which was originally introduced in [72] and later influenced various tweakable block cipher constructions [14]. Our generalization, so-called gSTK, is particularly interesting as it can apply to bit-oriented ciphers (in contrary to STK), while ensuring sufficient diffusion within the round keys.

Outline. In Section 2, we present the uKNIT framework and in Section 3 a method to automatically generate uKNIT ciphers instances for SPNs, based on a genetic algorithm. In Section 4, we concentrate on the case of low-latency, explaining the rationale for our low-latency block cipher proposal uKNIT-BC, later fully specified in Section 5. An exhaustive security analysis of uKNIT-BC is conducted in Section 6, while implementation benchmarks of the cipher and comparison with competitors are given in Section 7. Finally, we discuss and showcase possible other usages of uKNIT in Section 8 and conclude in Section 9.

2 The uKNIT design framework

In symmetric-key cryptography, most block ciphers and other primitives rely on an iterative design paradigm, where a sequence of rounds $R_0, R_1, \ldots, R_{r-1}$ is applied to the input and where each round R_i applies the same transformation R (up to a small variation, usually a constant value or even a rotation value, as was used to build the 64-bit ARX-based S-box Alzette [12]). For example, an r-round iterative block cipher E taking as input a plaintext P and a key K can be written as:

$$E(P, K) = R_{r-1} \circ R_{r-2} \circ \cdots \circ R_0(P, K).$$

In the case of an SPN block cipher, we would typically have

$$R_i(X, K) = L \circ S(X \oplus K_i \oplus c_i)$$

where S stands for the substitution layer, L for the (usually linear) permutation layer, K_i for the subkey generated at round i from the master key K, and c_i a round dependent constant.

Iterative primitives are usually created directly via a top-down approach: the designer crafts the function R (S and L in the case of SPNs) according to its security/performance needs and this immediately defines the entire primitive. To ensure good performances, the designers can, of course, choose components S and L that are likely to behave well for the targeted efficiency criterion. For security, they should make sure the components provide strong security when repeatedly iterated. Some structure usually helps in this regard, the wide-trail strategy [48] for the AES block cipher being an excellent example.

To the best of our knowledge, examples of existing symmetric-key cryptographic primitives that are not purely iterative constructions would be the Kaliski-Robshaw block cipher [73] or the MD4/MD5/SHA-1 hash functions. In both cases, the few "rounds" composing the primitives use a different internal component (a different Boolean function), in the hope that this would complicate the attacker's task. For example, a particular strategy to find a good differential characteristic for the first round might fail for the second round. Yet, these constructions remain very iterative. First, only a small function within the round differs. Secondly, each round is in fact composed of many "steps" that are actually the same. Thus, these constructions remained built classically, the designers did not analyze nor leverage the possible special interactions stemming from the rounds being slightly different.

Another line of work deviating a little from the pure iterative constructions is the arithmetization-oriented family of primitives `LowMC` [1] and `RASTA` [57]. In these SPN designs, the substitution layer S is fixed, but the permutation layer L is chosen pseudo-randomly at each round. However, these designs do not try to precisely analyze and leverage any security or performance gain by having different L at each round (as they are supposed to look randomly chosen). Again, these primitives were created using a top-down approach, where all the rounds were specified at the same time.

Finally, we can mention constructions such as `HADES` [65] and `PRINCE` [35] that are classical iterative structures, but where a special round portion is present at the middle of the cipher only.

2.1 The `uKNIT` ciphers space

We propose `uKNIT`, a simple method to build ciphers, generalizing the classical iterative constructions. A `uKNIT` primitive is defined by a sequence of rounds $R_0, R_1, \ldots, R_{r-1}$ applied to the input, but where each round R_i does not necessarily apply the same transformation. Reusing our block cipher example, we would typically have

$$R_i(X, K) = L_i \circ S_i(X \oplus K_i \oplus c_i)$$

where layers L_i and S_i might be completely distinct.

One obvious benefit from the `uKNIT` framework is that the space of the functions considered is larger, iterative constructions being a subset of `uKNIT` ones. A larger search space means candidates with potentially better security/performance trade-offs. In addition, with their very distinct rounds, `uKNIT` ciphers present a natural tendency to avoid strong alignment. More importantly, `uKNIT` ciphers space allows a paradigm shift in how we build symmetric-key primitives. Instead of crafting the scheme directly with a top-down approach, with `uKNIT` one can be much more exotic in how ciphers are created. One could use an incremental process where rounds are added one at a time, both in the forward (appending a round) or backward (pre-pending a round) direction, trying to optimize some fitness function f. This allows to optimize locally the cipher's design choices, expecting that this improvement will translate on a global scale. Given an existing construction with r rounds, one can build a set of $(r+1)$-round candidates (or $(r+s)$ rounds, where s is a relatively small integer) and select the one that maximizes f. One can even consider simply updating a r-round candidate to a new r-round one with a higher value according to the fitness function. Another possibility is to combine smaller ciphers to create larger ones: from a r_1-round candidate and another r_2-round candidate, we can produce a $(r_1 + r_2)$-round one by concatenating the rounds. Note that f can be fully adapted to the use case (in terms of security and performance criterion), which makes `uKNIT` a very generic symmetric-key construction framework.

2.2 The knitting methodology: gradually building `uKNIT` ciphers

We describe our methodology which we instantiate in Section 3 for the case of SPN ciphers. We assume that the designer has a goal (or a set of goals) for the cipher, represented by the fitness function f. We further consider that the designer has access to performance evaluation and cryptanalysis tools to evaluate the fitness function on any cipher candidate. The methodology is to gradually build the cipher up to i rounds, a process that we refer to as *knitting* a cipher. When building the i-round cipher, we take as input a group of ciphers of i or less rounds, but that does not satisfy our goals. These ciphers are fed to the optimization algorithm which has access to the analysis tools and eventually the optimization algorithm is expected to output an i-round cipher that is better, with respect to the fitness function, than all the input ciphers. This process is repeated until the cipher meets our goals. We can also vary the optimization algorithm at different steps of the process, in order to achieve a good trade-off between computational power and cipher behaviour. One step of this process is summed up in Figure 1.

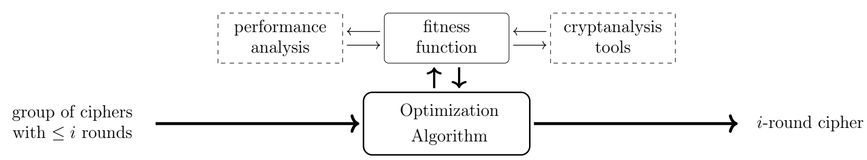

Fig. 1: One step of our knitting methodology.

There are many ways to interpret this methodology. For example, consider the process of designing an r-round cipher starting from a $(r-2)$-round cipher. We can consider that we run the methodology twice, once to get an $(r-1)$-round cipher, then to get an r-round cipher, or simply run it once to jump from $r-2$ to r, or even run it many times before we get from $r-2$ to $r-1$, it is a matter of different interpretations, as all these descriptions can be referring to the same execution.

3 Application of `uKNIT` to SPNs

The `uKNIT` cipher space is extremely large, which naturally triggers the question of how to find a good candidate within this space. We provide in this section one practical solution to knit an SPN cipher, mainly based on a genetic search, as well as a smart brute-force search when necessary.

Genetic search algorithms are evolutionary algorithms that are commonly employed to solve multi-objective optimization problems and offer several advantages, including the ability to handle complex and nonlinear optimization challenges. Before we introduce the genetic search and the smart brute-force algorithms, we describe the global search structure along which we knit the cipher.

3.1 The fitness computation

During the search, we need to evaluate the fitness of the current candidate, in terms of performance and security. Given a set of tools that can automatically evaluate the performance and the security of a candidate, a specific function needs to be defined to assign it a score. This function acts as a compass and depends on the use case considered: what platform, what performance criteria, what security target, etc. It can be computed from exact evaluations or merely approximations. It might even dynamically change during the search process (if some criterion is favored at the beginning of the search and another one towards the end).

Remark. To reduce the number of computations required during the security evaluations, especially when dealing with a large number of rounds, it might be useful to set an upper bound on the number of rounds we are analyzing. An upper bound can be chosen as the number of rounds that an attacker uses as a distinguisher for a key recovery attack for example. In other words, we can choose to only study "windows" of rounds from the cipher candidates, instead of the entire ciphers. As such, we propose the following definition to facilitate the description of the process.

Definition 1 (Window). *For a cipher C that has r rounds, the i^{th} l-length window is the l consecutive rounds of C starting from the i^{th} round, where $0 \leq i < r$ and $1 \leq l \leq r - i$. The i^{th} l-length window is denoted by $\mathcal{W}(i, l)$.*

Example. The window $\mathcal{W}(2, 8)$ refers to the 8-round cipher obtained by extracting rounds 2 through 9 from the cipher.

3.2 The search - Knitting an SPN cipher

The biggest challenge when knitting an SPN cipher is the huge search space inherent from `uKNIT`. To control the variability of the search, we can construct the cipher part by part. As a starting point, we generate a set of random x-round ciphers (x being a relatively small value), evaluate and sort these x-round candidates according to their fitness. These candidates are the first generation of the genetic search. Then, we trigger the generation evolution by breeding and mutation.

In each generation, we discard the bad performing ciphers and derive new candidates from the better performing ones. This continues for several loops (or generations). Once we are satisfied with the set of x-round ciphers, we add one round at a time to generate ciphers with a higher number of rounds.

Alternative optimization approach. If the computational power is limited, the search can be divided into two phases if needed. We can employ a genetic algorithm to search for candidate ciphers up to round i. In this phase, the number of ciphers that require evaluation can grow rapidly (in the case of `uKNIT-BC`, it easily exceeds 100,000 candidates). The computational power constraints are primarily dictated by the time required for the fitness function to evaluate the candidates. For the next $r - i$ rounds, we can use a smart brute-force algorithm to further extend the number of rounds. However, up to computational power limitations, we recommend using the genetic algorithm as much as possible, as it seems to consistently produce better candidates compared to the brute-force approach. Figure 2 provides an overview of the entire process. In fact, we use the pure genetic approach in the remainder of the paper.

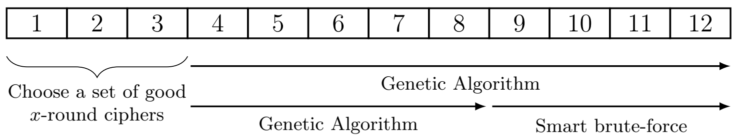

Fig. 2: Overview of the search process to knit an SPN cipher.

3.3 Genetic algorithm

A genetic algorithm is a search heuristic inspired by the principles of evolution and natural selection. It is particularly effective for solving optimization problems where the density of good solutions is limited due to a large solution space, making brute-force methods inefficient or impractical.

In the following paragraphs, we examine each component of our genetic algorithm and explain how they contribute to the overall search process. We provide in the description some precise parameters values that we found to be working well during our experiments. Of course, these depend on the use cases and the cipher properties. The designer should not hesitate to test/adapt them.

Overview. At a high level, Figure 3 illustrates the flow of our genetic algorithm. The process begins with initialization, during which the population is generated. We then evaluate the *fitnesss* of each candidate in this population to identify two key groups: the *breeding* population (those selected to breed before being eliminated) and the *surviving* population (those that continue to the next round).

The two groups undergo *breeding* and *cloning*, respectively, and may experience a potential *mutation* before moving on to the next generation. This cycle continues for some generations. Afterward, we append two new components, a permutation layer and a substitution layer, to the current cipher candidates. This process repeats until we reach the desired level of security and performance.

Initialization. For the initialization part of the search algorithm, we require a pool of ciphers. We have set the number of candidates to be 200, which turned out to be a good trade-off in our experiments. We construct each candidate cipher C in this manner:

$$C = S^{x-1} \circ L^{x-2} \circ S^{x-2} \circ \cdots \circ L^0 \circ S^0$$

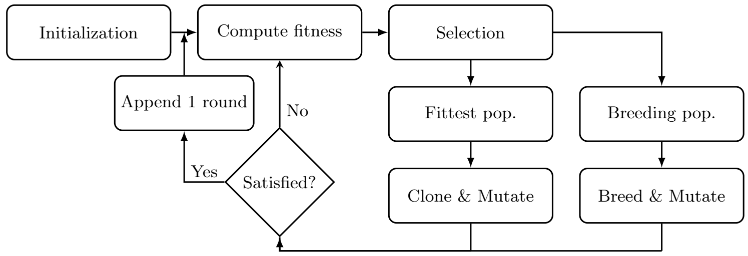

Fig. 3: The flow of the genetic algorithm to search for SPN ciphers.

where S^i and L^i are chosen randomly from sets $\boldsymbol{S}$ and $\boldsymbol{L}$ respectively. These are sets of substitution and permutation layers that we have pre-set in the beginning. The choice of these sets for the case of `uKNIT-BC` is discussed in Section 4. For the lower number of rounds, we set each round to have 100 generations. This value can be adjusted and is dependent on the available computational power and the complexity of the fitness function.

Selection. This process throws away the weaker candidates, following the concept of "survival of the fittest". However, considering only the *fitness* may cause the population to converge too quickly. Thus, we have to bring in some *diversity*, as well. Overall, the selection process is split into two parts:

- **Selecting the fittest ciphers.** The top 10 ciphers (sorted by on *fitness*) are selected. This set of ciphers is known as the "previous generation" as they are preserved until the next elimination, unless it is the last generation of its respective rounds. To extend the influence on the next generation, these ciphers are placed into the next generation directly. Additionally, mutated copies of these ciphers are introduced as well.
- **Selecting the breeding population.** The set of ciphers we select here will breed the next generation of ciphers. The process of selecting this group is based on both its fitness and a diversity measurement from a new candidate to the current pool of candidates:
  1. Initialize an empty set $\mathcal{C}$
  2. For each cipher C in the population set: Compute the diversity of C from all $C' \neq C \in \mathcal{C}$
  3. Normalize the fitness and diversity scores[5]
  4. Compute the score for each cipher: $a \cdot (C_{\text{fitness}}) + b \cdot (C_{\text{diversity}})$ with $a = 1$ and $b = 10$
  5. Select the cipher with the top score and place it in $\mathcal{C}$
  6. Repeat from Step 2 until we have obtained 40% of the population size.

The distance of a cipher C to another cipher C' is hard to quantify as we neither have a notion of quantifiable distance between S-boxes nor the linear layers that considers their cryptographic properties. Thus, for the substitution layer, we simply count the number of differing S-boxes and for the linear layer,

[5] We rescale the fitness and diversity scores be the same range of [0,1].

we count the number of different entries in the (binary) matrix. The exact details of the diversity computation are shown in Algorithm 1 of Appendix A.

Breeding. There are three types of breeding we implement: single-point crossover, double-point crossover and uniform crossover. To illustrate a single-point crossover, consider two ciphers C and C' as the parents in a chain form:

$$C : S_0 - L_0 - S_1 - L_1 - ... - S_{x-1}$$
$$C' : S'_0 - L'_0 - S'_1 - L'_1 - ... - S'_{x-1}$$

then a single point crossover chooses one part of the link and swaps the remaining parts of the chain with the other parent to create two offspring:

$$C'' : S_0 - L_0 - S_1 - L_1 - S'_2 - L'_2 - ... - S'_{x-1}$$
$$C''' : S'_0 - L'_0 - S'_1 - L'_1 - S_2 - L_2 - ... - S_{x-1}$$

A double point crossover chooses two points instead of one and swaps the parts accordingly and a uniform crossover would be a random mixture of S-boxes and linear layers. Note that a uniform crossover is very likely to destroy any cryptographic properties across different rounds and hence, it is assigned a lower probability. The breeding process proceeds as follow:

1. Randomly select randomly with uniform probability two candidates C and C' from the breeding population.
2. Let C and C' undergo either single-point, double-point, or uniform crossover with probability $0.4, 0.4$ and 0.2, respectively.
3. With a probability of 0.05, the new ciphers undergo mutation. If the new candidates after breeding are already included in the set of offspring, then this probability is increased to 1. The details of the mutation for the case of `uKNIT-BC` are explained in Section 4.
4. Repeat this process until we obtain a total of 200 new ciphers.

Remarks. The population size of 200 was selected to ensure a diverse range of ciphers while keeping the total evaluation time manageable. In our setup, using a server with a dual-socket AMD EPYC 7401 server with 48 physical cores (96 logical threads). To optimize resource usage, we limited execution to 90 threads and the computation took approximately seven days to complete. The probabilities are chosen after a few trial and error and we tend to favor single-point and double-point as they preserve most of the cipher's structure.

3.4 Smart brute-force

While genetic algorithm should be favored, we introduce a smart brute-force method in the case where the genetic algorithm is spending an excessive amount of time evaluating the large number of candidates. We emphasize that this method is simply a way to reduce the number of candidates we need to evaluate, thus decreasing the time complexity by a constant factor. This method can be applied after we have obtained fairly decent candidates with high number of rounds. Unlike a naïve brute-force method, this smart brute-force takes into account some specific factors, which we discuss here.

First, note that in the smart brute-force approach, we do not employ the concept of generations, or rather, it can viewed as if there is only 1 generation per round. However, as compensation, we can afford to increase the number of candidates.

The smart brute-force approach basically consists in adding a new round, alternating at the start or the end of the original candidate, such that the fitness function is locally optimized. More precisely, the new round is not generated randomly, but by choosing carefully its sub-components (S-Box and linear layer) to heuristically increase the fitness function.

For instance, in the case where the target security is the resistance against classical differential cryptanalysis, the smart brute force approach takes in an x-round cipher as well as one of its best differential characteristic. This approach generates many potential linear layers for the additional round and selects one that maximizes the number of active S-boxes in the new round based on the best differential characteristic given. The output is an $x + 1$-round cipher.

4 Design rationale of the `uKNIT-BC` block cipher

We apply here our SPN search strategy to the case of low-latency block cipher. We use candidates of $x = 3$ rounds to populate our first generation.

4.1 Fitness computation during the search

Our performance goal is to minimize the total cipher's latency, while providing enough security against state-of-the-art attacks. Therefore, our fitness or objective function must account for both factors. To achieve this, we rely on open-source tools to evaluate these metrics. While there are various methods to measure a cipher's security, we chose to preliminarily assess it based on the best differential characteristic and linear trail.

To obtain the best differential characteristic and linear trail, we automatically convert a cipher candidate into SAT models that describe its differential and linear properties. These models are then analyzed by a SAT solver. The modeling method we used follows the techniques described in [106]. For this purpose, we use the SAT solver `CaDiCaL` [23], but our model is compatible with any SAT solver that accepts DIMACS format. For the latency measurement, we use `OpenLane` [101], an open-source automated RTL to GDSII flow that leverages other available open-source CAD tools such as Yosys [116], a set of optimization scripts and synthesis strategies for latency and area and an open-source PDK known as Skywater 130nm [6], which is a collaboration between Google and SkyWater Technology Foundry. Unlike other open-source PDKs, Skywater 130nm has been silicone-proven both academically and commercially.

[6] https://github.com/google/skywater-pdk

After obtaining the probability of the best differential characteristic ($prob_d$), the bias of the best linear trail ($bias_l$), and the latency of the cipher (lat), the fitness of a candidate is computed as:

$$\frac{\min\{-\log_2(prob_d), -2 \cdot \log_2(bias_l)\}^2}{lat}$$

Remark. While it may look more intuitive to have the above expression to be $\frac{\text{security}}{\text{latency}}$, the security does not scale linearly with the number of rounds (whereas it does for latency). In particular, in the early stages where the number of rounds is small, a proportionate increase in security should be prioritized over a proportionate decrease in latency. The above expression is selected during the initial testing phase where we tested a few different expressions and this expression produces candidates that are consistent with our goals for the cipher.

4.2 Structure selection

As we are using a genetic algorithm to automate the search process, we are concerned about having a good starting point and properly defining the set of possible components within our search parameters. Therefore, our initial starting point is somewhat influenced by existing low-latency and low-energy designs such as `PRINCE` [41,39], `MANTIS` [14] and `MIDORI` [7].

Type of construction. For our construction, we opted for the SPN structure with a 64-bit state size. The extensive amount of cryptanalysis conducted on SPN ciphers has given cryptanalysts a deeper understanding of this structure and, naturally, one significant advantage of this choice is the wider availability of automated tools optimized for this task. While we briefly considered the Feistel construction, it proved to be unsuitable for a low-latency context, as only half the state is processed at any given time. Additionally, using a 64-bit structure ensures that the search space will not be too large for automated tools to handle. It is important to note that mutations within our genetic algorithm do not alter the type of structure chosen.

Number of rounds. During the search, a constant evaluation of security and performance is required for the fitness function. One problem we encountered when we attempted to generate ciphers with a short number of rounds was that the construction required much stronger S-boxes and linear layers. This caused the SAT solver to have a hard time solving the model given and thus, slowing down the process significantly. Moreover, ciphers with fewer rounds are also more vulnerable to meet-in-the-middle (MitM) attacks. With the 64-bit SPN structure of `uKNIT-BC` and its (probably sparse) diffusion layer, we evaluated that at least 10 rounds would be needed to resist MitM attacks. From there, we did not know in advance how many rounds would ensure enough security according to our criterion, but a first rough evaluation indicated a number of rounds around 12 to 14.

4.3 Choice of substitution layers

Initialization. For the substitution layer, we opted for 4-bit S-boxes due to their extensive study and documentation. These S-boxes can be categorized based on affine equivalence classes, with S-boxes within the same class sharing very similar security properties. This categorization allows us to efficiently eliminate entire sets of S-boxes when necessary. This is particularly important as unlike other designs, we do not limit ourselves to using the same S-box throughout the substitution layer, or even within a single layer. Consequently, the search space is very large. Initially, we considered all possible 4-bit S-boxes, excluding those with undesirable security properties, such as those that contain linear components or probability-one differential transitions. While this approach enabled us to design ciphers with slightly lower latency but stronger security properties, the complexity of these ciphers made them too challenging for our automated tools to analyze, particularly when evaluating a large number of candidates. Eventually, we restricted our selection to the S-box used in `MANTIS` (which is also `MIDORI`'s Sb_0) as well as the S-boxes that are simple bit-transpositions of it, affecting both the inputs and outputs. The `MANTIS` S-box was chosen for its notably lower latency compared to other S-boxes, and applying bit transpositions will not change its latency. Surprisingly, this decision significantly sped up the performance of the automated tool.

Mutation. For the S-boxes, we have identified four mutations meant to reflect an increasing distance in terms of the S-box properties:

1. A bit permutation on the output
2. A linear permutation on the output
3. An affine permutation on the output
4. A swap of indices: $S[i] \longleftrightarrow S[j]$ for some $i, j \in \{0, ..., 15\}$

The order above is in an increasing order of changes. The first three mutations allow many of the desired properties to be preserved as they are in the same affine equivalence (AE) class whereas a swap of indices will most likely change its AE class. In the case of low-latency purposes, having a linear or affine permutation is not desirable due to the increase number of XOR gates required. Indeed, in our initial empirical results showed that, while there is an increase in the security level of the resultant pool of candidates, it is not worth the increase in latency. Thus, for `uKNIT-BC`, we eventually decided to set the mutation to only allow bit permutations only.

4.4 Choice of linear layers

For our low-latency cipher design, the depth of the linear circuit is a critical factor, just as it is in other ciphers targeting minimal latency. To ensure maximum diffusion for each output bit, we restrict the set of possible circuits to be a set where each output bit is computed through a series of p-XOR gates. This configuration corresponds to having $p+1$ '1's in each row of the linear transformation matrix. To prevent excessive fan-out where a single signal is used in too many places, each input bit is also used in p-XOR gates. This is equivalent to having $p+1$ '1's in each column of the matrix. Under these conditions, p cannot be odd if we want the linear circuit to be invertible. Therefore, if p is odd, we allow one row or column to have $(p-1)$-XOR gates instead.

In our design, we considered cases where $p = 0,\ 1$, and 2. We did not explore $p \geq 3$ as this would increase the depth of the circuit by one, which would negatively impact latency when taking the key addition into account (refer to Figure 4 for an illustration of XOR depth) .

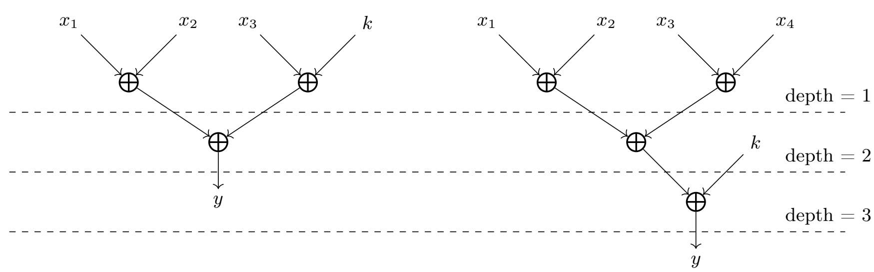

Fig. 4: An illustration of the depth with 4 and 5 variables (including the keys).

Initialization. Almost-MDS matrices are matrices that achieve a branch number that is one less than that of an MDS matrix of the same dimensions. This property is significant because it offers a strong level of diffusion (often measured in branch number) while maintaining relatively low complexity in terms of the number of XOR gates required. One example is the linear layer used in `MIDORI`. While this almost-MDS property is usually reserved for linear transformation over the vector spaces of finite fields (e.g. $GF(2^K)^M \rightarrow GF(2^K)^N$), it is possible to obtain a branch number equivalent to an almost-MDS matrix while not working on this set of transformations. For instance, in the case of `PRINCE`, the matrices used are 16×16 binary matrices that cannot be defined as a 4×4 matrix over $GF(2^4)$. However, the observed effect of `PRINCE`'s MixColumns is that the branch number (at the nibble level) is 4, equivalent to that of an almost-MDS matrix for a 4×4 matrix defined over $GF(2^4)$. We give the values of the `MIDORI` and `PRINCE` matrices in Appendix D.

We aim to leverage these almost-MDS matrices or other matrices that provide the same branch number to achieve an optimal balance between security (via strong diffusion) and efficiency (via minimal latency). However, we only use them as a starting search point, and apply several transformations as part of the genetic algorithm. As we are concerned about the branch number when we look at the nibble level (we care about active S-boxes), performing a row-wise or column-wise swaps within the block matrix (with size 4×4) can preserve the branch number. Thus, for the initialization phase, we consider the case where we are allowed to do elementary row swap (ERS) and column swap operations (ECS) at the bit-evel, but limited to swaps within the block itself. More specifically, we follow these steps to generate our initial linear layer:

1. Randomly select either $\tilde{M}^{(0)}_{\texttt{PRINCE}}$ or $M_{\texttt{MIDORI}}$.
2. Randomly select either to swap row or column
3. $b \xleftarrow{\$} \{0, 1, 2, 3\}$
4. Apply a random number of ERS (or ECS) operations on the rows (columns) indices chosen from $\{4b, 4b+1, 4b+2, 4b+3\}$
5. Repeat Step 2 to 4 for a random number of times from 1 to 1000
6. Repeat Step 1 to 5 to obtain four of them for each of the 16-bit columns

Although the ERS and ECS mentioned above allow for some diffusion to other columns (not exactly a MixColumns), to ensure the various cells are mixed thoroughly, we also implemented the ShiftRows operation identical to that of `PRINCE` after the matrix multiplication operation for all the candidates:

$$\begin{bmatrix} s_0 & s_4 & s_8 & s_{12} \\ s_1 & s_5 & s_9 & s_{13} \\ s_2 & s_6 & s_{10} & s_{14} \\ s_3 & s_7 & s_{11} & s_{15} \end{bmatrix} \rightarrow \begin{bmatrix} s_0 & s_4 & s_8 & s_{12} \\ s_5 & s_9 & s_{13} & s_1 \\ s_{10} & s_{14} & s_2 & s_6 \\ s_{15} & s_3 & s_7 & s_{11} \end{bmatrix}.$$

We will discuss briefly on the size of the pool of possible linear layers. In $M_{\texttt{MIDORI}}$, the 4×4 matrices are either the all-zero matrix or the identity matrix, while the all-zero matrix will neither be affected by ECS nor the ERS, we have a total of 24 possible arrangements for each of the identity matrix. This results in a total of $24^9 \approx 2^{41.26}$ possible choices. In the case of $\tilde{M}^{(0)}_{\texttt{PRINCE}}$, it is $4 \times 24 = 96$ possible arrangements for each of the 16 4×4 blocks, resulting in a total of $96^{16} \approx 2^{105.36}$. The large search space from the linear layers alone warrants the use of genetic algorithm to search.

Mutation. In the linear layer, represented by a 64×64 binary matrix, the mutation function operates by randomly selecting two rows and swapping them. The same process is then applied to the columns. This is equivalent to rewiring two input and output bits in the linear layer. While this operation carries a high probability of disrupting the branch number, our experiments show that as long as the number of swaps is kept low, the resulting candidates often demonstrate enhanced security, particularly in terms of their best differential characteristics.

4.5 The key schedule

Jean *et al.* [72] proposed a generalized construction that builds key schedules for key alternating ciphers, dubbed as the Superposition-Tweak-key (STK) construction. For a block cipher with block size n, the (twea)key is divided into p blocks, each of size n. Each key block is processed independently. Each round, a function h' permutes the nibbles of each block. Then, an LFSR is applied to each nibble. In the same block, the same LFSR is applied to all nibbles, while different blocks must have different LFSRs. Last but not least, the key blocks are XORed together to generate the round key.

The goal of this construction is to ensure that when the cipher is used with two related keys with a known difference, the number of nibbles where the key blocks have non-zero difference but the corresponding round key has 0 difference is limited. Indeed, the construction achieves this goal efficiently, and has been used in several TBC designs. In [44], Cogliati *et al.* studied extending the STK framework to more than 3 branches (as in the first generation of STK-based ciphers), correcting an error in another proposal [91]. In [75], Khairallah *et al.* studied how smart mode designs coupled with STK-based TBCs can lead to efficient implementations and cheap side-channel countermeasures, which is relevant in the domain of low-latency ciphers, since expensive masking is not an option. However, the original presentation of the STK construction has two drawbacks for our use case:

1. The STK construction was particular to `AES`-like ciphers, where the whole cipher is nibble- or byte-oriented. Thus, it may not be suitable for bit-oriented ciphers.
2. The number of rounds in our proposal is small. Thus, having a key schedule where the nibbles do not interact with each other can lead to slow diffusion.

For these reasons, we need a generalization of the STK construction that can work for bit-oriented ciphers, and has sufficient diffusion in the round keys. In order to do so, we have to view the round keys as bit vectors. In Definition 2, we give a mathematical representation of any linear key schedule, viewed over binary vector spaces.

Definition 2. *Let p, n, k be three positive integers, where n is the block size, k is the (twea)key size, and $k = np$. The master key K_m is a vector from the vector space $\mathbb{F}_2^k$. For $i \in \{0, 1, \ldots, r\}$, where r is the number of rounds, $K_i \in \mathbb{F}_2^n$ are the round (twea)keys. Then, any linear key schedule can be represented as a sequence of $n \times k$ matrices over $\mathbb{F}_2$: $G_0, G_1, \ldots, G_r$, such that $K_i = G_i K_m$. We call the set of matrices $\mathbf{G} = \{G_0, G_1, \ldots, G_r\}$ a linear key schedule.*

Given Definition 2, we can now give a stronger goal for the key schedule, but does not only work for nibble-oriented ciphers.

Definition 3. *Let $\mathbf{G}$ be an r-round linear key schedule according to Definition 2. The key schedule is a generalized STK (gSTK) key schedule if for any p indices $0 \leq i_0 < i_1 < \ldots < i_{p-1} \leq r$, $[\, G_{i_0}^T \; G_{i_1}^T \; \cdots \; G_{i_{p-1}}^T \,]$ is a full rank matrix, where G^T is the transpose matrix of G.*

It is easy to see why the property in Definition 3 captures the essence of the STK construction. Note that if we select $p' < p$ round keys, it must hold that there are many keys K_m that lead to the same set of p' round keys. Thus, an adversary with full control over the key difference can choose a set of p' round keys such that $K_m \neq K'_m$, but the round keys are equal. We want to make sure that this does not hold for $p' \geq p$. Thus, we want that the relation between any set of p round keys and the input key to be bijective. Definition 3 is a more formal way of writing this. For small r, it is easy to check whether this property holds. It boils down to checking the determinants of $\binom{r}{p}$ matrices of size $k \times k$.

Another interesting observation is that a powerful adversary can always choose a key such that a specific set of p rounds keys take a specific value. However, this determines all the other round keys. Thus, we can set G_0 to G_{p-1} such that the first p rounds keys are simply blocks of the input keys. This allows us to reduce the latency in unrolled key schedule as for the first p key additions, the round keys are readily available, and the p^{th} round key is only used after p rounds, so we can afford to use a circuit with somewhat higher latency. Since the linear key schedule is typically lighter than the cipher, the key schedule has minimal effect on the overall latency. The challenge now becomes how to select the matrices. In the remainder of this section, we shall focus on the case of $n = 64$, $k = 128$ and $p = 2$, and discuss possible options of selecting the matrices in efficient and smart ways.

Based on our observations, we assign $G_0 = [I\ 0]$ and $G_1 = [0\ I]$. Then, the design problem becomes: Find $(r-1)$ 64×128 matrices $G_2, \ldots, G_r$ such that

$$\begin{bmatrix} G_i \\ G_j \end{bmatrix}, \begin{bmatrix} I & 0 \\ & G_i \end{bmatrix} \text{ and } \begin{bmatrix} 0 & I \\ & G_i \end{bmatrix} \text{ are all invertible } \forall\ 2 \leq i < j \leq r.$$

We now re-introduce some simplifications from the STK construction to reduce our search space.

Method I: We consider the case where each block of the key is treated independently, and then the different blocks are XORed to get each round key. This translates to choosing $2r-2$ 64×64 matrices $A_2, \ldots, A_r$ and $B_2, \ldots, B_r$, s.t.

$$A_i, B_i \text{ and } \begin{bmatrix} A_i & B_i \\ A_j & B_j \end{bmatrix} \text{ are all invertible } \forall\ 2 \leq i < j \leq r.$$

Method II: We refine the analysis further by considering an iterative structure. We choose 2 64×64 invertible matrices A and B such that

$$\begin{bmatrix} A_i & B_i \\ A_j & B_j \end{bmatrix} \text{ is invertible } \forall\ 1 \leq i < j \leq r-1.$$

This allows us to simplify the condition to check to a condition on the differences between repeated iterations of A and B. In particular, A and B satisfy the gSTK requirement if

$$0 \neq \det\left(\begin{bmatrix} A^i & B^i \\ A^j & B^j \end{bmatrix}\right) = \det(A^i)\det(B^j - A^j A^{-i} B^i) =$$

$$\det(A^i)\det(B^j - A^{j-i}B^i) = \det(A^i)\det(B^{j-i} - A^{j-i})\det(B^i) \qquad (1)$$

which translates to A and B being invertible, and $B^l - A^l$ is invertible for $1 \leq l \leq r-2$.

Method III: This method, and Method IV, use a nibble structure, but we have faster diffusion compared to just nibble permutations. Instead of defining A and B as binary matrices, we define them as matrices over the finite field $\mathrm{GF}(2^b)$, where b is typically 4 or 8. We also define $B = AC$, where $C = cI$, for $c \in \mathrm{GF}(2^b)$ and $c \neq 0$ and $c^i \neq 1 \;\forall\; 1 \leq r$. We can show that this is sufficient since C commutes with any matrix: $AC = AcI = cAI = cIA = CA$. Thus,

$$\det((AC)^r - A^r) = \det(A^r C^r - A^r) = \det(A^r)\det(C^r - I) = \det(A^r)\det((c^r - 1)I)$$

Incidentally, if A consists of elements 0 and 1 only, and each row has only one non-zero element, then this method coincides with the original STK construction.

If c is a primitive element of a field defined by a primitive polynomial, then the multiplication can be implemented by a Linear Feedback Shift Register (LFSR) of maximal length $2^b - 1$ and the condition is satisfied as long as $r \geq 2^b - 1$. For $b = 4$, multiple LFSRs can suffice, such as the Galois LFSR defined by the primitive polynomial $x^4 + x + 1$ and the Fibonacci LFSR defined by the primitive polynomial $x^4 + x^3 + 1$. In fact, the two are defined over two isomorphic fields and we use the latter in our design. See [110, Section 7.4] on how to implement LFSRs from primitive polynomials using both methods, labelled in the book as Method I (Fibonacci LFSR) and II (Galois LFSR).

Method IV: We could use different matrices for different rounds on the form $B_i = c^{i-2} A_i$ and the analysis follows.

An interesting observation in methods III and IV is that as long as the matrix/matrices A are invertible and c is of a sufficiently large order, then the choice of A does not affect the gSTK property and we can use any matrix, from nibble permutations, all the way up to MDS matrices or very dense matrices.

Rationale of the key schedule of `uKNIT-BC`. Although we do not claim any security for `uKNIT-BC` in the related-key setting, we still want a well-designed key schedule as it enhances the security against key-recovery attacks by introducing non-trivial relations between round keys.

We expect to achieve two goals for the key schedule:

- It should not be too heavy such that it increases the overall area and latency;
- It should be easy to model by automatic search tools, as it will facilitate the search and provide lower bounds against the related-key differential attacks.

The two goals require the design of key schedule be simple, thus the gSTK framework discussed above is ideal for us. As such, we instantiate a particular instance of the gSTK, using Method III.

According to Method III, the first two round keys use the master keys directly. For the remaining round keys, we only need to choose proper $A \in \mathrm{GF}(2^4)^{4\times4}$ and $C = cI$. First, to avoid the heavy field multiplication, we choose an LFSR used by `SKINNY-64` to play the role of c. Second, for the choice of A, we define $A = P \circ M$ where P is a nibble-permutation matrix, while $M \in F_{2^4}^{16\times16}$ is a matrix with some XORs that provide a stronger diffusion. To make the key schedule simple, we restrict that all the entries of M are either 0 or 1. which is inline with the rationale that some previous tweakable block cipher designs have considered. Using some XORs in M would speed up the diffusion, but too many XORs would also significantly complicate the related-key differential lower bounds search. Therefore, we chose M that contains one XOR per 4 rows (columns) for `uKNIT-BC` key schedule (see Section 4.5). As for P, we use a brute-force search to search among all cyclic permutations such that for every four rounds, each key position must be in position 3, 6, 9 or 12 where an XOR operation is applied. The criteria for a good choice of P is one that has a decent amount of diffusion. Eventually, we chose one that after 11 iterations of $G = [P \circ M, P \circ M \circ L_{LFSR}]$ (L_{LFSR} is a matrix corresponding to applying an LFSR to each nibble), every nibble of K_{12} is a function of at least 10 nibbles of K_m. P is given in Section 4.5.

Such a design achieves a good balance between the diffusion speed and the search efficiency for the security lower bounds. With the SAT tools, we check the lower bounds for the related-key differential probability for all windows. The data is shown in Table 12 of Appendix E.1.

5 Specifications of the low-latency block cipher `uKNIT-BC`

Since each component of the cipher is distinct, its description is more complex compared to other conventional ciphers. As far as possible, we try to give a compact specification of our cipher. In Appendix B, we give the specification of `uKNIT-BC`. In Appendix C, we also give an alternate representation of the cipher. We also provide a GitHub repository containing the implementation and test vectors here:
https://anonymous.4open.science/r/uKNIT-implementations-7ABA

5.1 Overview

`uKNIT-BC` is a 64-bit block, 128-bit key block cipher that contains 12 rounds (a total of 12 substitution layers and 11 linear layers). It also has 13 round-key additions. Each round, except the final one, consists of two layers: substitution layer and linear layer. The final round contains only the substitution layer. Figure 5 describes the overview of `uKNIT-BC`. In our description, each n-bit variable is a bit column vector indexed $0, 1, \ldots, n-1$ from top to bottom. When we refer to a nibble vector, the indexing order is the same and nibble i refers to the bits $4i$ to $4i+3$, from top to bottom.

5.2 Substitution layers

The 4-bit S-boxes applied to each nibble of the internal state in `uKNIT-BC` can be represented by $(D \circ S_{\texttt{MANTIS}} \circ B)(x)$ where $S_{\texttt{MANTIS}}$ is the `MANTIS` S-box ($S_{\texttt{MANTIS}}$[x]= $[\texttt{c}, \texttt{a}, \texttt{d}, \texttt{3}, \texttt{e}, \texttt{b}, \texttt{f}, \texttt{7}, \texttt{8}, \texttt{9}, \texttt{1}, \texttt{5}, \texttt{0}, \texttt{2}, \texttt{4}, \texttt{6}]$) and D and B are transposition matrices given in Table 4 of Appendix B.1.

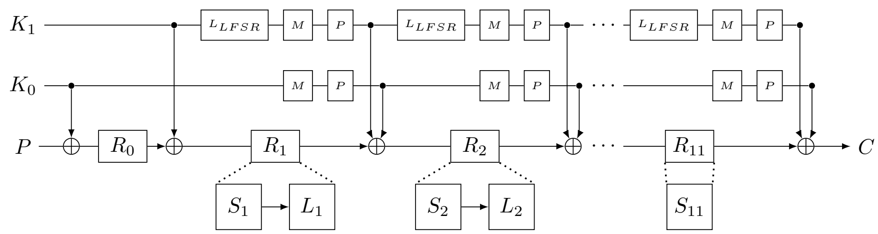

Fig. 5: The structure of uKNIT-BC including the key schedule.

5.3 Linear layers

Our linear layers L_i are very sparse 64×64 binary matrices applied on the entire internal state. Since we have exactly 3 indices in each row having "1" with the rest being "0", we can describe the matrices solely based on these indices. Table 7 and 8 of Appendix B.2 provide the list of these indices.

5.4 Key schedule

The key schedule of uKNIT-BC is depicted in Figure 5. Given the 128-bit master key $K_m = K_0||K_1$, K_0 and K_1 are used as the round keys of the first two rounds. For $i \geq 2$, the round key K_i is computed by

$$K_0 \leftarrow P \circ M(K_0), \quad K_1 \leftarrow P \circ M \circ L_{LFSR}(K_1),$$
$$K_i \leftarrow K_0 \oplus K_1,$$

where L_{LFSR} is a linear operation that applies the SKINNY-64 LFSR to each nibble of K_1. $L_{LFSR} : (x_3||x_2||x_1||x_0) \rightarrow (x_2||x_1||x_0||x_3 \oplus x_2)$. The permutation P is defined as $P = [3, 8, 13, 2, 15, 9, 11, 5, 0, 6, 14, 10, 7, 12, 4, 1]$. More precisely, the 64-bit input key K is split into 16 nibbles, and the output is $K'[i] \leftarrow K[P[i]]$, where $K[i]$ is the i^{th} nibble.

Finally, M is a matrix defined as $M = \begin{bmatrix} M' & & & \\ & M' & & \\ & & M' & \\ & & & M' \end{bmatrix}$ where $M' = \begin{bmatrix} 1&0&0&0 \\ 0&1&0&0 \\ 0&0&1&0 \\ 1&0&0&1 \end{bmatrix}$.

5.5 Decryption of uKNIT-BC

As the circuits of uKNIT-BC encryption and decryption are different, we more recommend using uKNIT-BC for modes of operation that do not require much decryption. However, since the starting points of our genetic search algorithm are matrices of PRINCE and MANTIS, the decryption function for the data path of uKNIT-BC also enjoys the low-latency feature. Inherently, the inverse S-boxes are still the MANTIS S-box with some bit permutations and the inverse functions of the linear layers in uKNIT-BC ensure that each output bit is obtained by performing two XOR operations on three input bits. Therefore, the depths of the inverses function of the linear layers in uKNIT-BC are also 2 layers.

Like other SPN ciphers, the decryption function of uKNIT-BC is also executed round by round in reverse order, applying the inverse functions of the substitution and linear layers layers. Since the round function of each round in uKNIT-BC is different, we also need to describe the inverse functions of the substitution layer and the linear layer for each round. To correspond with the encryption function, we describe them in order from the first round to the last round.

Inverses of substitution layers. The inverse functions of the 4-bit S-boxes are applied to the internal state of uKNIT-BC. Since each 4-bit uKNIT-BC S-box can be represented as $(D \circ S_{\texttt{MANTIS}} \circ B)(x)$ (D and B are provided in Table 4) and $S_{\texttt{MANTIS}}$ is involutory, the inverse of each S-box is represented as $(B^{-1} \circ S_{\texttt{MANTIS}} \circ D^{-1})(x)$. B^{-1} and D^{-1} are easily obtained from Table 4, as listed in Table 5.

Inverses of linear layers. The inserves of linear layers are also sparse 64×64 binary matrices applied to the internal state. Each row of these matrices contains three "1" with the rest bing "0". Thus, we describe these inverse linear layers in a similar way with these indices. Tables 9 and 10 of Appendix B.2 provide the list of these indices.

6 Security analysis of uKNIT-BC

In this section, we exhibit the extensive state-of-the-art cryptanalysis we performed on uKNIT-BC, see in Table 1 the best key-recovery attacks we obtained. Due to page limitation, we only provide here a summary, but all the details and more analysis are provided in Appendix E.

Table 1: Overview of our main key-recovery attacks on round-reduced uKNIT-BC, for which the full number of rounds is 12.

Attack	Rounds	Targeted Win.	Time	Data	Reference
Differential	10	$\mathcal{W}(0,10)$	2^{110} Enc.	$2^{55.7}$ CP	Section E.1
Impossible differential	10	$\mathcal{W}(1,10)$	2^{93} Enc.	2^{55} CP	Appendix E.4
Demirci-Selçuk MitM	9	$\mathcal{W}(0,9)$	2^{87} Enc.	2^{61} CP	Appendix E.7
Differential-linear	9	$\mathcal{W}(1,9)$	$2^{92.6}$ Enc.	$2^{53.6}$ CP	Appendix E.9

Security claims and attack model. We claim that there is no attack that can break the full uKNIT-BC with less than 2^{112} time complexity and 2^{47} (chosen / adaptively-chosen) plaintext-ciphertext pairs (2^{50} bytes). These two numbers consider the NIST lightweight cryptography requirement [93], and they are similar to what is claimed for PRINCEv2. We do not claim any security regarding related-key, known-key or chosen-key attacks.

We did a complete cryptanalysis on uKNIT-BC and did not find any attack that threatens its security: simple and multiple differential cryptanalysis (Appendices E.1 and E.2), linear cryptanalysis (Appendix E.3), impossible differential cryptanalysis (Appendix E.4), zero-correlation cryptanalysis (Appendix E.5), integral attacks (Appendix E.6), Demirci-Selçuk meet-in-the-middle attack (Appendix E.7), boomerang and rectangle attacks (Appendix E.8), (higher-order) differential-linear attacks (Appendix E.9), invariant attacks (Appendix E.10), slide attacks and internal differential attacks (Appendix E.11),

We encourage third-party cryptanalysis on any (consecutive) windows, even surpassing the complexity limitations we set, as they are beneficial to explore the security margin of `uKNIT-BC`.

7 Implementations and benchmarks

General comparison. We synthesized the different ciphers for the TSMC 65nm technology library using design compiler. For each cipher, we derived two measurements: the first one is a combinational unconstrained circuit as a baseline. In the second, For the second result, we place each cipher between input and output registers and set the target clock period to $1ns$. For all ciphers, this goal is unattainable. However, the synthesis algorithm outputs the closest netlist it could reach to this goal, as the expense of larger area. In both cases, we use the `compile_ultra` command. For `uKNIT-BC`, we also included the results of the circuit synthesized for the maximum achievable frequency of `PRINCEv2` [39]. While `uKNIT-BC` is competitive even at its own maximum achievable frequency, it does not provide a fair comparison as `PRINCEv2` cannot even reach that frequency. Thus, it is a more fair comparison to also include the area gain when only the maximum achievable frequency of `PRINCEv2` is targeted. We also include the results with the key schedule and with precomputed round keys (key side loading). The results are given in Table 2. In the comparison, we include most of the ciphers that claim to be designed with low latency in mind. However, they satisfy different security goals. `KoalaP` is a public permutation used in a Variable-Input-Length PRF (VIL-PRF), which takes many blocks and the latency is for how fast each block is absorbed. If it is used with a fixed 64-bit input length, it requires two calls to the permutation, doubling the latency, making it slower that `uKNIT-BC`. `Gleeok128` [3] and `Orthros` [8] are Fixed-Input-Length PRFs (FIL-PRFs). They are not designed to resist the same type of attacks as `uKNIT-BC`, so they can tolerate having lower latency for 128-bit blocks. That being said, from a pure latency point of view, we do in fact have lower latency, and in Appendix F we discuss how to build a PRF from `uKNIT-BC`, not even considering using less rounds. `BipBip` [15] has a 24-bit block, yet its latency is not that much better than `uKNIT-BC` (less than 3%). `Qarmav1` [4] is a TBC with large block size and are both slower than `uKNIT-BC`. Among BCs, We have implemented `MIDORI` and `MANTIS` with 7 rounds on either side of the middle round (with no tweak and similar security claim to `PRINCEv2` and `uKNIT-BC`). Both of these ciphers are more costly than `PRINCEv2`, but we included them in the table for completeness. `SPEEDY` [81] is a 192-bit BC, which comes in three variants differing mainly in the number of rounds; 5, 6 and 7 rounds. The large block size makes the area very large for all variants, and impacts its usability in applications that require a small block size. uKNIT-BC is significantly faster than the 7-round variant and moderately faster than the 6-round variant, while using only a fraction of the area. The 5-round variant is faster than most other ciphers on the list. However, a few points must be noted:

1. The design goals of the different ciphers are different and the head-to-head comparison is not straightforward.
2. The uKNIT framework can be applied to wide block sizes, such as 192 bits. Although we leave that for future work, in the next section we show examples of the applicability of the uKNIT framework to other use cases than uKNIT-BC. It is likely that the larger block size gives more degrees of freedom, and we can capture this in the uKNIT framework.
3. The security of 5-round SPEEDY has been under scrutiny, with a very slim security margin [37,20]. In addition, while the 7-round variants achieve much higher security, their security claims have been broken in [115].

Last but not least, the candidate that is closest to uKNIT-BC in terms of security model and block size is PRINCEv2. *The ideal way to assess the power of the* uKNIT *framework is to compare its outcome* uKNIT-BC *against the best cipher with the same goal, application and parameters (key and block sizes), and such BC happens to be* PRINCEv2. uKNIT-BC has $\sim$ 10% lower latency, and for the lowest latency of PRINCEv2, we need only half the are with precomputed round keys of $\sim$ 18% less area with key schedule. For the remainder of this section, we provide more in-depth benchmarking compared exclusively to PRINCEv2.

Power consumption. We believe a straightforward comparison of different circuits synthesized for different targets, then setting the frequency to a nominal value, *e.g.* 10 MHz, is not very informative. This is especially true if the circuit used in the comparison is synthesized with maximum achievable frequency in mind. The synthesizer can allocate a very large area to achieve such frequency which increases power consumption. Thus, estimating the power of this particular circuit at a much lower frequency gives an inaccurate picture of how the cipher is used. Rather, if we target a low frequency, we should estimate the power using a circuit that is optimized either for area or for power consumption, not for frequency. Besides, comparing the power consumption of ciphers with different block sizes is also not very informative. Thus, we compare our proposal to PRINCEv2 and we follow a different approach. We synthesize each cipher for specific frequencies, and use the circuit corresponding to each frequency to estimate the power consumption. In case of the maximum achievable frequency for PRINCEv2, we synthesize uKNIT-BC for the same frequency and set the circuit of PRINCEv2 at that frequency. In case of the maximum achievable frequency for uKNIT-BC, we set the frequency of that circuit as such. Besides, we set the switching activity of the key bits to 0. The key is loaded once and used to encrypt many blocks. Thus, it is unreasonable to assume that the key values, and key schedule gates, are toggling all the time. It is a standard practice to simulate real operating conditions to estimate and optimize power consumption. The results are presented in Table 14 (top). The results indeed show the subtleties of comparing power consumption.

Table 2: Comparison of different low latency primitives using TSMC 65nm. The first row of each cipher is the unconstrained combinational circuit, and the second row is the single cycle circuit with target latency of $1ns$. For `KoalaP` [2], the first row is just the permutation, while the second row is the latency is the time the PRF takes to absorb 1 64-bit block per cycle. For the VIL-PRF latency of `KoalaP`, we need to multiply the permutation latency by $1 + n_b$ where n_b is the number of input 64-bit blocks per 257-bit output block.

	Name	**Block Size**	**Latency** (ns)	**Area** (μm^2)
FIL-PRF	`Gleeok128` [3]	128	3.45	73,078.92
		128	1.61	133,343.99
	`Orthros` [8]	128	2.66	40,932.36
		128	1.59	77,437.08
TBC	`BipBip` [15]	24	4.03	39,278.52
		24	1.45	60,630.12
	`MANTIS` [14]	64	3.39	13,359.60
		64	2.01	31,020.48
	`Qarmav1` 9 rnds [4]	128	4.84	42,787.08
		128	2.74	94,944.23
Public Perm.	`KoalaP` [2]	64	1.46	24,104.88
		64	1.16	52,965.36
BC	`MIDORI` [7]	64	3.46	13,367.16
		64	2.05	30,475.44
	`SPEEDY` 5 rnds [81]	192	2.63	32,565.96
		192	1.26	66,251.16
	`SPEEDY` 6 rnds [81]	192	3.13	39,681.36
		192	1.52	77,387.40
	`SPEEDY` 7 rnds [81]	192	3.75	46,826.64
		192	1.79	88,331.04
	`PRINCEv2` [39]	64	2.90	12,006.72
		64	1.65	27,564.12
	`uKNIT-BC` (precomputed keys)	64	2.58	10,685.88
		64	1.64	14,587.92
		64	1.49	21,779.27
	`uKNIT-BC`	64	2.53	15,859.80
		64	1.64	22,963.67
		64	1.48	30,436.20
	`uKNIT-BC` Decryption (precomputed keys)	64	2.50	9,842.75
		64	1.64	14,664.60
		64	1.49	23,095.08

In the medium range of frequency ($250 \sim 500$ MHz), `uKNIT-BC` experiences approximately $25\% \sim 35\%$ improvement without the key schedule and approximately $8\% \sim 19\%$ with key schedule. At `PRINCEv2` maximum achievable frequency, `uKNIT-BC` reaches 44% and 55% improvement over `PRINCEv2` with and without the key schedule, respectively. This massive gain is attributed to the fact that `uKNIT-BC` reaches this frequency without extensive optimization, while `PRINCEv2` requires very high optimization effort and enlarged area. This is also why we observe a widening gap between the two ciphers, until we reach a range of frequencies for which PRINCEv2 is unsynthesizable. The power consumption of uKNIT-BC at maximum achievable frequency with key schedule is only marginally higher than PRINCEv2 at the maximum achievable frequency. Due to the frequency difference, this implies uKNIT-BC consumes 7.5% less energy. At low frequencies, uKNIT-BC consumes 20.9% less power without key schedule, but has higher consumption with key schedule due to the effects of leakage power consumption in the gates of the key schedule.

FDSOI 28nm. As further verification of our analysis, we replicated our results for PRINCEv2 and uKNIT-BC (with and without key schedule) using the FDSOI 28nm 1.1V standard cell library. Table 14 (mid) includes the power results, while Table 14 (bottom) includes the area results. We observe the same trends, and even higher gains in terms of power consumption as the latency is increased. In fact, uKNIT-BC can reach the GHz range, while PRINCEv2 cannot.

Combined encryption and decryption. We acknowledge that it is cheaper for PRINCEv2 to have a combined encryption-decryption circuit, due to its reflection property. However, the area of a combined encryption-decryption circuit for uKNIT-BC is less $40,000\mu m^2$ compared to $27,000\mu m^2$ for PRINCEv2, at the maximum frequency possible by PRINCEv2. Although some may view this as a limitation, we believe that whether such an implementation is needed depends heavily on the application and mode of operation. We do not recommend using a simple block-cipher mode of operation with a 64-bit block cipher, but we recommend using the XoP construction (see Appendix F), which requires two encryption circuits rather than encryption-decryption. In this use case, PRINCEv2 is actually more expensive. In addition, we believe that reaching lower latency is worth the area sacrifice for the right applications, and we view the fact that, for the same frequency, the combined encryption-decryption circuit is still less than twice PRINCEv2 as positive.

8 Discussion

8.1 Alternative use-cases

Although we have applied the uKNIT framework specifically to the design of low-latency ciphers, its capabilities extend beyond this particular application. By simply replacing the security-latency criterion with another metric, the framework can be adapted for different cipher design objectives (potentially again mixing performance and security objectives). Additionally, although this paper uses the uKNIT framework for a 64-bit low-latency cipher design, its potential is much greater than this, which also applies to designing 128-bit ciphers and other cipher sizes.

As a proof of concept, we applied our genetic algorithm in the uKNIT framework to SPECK-32 and SPECK-128 [10], allowing rotation values to vary between rounds. Different rotation values lead to a cipher with about the same performance per round as the original speck, but the security is greatly improved.

Table 3: Comparison of the **probability of the best differential characteristic** of SPECK-32 and SPECK-128 to variants that use different **rotation values** each round (left table); and of the **minimum number of active S-boxes** in AES to a variant uses uses different **byte-permutation** each round (right table). The rotation values for the variant SPECK-32 is [(10, 13), (10, 2), (3, 1), (9, 12), (14, 8), (5, 2), (5, 15), (13, 15)] for the first 8 rounds. For SPECK-128, the rotation values are [(23, 4), (21, 20), (18, 16), (14, 16), (10, 10), (8, 20)] for the first 6 rounds. For AES the 6 byte-permutations are provided in Appendix G.

		Rounds				
		5	6	7	8	9
SPECK-32	orig.	9	13	18	24	30
	diff.	12	19	25	30	-
SPECK-128	orig.	10	15	21	-	-
	diff.	12	21	-	-	-

		Rounds			
		3	4	5	6
AES	orig.	9	25	26	30
	diff.	9	25	28	34

We achieve this by setting the initial rotation values to be the same as SPECK. However, with each generation, the rotation at each round has a probability of increasing or decreasing by 1. Table 3 (left) compares the probabilities of the best differential characteristics obtained when using different round rotations versus the original cipher. The results show a significant security improvement, as measured by the probability of the best differential characteristic, when different rotations are used for each round. Note that SPECK designers mention in [11] an extra criterion on the rotation values, by minimizing the distance to multiple of 8 (for faster performance on certain micro-controllers. If we also take this criterion into account, we could find rotation values on 8 rounds that have a distance lower than that of SPECK (thus potentially leading to increased performances), while also improving security bounds.

We applied the same concept to AES [49]. Although evaluating the differential characteristics of AES is highly time-consuming, the security of AES (in terms of a lower bound on the differential probability) can be assessed using the wide-trail strategy. Similarly, we can modify our security evaluation function to incorporate the wide-trail strategy. In this case, we varied the ShiftRows (to a more generic byte-permutation) operation for each round. The results are presented in Table 3 (right).

8.2 Time complexity and optimality

We emphasize that we do not claim that our design strategy leads to optimal constructions. However, the uKNIT framework indeed provides a way to find good candidates from a very large search space (much larger than the original same-round cipher design paradigms). One may argue that it is unsurprising that using different round functions can lead to better performance, however, no work has paid attention to exploring such design possibilities for the full cipher (one can mention the ARX-based S-box of Alzette [12]). The uKNIT framework takes the first main step in this direction: we are the first to take full advantage of this design idea to design a full-fledged cipher.

The `uKNIT` framework provides a structured and guided approach to exploring this search space and identifying improved designs. Since the framework evaluates ciphers' strength based on various metrics, its time complexity is directly proportional to the time required to evaluate a single cipher (for performance and security), with the multiplier depending on the chosen hyperparameters. Consequently, if a design is infeasible to evaluate using existing methods due to time constraints, `uKNIT` will also be unable to evaluate it.

During the early stages of this research, we encountered candidates which exhibited exceptionally strong security-to-latency ratios. However, due to the extensive time required to evaluate even a single cipher, we had no choice but to abandon them in favor of alternatives whose security could be feasibly assessed.

It is important to note also that the `uKNIT` framework is not limited to evaluating security based on the best differential characteristic. Any assessable security metric could be used. As demonstrated with `AES`, the security metric can be adapted, like calculating the minimum number of active S-boxes, offering an alternative evaluation approach for faster search if time complexity becomes an issue.

9 Conclusion

In this paper, we introduced a new design framework called `uKNIT`, aimed at creating ciphers round-by-round with various performance/security objectives and breaking for the first time the round alignment paradigm that prevailed in the field. To showcase that excellent cipher candidates do exist within this gigantic search space, we proposed a genetic search algorithm for the case of SPN schemes and we instantiated a specific example focused on creating an ultra-low latency block cipher, `uKNIT-BC`. It outperforms the state-of-the-art low-latency cipher (`PRINCEv2`) in both security and performance. Additionally, we generalized the STK construction for key scheduling, enabling its application to bit-oriented ciphers. To the best of our knowledge, this is also the first attempt at fully automating a cipher's design process. Automation enables us to explore uncharted territories more effectively, paving the way for innovative cryptographic schemes.

Acknowledgments

We thank the anonymous reviewers for the relevant comments on the first version of our paper. This research was supported by the Seagate Technology LLC grant "Low-Latency Lightweight Cryptography" and the Singapore NRF Investigatorship grant NRF-NRFI08-2022-0013. The second author is funded by the Wallenberg-NTU Presidential Postdoctoral Fellowship.

References

1. Albrecht, M.R., Rechberger, C., Schneider, T., Tiessen, T., Zohner, M.: Ciphers for MPC and FHE. In: Oswald, E., Fischlin, M. (eds.) Advances in Cryptology - EUROCRYPT 2015. LNCS, vol. 9056, pp. 430–454. Springer (2015), https://doi.org/10.1007/978-3-662-46800-5_17
2. Amiri-Eliasi, P., Belkheyar, Y., Daemen, J., Ghosh, S., Kuijsters, D., Mehrdad, A., Mella, S., Rasoolzadeh, S., Assche, G.V.: Koala: A Low-Latency Pseudorandom Function. IACR Cryptol. ePrint Arch. p. 1249 (2024), https://eprint.iacr.org/2024/1249
3. Anand, R., Banik, S., Caforio, A., Ishikawa, T., Isobe, T., Liu, F., Minematsu, K., Rahman, M., Sakamoto, K.: Gleeok: A Family of Low-Latency PRFs and its Applications to Authenticated Encryption. IACR Trans. Cryptogr. Hardw. Embed. Syst. 2024(2), 545–587 (2024), https://doi.org/10.46586/tches.v2024.i2.545-587
4. Avanzi, R.: The QARMA Block Cipher Family. Almost MDS Matrices Over Rings With Zero Divisors, Nearly Symmetric Even-Mansour Constructions With Non-Involutory Central Rounds, and Search Heuristics for Low-Latency S-Boxes. IACR Trans. Symmetric Cryptol. 2017(1), 4–44 (2017), https://doi.org/10.13154/tosc.v2017.i1.4-44
5. Avanzi, R., Banik, S., Dunkelman, O., Eichlseder, M., Ghosh, S., Nageler, M., Regazzoni, F.: The QARMAv2 Family of Tweakable Block Ciphers. IACR Trans. Symmetric Cryptol. 2023(3), 25–73 (2023), https://doi.org/10.46586/tosc.v2023.i3.25-73
6. Avanzi, R., Dunkelman, O., Minematsu, K.: MATTER: A Wide-Block Tweakable Block Cipher. IACR Cryptol. ePrint Arch. p. 1186 (2024), https://eprint.iacr.org/2024/1186
7. Banik, S., Bogdanov, A., Isobe, T., Shibutani, K., Hiwatari, H., Akishita, T., Regazzoni, F.: Midori: A Block Cipher for Low Energy. In: Iwata, T., Cheon, J.H. (eds.) Advances in Cryptology - ASIACRYPT 2015. LNCS, vol. 9453, pp. 411–436. Springer (2015), https://doi.org/10.1007/978-3-662-48800-3_17
8. Banik, S., Isobe, T., Liu, F., Minematsu, K., Sakamoto, K.: Orthros: A Low-Latency PRF. IACR Cryptol. ePrint Arch. p. 390 (2021), https://eprint.iacr.org/2021/390
9. Bar-On, A., Dunkelman, O., Keller, N., Weizman, A.: DLCT: A New Tool for Differential-Linear Cryptanalysis. In: Ishai, Y., Rijmen, V. (eds.) Advances in Cryptology - EUROCRYPT 2019. LNCS, vol. 11476, pp. 313–342. Springer (2019), https://doi.org/10.1007/978-3-030-17653-2_11
10. Beaulieu, R., Shors, D., Smith, J., Treatman-Clark, S., Weeks, B., Wingers, L.: The SIMON and SPECK Families of Lightweight Block Ciphers. IACR Cryptol. ePrint Arch. p. 404 (2013), http://eprint.iacr.org/2013/404
11. Beaulieu, R., Shors, D., Smith, J., Treatman-Clark, S., Weeks, B., Wingers, L.: Notes on the design and analysis of SIMON and SPECK. Cryptology ePrint Archive, Paper 2017/560 (2017), https://eprint.iacr.org/2017/560
12. Beierle, C., Biryukov, A., dos Santos, L.C., Großschädl, J., Perrin, L., Udovenko, A., Velichkov, V., Wang, Q.: Alzette: A 64-Bit ARX-box - (Feat. CRAX and TRAX). In: Micciancio, D., Ristenpart, T. (eds.) Advances in Cryptology - CRYPTO 2020. LNCS, vol. 12172, pp. 419–448. Springer (2020), https://doi.org/10.1007/978-3-030-56877-1_15

13. Beierle, C., Canteaut, A., Leander, G., Rotella, Y.: Proving Resistance Against Invariant Attacks: How to Choose the Round Constants. In: Katz, J., Shacham, H. (eds.) Advances in Cryptology - CRYPTO 2017. LNCS, vol. 10402, pp. 647–678. Springer (2017), https://doi.org/10.1007/978-3-319-63715-0_22
14. Beierle, C., Jean, J., Kölbl, S., Leander, G., Moradi, A., Peyrin, T., Sasaki, Y., Sasdrich, P., Sim, S.M.: The SKINNY Family of Block Ciphers and Its Low-Latency Variant MANTIS. In: Robshaw, M., Katz, J. (eds.) Advances in Cryptology - CRYPTO 2016. LNCS, vol. 9815, pp. 123–153. Springer (2016), https://doi.org/10.1007/978-3-662-53008-5_5
15. Belkheyar, Y., Daemen, J., Dobraunig, C., Ghosh, S., Rasoolzadeh, S.: BipBip: A Low-Latency Tweakable Block Cipher with Small Dimensions. IACR Trans. Cryptogr. Hardw. Embed. Syst. 2023(1), 326–368 (2023), https://doi.org/10.46586/tches.v2023.i1.326-368
16. Belkheyar, Y., Daemen, J., Dobraunig, C., Ghosh, S., Rasoolzadeh, S.: Introducing two Low-Latency Cipher Families: Sonic and SuperSonic. IACR Cryptol. ePrint Arch. p. 878 (2023), https://eprint.iacr.org/2023/878
17. Bellini, E., Gérault, D., Grados, J., Makarim, R.H., Peyrin, T.: Boosting Differential-Linear Cryptanalysis of ChaCha7 with MILP. IACR Trans. Symmetric Cryptol. 2023(2), 189–223 (2023), https://doi.org/10.46586/tosc.v2023.i2.189-223
18. Bellini, E., Gérault, D., Grados, J., Makarim, R.H., Peyrin, T.: Fully Automated Differential-Linear Attacks Against ARX Ciphers. In: Rosulek, M. (ed.) Topics in Cryptology - CT-RSA 2023. LNCS, vol. 13871, pp. 252–276. Springer (2023), https://doi.org/10.1007/978-3-031-30872-7_10
19. Beyne, T.: Block Cipher Invariants as Eigenvectors of Correlation Matrices. In: Peyrin, T., Galbraith, S.D. (eds.) Advances in Cryptology - ASIACRYPT 2018. LNCS, vol. 11272, pp. 3–31. Springer (2018), https://doi.org/10.1007/978-3-030-03326-2_1
20. Beyne, T., Neyt, A.: Note on the cryptanalysis of Speedy. Cryptology ePrint Archive, Paper 2024/262 (2024), https://eprint.iacr.org/2024/262
21. Beyne, T., Rijmen, V.: Differential Cryptanalysis in the Fixed-Key Model. In: Dodis, Y., Shrimpton, T. (eds.) Advances in Cryptology - CRYPTO 2022 - 42nd Annual International Cryptology Conference, CRYPTO 2022, Santa Barbara, CA, USA, August 15-18, 2022, Proceedings, Part III. Lecture Notes in Computer Science, vol. 13509, pp. 687–716. Springer (2022), https://doi.org/10.1007/978-3-031-15982-4_23
22. Beyne, T., Verbauwhede, M.: Integral Cryptanalysis Using Algebraic Transition Matrices. IACR Trans. Symmetric Cryptol. 2023(4), 244–269 (2023), https://doi.org/10.46586/tosc.v2023.i4.244-269
23. Biere, A., Faller, T., Fazekas, K., Fleury, M., Froleyks, N., Pollitt, F.: CaDiCaL 2.0. In: Gurfinkel, A., Ganesh, V. (eds.) Computer Aided Verification - CAV 2024. LNCS, vol. 14681, pp. 133–152. Springer (2024)
24. Biham, E., Biryukov, A., Shamir, A.: Cryptanalysis of Skipjack Reduced to 31 Rounds Using Impossible Differentials. In: Stern, J. (ed.) Advances in Cryptology - EUROCRYPT '99. LNCS, vol. 1592, pp. 12–23. Springer (1999), https://doi.org/10.1007/3-540-48910-X_2
25. Biham, E., Dunkelman, O., Keller, N.: The Rectangle Attack - Rectangling the Serpent. In: Pfitzmann, B. (ed.) Advances in Cryptology - EUROCRYPT 2001. LNCS, vol. 2045, pp. 340–357. Springer (2001), https://doi.org/10.1007/3-540-44987-6_21

26. Biham, E., Dunkelman, O., Keller, N.: New Combined Attacks on Block Ciphers. In: Gilbert, H., Handschuh, H. (eds.) Fast Software Encryption - FSE 2005. LNCS, vol. 3557, pp. 126–144. Springer (2005), https://doi.org/10.1007/11502760_9
27. Biham, E., Shamir, A.: Differential Cryptanalysis of DES-like Cryptosystems. In: Menezes, A., Vanstone, S.A. (eds.) Advances in Cryptology - CRYPTO '90. LNCS, vol. 537, pp. 2–21. Springer (1990), https://doi.org/10.1007/3-540-38424-3_1
28. Biryukov, A., Shamir, A.: Structural Cryptanalysis of SASAS. In: Pfitzmann, B. (ed.) Advances in Cryptology - EUROCRYPT 2001. LNCS, vol. 2045, pp. 394–405. Springer (2001), https://doi.org/10.1007/3-540-44987-6_24
29. Biryukov, A., Wagner, D.A.: Slide Attacks. In: Knudsen, L.R. (ed.) Fast Software Encryption - FSE '99. LNCS, vol. 1636, pp. 245–259. Springer (1999), https://doi.org/10.1007/3-540-48519-8_18
30. Biryukov, A., Wagner, D.A.: Advanced Slide Attacks. In: Preneel, B. (ed.) Advances in Cryptology - EUROCRYPT 2000. LNCS, vol. 1807, pp. 589–606. Springer (2000), https://doi.org/10.1007/3-540-45539-6_41
31. Blondeau, C., Bogdanov, A., Wang, M.: On the (In)Equivalence of Impossible Differential and Zero-Correlation Distinguishers for Feistel- and Skipjack-Type Ciphers. In: Boureanu, I., Owesarski, P., Vaudenay, S. (eds.) Applied Cryptography and Network Security - ACNS 2014. LNCS, vol. 8479, pp. 271–288. Springer (2014), https://doi.org/10.1007/978-3-319-07536-5_17
32. Bogdanov, A., Leander, G., Nyberg, K., Wang, M.: Integral and Multidimensional Linear Distinguishers with Correlation Zero. In: Wang, X., Sako, K. (eds.) Advances in Cryptology - ASIACRYPT 2012. LNCS, vol. 7658, pp. 244–261. Springer (2012), https://doi.org/10.1007/978-3-642-34961-4_16
33. Bogdanov, A., Rijmen, V.: Linear hulls with correlation zero and linear cryptanalysis of block ciphers. Des. Codes Cryptogr. 70(3), 369–383 (2014), https://doi.org/10.1007/s10623-012-9697-z
34. Bogdanov, A., Wang, M.: Zero Correlation Linear Cryptanalysis with Reduced Data Complexity. In: Canteaut, A. (ed.) Fast Software Encryption - FSE 2012. LNCS, vol. 7549, pp. 29–48. Springer (2012), https://doi.org/10.1007/978-3-642-34047-5_3
35. Borghoff, J., Canteaut, A., Güneysu, T., Kavun, E.B., Knezevic, M., Knudsen, L.R., Leander, G., Nikov, V., Paar, C., Rechberger, C., Rombouts, P., Thomsen, S.S., Yalçin, T.: PRINCE - A Low-Latency Block Cipher for Pervasive Computing Applications - Extended Abstract. In: Wang, X., Sako, K. (eds.) Advances in Cryptology - ASIACRYPT 2012. LNCS, vol. 7658, pp. 208–225. Springer (2012), https://doi.org/10.1007/978-3-642-34961-4_14
36. Boura, C., Canteaut, A.: Another View of the Division Property. In: Robshaw, M., Katz, J. (eds.) Advances in Cryptology - CRYPTO 2016. LNCS, vol. 9814, pp. 654–682. Springer (2016), https://doi.org/10.1007/978-3-662-53018-4_24
37. Boura, C., David, N., Boissier, R.H., Naya-Plasencia, M.: Better Steady than Speedy: Full Break of SPEEDY-7-192. In: Hazay, C., Stam, M. (eds.) Advances in Cryptology - EUROCRYPT 2023. LNCS, vol. 14007, pp. 36–66. Springer (2023), https://doi.org/10.1007/978-3-031-30634-1_2
38. Boura, C., Naya-Plasencia, M.: Symmetric Cryptography, Volume 2: Cryptanalysis and Future Directions. John Wiley & Sons (2024)
39. Bozilov, D., Eichlseder, M., Knezevic, M., Lambin, B., Leander, G., Moos, T., Nikov, V., Rasoolzadeh, S., Todo, Y., Wiemer, F.: PRINCEv2 - More Security for (Almost) No Overhead. In: Dunkelman, O., Jr., M.J.J., O'Flynn, C. (eds.) Selected Areas in Cryptography - SAC 2020. LNCS, vol. 12804, pp. 483–511. Springer (2020), https://doi.org/10.1007/978-3-030-81652-0_19

40. Canale, F., Güneysu, T., Leander, G., Thoma, J.P., Todo, Y., Ueno, R.: SCARF - A Low-Latency Block Cipher for Secure Cache-Randomization. In: Calandrino, J.A., Troncoso, C. (eds.) USENIX Security Symposium, 2023. pp. 1937–1954. USENIX Association (2023), https://www.usenix.org/conference/usenixsecurity23/presentation/canale
41. Canteaut, A., Fuhr, T., Gilbert, H., Naya-Plasencia, M., Reinhard, J.: Multiple Differential Cryptanalysis of Round-Reduced PRINCE. In: Cid, C., Rechberger, C. (eds.) Fast Software Encryption - FSE 2014. LNCS, vol. 8540, pp. 591–610. Springer (2014), https://doi.org/10.1007/978-3-662-46706-0_30
42. Chakraborty, D., Hadipour, H., Nguyen, P.H., Eichlseder, M.: Finding Complete Impossible Differential Attacks on AndRX Ciphers and Efficient Distinguishers for ARX Designs. IACR Trans. Symmetric Cryptol. 2024(3), 84–176 (2024), https://doi.org/10.46586/tosc.v2024.i3.84-176
43. Cid, C., Huang, T., Peyrin, T., Sasaki, Y., Song, L.: Boomerang Connectivity Table: A New Cryptanalysis Tool. In: Nielsen, J.B., Rijmen, V. (eds.) Advances in Cryptology - EUROCRYPT 2018. LNCS, vol. 10821, pp. 683–714. Springer (2018), https://doi.org/10.1007/978-3-319-78375-8_22
44. Cogliati, B., Jean, J., Peyrin, T., Seurin, Y.: A Long Tweak Goes a Long Way: High Multi-user Security Authenticated Encryption from Tweakable Block Ciphers. IACR Communications in Cryptology 1(2) (2024)
45. Cui, T., Jia, K., Fu, K., Chen, S., Wang, M.: New Automatic Search Tool for Impossible Differentials and Zero-Correlation Linear Approximations. IACR Cryptol. ePrint Arch. p. 689 (2016), http://eprint.iacr.org/2016/689
46. Daemen, J., Govaerts, R., Vandewalle, J.: Correlation Matrices. In: Preneel, B. (ed.) Fast Software Encryption - FSE 1994. LNCS, vol. 1008, pp. 275–285. Springer (1994), https://doi.org/10.1007/3-540-60590-8_21
47. Daemen, J., Knudsen, L.R., Rijmen, V.: The Block Cipher Square. In: Biham, E. (ed.) Fast Software Encryption - FSE '97. LNCS, vol. 1267, pp. 149–165. Springer (1997), https://doi.org/10.1007/BFb0052343
48. Daemen, J., Rijmen, V.: The Wide Trail Design Strategy. In: Honary, B. (ed.) Cryptography and Coding, 8th IMA International Conference. LNCS, vol. 2260, pp. 222–238. Springer (2001), https://doi.org/10.1007/3-540-45325-3_20
49. Daemen, J., Rijmen, V.: The Design of Rijndael: AES - The Advanced Encryption Standard. Information Security and Cryptography, Springer (2002), https://doi.org/10.1007/978-3-662-04722-4
50. Dai, W., Hoang, V.T., Tessaro, S.: Information-Theoretic Indistinguishability via the Chi-Squared Method. In: Katz, J., Shacham, H. (eds.) Advances in Cryptology - CRYPTO 2017. LNCS, vol. 10403, pp. 497–523. Springer (2017), https://doi.org/10.1007/978-3-319-63697-9_17
51. Delobel, F., Derbez, P., Gontier, A., Rouquette, L., Solnon, C.: A CP-Based Automatic Tool for Instantiating Truncated Differential Characteristics. In: Chattopadhyay, A., Bhasin, S., Picek, S., Rebeiro, C. (eds.) Progress in Cryptology - INDOCRYPT 2023. LNCS, vol. 14459, pp. 247–268. Springer (2023), https://doi.org/10.1007/978-3-031-56232-7_12
52. Demirci, H., Selçuk, A.A.: A Meet-in-the-Middle Attack on 8-Round AES. In: Nyberg, K. (ed.) Fast Software Encryption - FSE 2008. LNCS, vol. 5086, pp. 116–126. Springer (2008), https://doi.org/10.1007/978-3-540-71039-4_7
53. Derbez, P., Fouque, P.: Exhausting Demirci-Selçuk Meet-in-the-Middle Attacks Against Reduced-Round AES. In: Moriai, S. (ed.) Fast Software Encryption - FSE 2013. LNCS, vol. 8424, pp. 541–560. Springer (2013), https://doi.org/10.1007/978-3-662-43933-3_28

54. Derbez, P., Fouque, P.: Automatic Search of Meet-in-the-Middle and Impossible Differential Attacks. In: Robshaw, M., Katz, J. (eds.) Advances in Cryptology - CRYPTO 2016. LNCS, vol. 9815, pp. 157–184. Springer (2016), https://doi.org/10.1007/978-3-662-53008-5_6
55. Derbez, P., Fouque, P., Jean, J.: Improved Key Recovery Attacks on Reduced-Round AES in the Single-Key Setting. In: Johansson, T., Nguyen, P.Q. (eds.) Advances in Cryptology - EUROCRYPT 2013. LNCS, vol. 7881, pp. 371–387. Springer (2013), https://doi.org/10.1007/978-3-642-38348-9_23
56. Dinur, I., Dunkelman, O., Shamir, A.: Collision Attacks on Up to 5 Rounds of SHA-3 Using Generalized Internal Differentials. In: Moriai, S. (ed.) Fast Software Encryption - FSE 2013. LNCS, vol. 8424, pp. 219–240. Springer (2013), https://doi.org/10.1007/978-3-662-43933-3_12
57. Dobraunig, C., Eichlseder, M., Grassi, L., Lallemand, V., Leander, G., List, E., Mendel, F., Rechberger, C.: Rasta: A cipher with low ANDdepth and few ANDs per bit. IACR Cryptol. ePrint Arch. p. 181 (2018), http://eprint.iacr.org/2018/181
58. Dobraunig, C., Eichlseder, M., Kales, D., Mendel, F.: Practical Key-Recovery Attack on MANTIS5. IACR Trans. Symmetric Cryptol. 2016(2), 248–260 (2016), https://doi.org/10.13154/tosc.v2016.i2.248-260
59. Dunkelman, O., Keller, N., Shamir, A.: Improved Single-Key Attacks on 8-Round AES-192 and AES-256. In: Abe, M. (ed.) Advances in Cryptology - ASIACRYPT 2010. LNCS, vol. 6477, pp. 158–176. Springer (2010), https://doi.org/10.1007/978-3-642-17373-8_10
60. Dunkelman, O., Keller, N., Shamir, A.: A Practical-Time Related-Key Attack on the KASUMI Cryptosystem Used in GSM and 3G Telephony. In: Rabin, T. (ed.) Advances in Cryptology - CRYPTO 2010. LNCS, vol. 6223, pp. 393–410. Springer (2010), https://doi.org/10.1007/978-3-642-14623-7_21
61. Dunkelman, O., Keller, N., Shamir, A.: A Practical-Time Related-Key Attack on the KASUMI Cryptosystem Used in GSM and 3G Telephony. J. Cryptol. 27(4), 824–849 (2014), https://doi.org/10.1007/s00145-013-9154-9
62. Dunkelman, O., Keller, N., Shamir, A.: Slidex Attacks on the Even-Mansour Encryption Scheme. J. Cryptol. 28(1), 1–28 (2015), https://doi.org/10.1007/s00145-013-9164-7
63. Gérault, D., Lafourcade, P., Minier, M., Solnon, C.: Computing AES related-key differential characteristics with constraint programming. Artif. Intell. 278 (2020), https://doi.org/10.1016/j.artint.2019.103183
64. Gorski, M., Lucks, S., Peyrin, T.: Slide Attacks on a Class of Hash Functions. In: Pieprzyk, J. (ed.) Advances in Cryptology - ASIACRYPT 2008. LNCS, vol. 5350, pp. 143–160. Springer (2008), https://doi.org/10.1007/978-3-540-89255-7_10
65. Grassi, L., Lüftenegger, R., Rechberger, C., Rotaru, D., Schofnegger, M.: On a Generalization of Substitution-Permutation Networks: The HADES Design Strategy. In: Canteaut, A., Ishai, Y. (eds.) Advances in Cryptology - EUROCRYPT 2020. LNCS, vol. 12106, pp. 674–704. Springer (2020), https://doi.org/10.1007/978-3-030-45724-2_23
66. Greene, P., Motley, M., Weeks, B.: ARADI and LLAMA: Low-Latency Cryptography for Memory Encryption. IACR Cryptol. ePrint Arch. p. 1240 (2024), https://eprint.iacr.org/2024/1240
67. Hadipour, H., Eichlseder, M.: Integral Cryptanalysis of WARP based on Monomial Prediction. IACR Trans. Symmetric Cryptol. 2022(2), 92–112 (2022), https://doi.org/10.46586/tosc.v2022.i2.92-112

68. Hall, C., Wagner, D.A., Kelsey, J., Schneier, B.: Building PRFs from PRPs. In: Krawczyk, H. (ed.) Advances in Cryptology - CRYPTO '98. LNCS, vol. 1462, pp. 370–389. Springer (1998), https://doi.org/10.1007/BFb0055742
69. Hu, K., Peyrin, T., Tan, Q.Q., Yap, T.: Revisiting Higher-Order Differential-Linear Attacks from an Algebraic Perspective. In: Guo, J., Steinfeld, R. (eds.) Advances in Cryptology - ASIACRYPT 2023. LNCS, vol. 14440, pp. 405–435. Springer (2023), https://doi.org/10.1007/978-981-99-8727-6_14
70. Hu, K., Sun, S., Wang, M., Wang, Q.: An Algebraic Formulation of the Division Property: Revisiting Degree Evaluations, Cube Attacks, and Key-Independent Sums. In: Moriai, S., Wang, H. (eds.) Advances in Cryptology - ASIACRYPT 2020. LNCS, vol. 12491, pp. 446–476. Springer (2020), https://doi.org/10.1007/978-3-030-64837-4_15
71. Jean, J., Nikolic, I.: Efficient Design Strategies Based on the AES Round Function. In: Peyrin, T. (ed.) Fast Software Encryption - FSE 2016. LNCS, vol. 9783, pp. 334–353. Springer (2016), https://doi.org/10.1007/978-3-662-52993-5_17
72. Jean, J., Nikolić, I., Peyrin, T.: Tweaks and Keys for Block Ciphers: The TWEAKEY Framework. In: Sarkar, P., Iwata, T. (eds.) Advances in Cryptology – ASIACRYPT 2014. pp. 274–288. Springer Berlin Heidelberg, Berlin, Heidelberg (2014)
73. Jr., B.S.K., Robshaw, M.J.B.: Fast Block Cipher Proposal. In: Anderson, R.J. (ed.) Fast Software Encryption - 1993. LNCS, vol. 809, pp. 33–40. Springer (1993), https://doi.org/10.1007/3-540-58108-1_3
74. Kelsey, J., Kohno, T., Schneier, B.: Amplified Boomerang Attacks Against Reduced-Round MARS and Serpent. In: Schneier, B. (ed.) Fast Software Encryption - FSE 2000. LNCS, vol. 1978, pp. 75–93. Springer (2000), https://doi.org/10.1007/3-540-44706-7_6
75. Khairallah, M., Yadhunathan, S., Bhasin, S.: Lightweight Leakage-Resilient PRNG from TBCs Using Superposition. In: Wacquez, R., Homma, N. (eds.) Constructive Side-Channel Analysis and Secure Design - COSADE 2024. LNCS, vol. 14595, pp. 197–217. Springer (2024), https://doi.org/10.1007/978-3-031-57543-3_11
76. Knudsen, L.: DEAL-a 128-bit block cipher. complexity 258(2), 216 (1998)
77. Knudsen, L.R., Wagner, D.A.: Integral Cryptanalysis. In: Daemen, J., Rijmen, V. (eds.) Fast Software Encryption - FSE 2002. LNCS, vol. 2365, pp. 112–127. Springer (2002), https://doi.org/10.1007/3-540-45661-9_9
78. Kounavis, M.E., Deutsch, S., Ghosh, S., Durham, D.: K-Cipher: A Low Latency, Bit Length Parameterizable Cipher. In: IEEE Symposium on Computers and Communications - ISCC 2020. pp. 1–7. IEEE (2020), https://doi.org/10.1109/ISCC50000.2020.9219582
79. Langford, S.K., Hellman, M.E.: Differential-Linear Cryptanalysis. In: Desmedt, Y. (ed.) Advances in Cryptology - CRYPTO '94. LNCS, vol. 839, pp. 17–25. Springer (1994), https://doi.org/10.1007/3-540-48658-5_3
80. Leander, G., Abdelraheem, M.A., Alkhzaimi, H., Zenner, E.: A Cryptanalysis of PRINTcipher: The Invariant Subspace Attack. In: Rogaway, P. (ed.) Advances in Cryptology - CRYPTO 2011. LNCS, vol. 6841, pp. 206–221. Springer (2011), https://doi.org/10.1007/978-3-642-22792-9_12
81. Leander, G., Moos, T., Moradi, A., Rasoolzadeh, S.: The SPEEDY Family of Block Ciphers Engineering an Ultra Low-Latency Cipher from Gate Level for Secure Processor Architectures. IACR Trans. Cryptogr. Hardw. Embed. Syst. 2021(4), 510–545 (2021), https://doi.org/10.46586/tches.v2021.i4.510-545

82. Li, H., Zhang, H., Hu, K., Liu, G., Qiu, W.: AlgSAT - A SAT Method for Verification of Differential Trails from an Algebraic Perspective. In: Zhu, T., Li, Y. (eds.) Information Security and Privacy - ACISP 2024. LNCS, vol. 14895, pp. 450–471. Springer (2024), https://doi.org/10.1007/978-981-97-5025-2_23
83. Liu, M., Lu, X., Lin, D.: Differential-Linear Cryptanalysis from an Algebraic Perspective. In: Malkin, T., Peikert, C. (eds.) Advances in Cryptology - CRYPTO 2021. LNCS, vol. 12827, pp. 247–277. Springer (2021), https://doi.org/10.1007/978-3-030-84252-9_9
84. Liu, Y., Xiang, Z., Chen, S., Zhang, S., Zeng, X.: A Novel Automatic Technique Based on MILP to Search for Impossible Differentials. In: Tibouchi, M., Wang, X. (eds.) Applied Cryptography and Network Security - ACNS 2023. LNCS, vol. 13905, pp. 119–148. Springer (2023), https://doi.org/10.1007/978-3-031-33488-7_5
85. Lucks, S.: The Saturation Attack - A Bait for Twofish. In: Matsui, M. (ed.) Fast Software Encryption - FSE 2001. LNCS, vol. 2355, pp. 1–15. Springer (2001), https://doi.org/10.1007/3-540-45473-X_1
86. Mahzoun, M., Kraleva, L., Posteuca, R., Ashur, T.: Differential Cryptanalysis of K-Cipher. In: IEEE Symposium on Computers and Communications - ISCC 2022. pp. 1–7. IEEE (2022), https://doi.org/10.1109/ISCC55528.2022.9912926
87. Matsui, M.: Linear Cryptanalysis Method for DES Cipher. In: Helleseth, T. (ed.) Advances in Cryptology - EUROCRYPT '93. LNCS, vol. 765, pp. 386–397. Springer (1993), https://doi.org/10.1007/3-540-48285-7_33
88. Mouha, N., Preneel, B.: Towards Finding Optimal Differential Characteristics for ARX: Application to Salsa20. Cryptology ePrint Archive, Paper 2013/328 (2013), https://eprint.iacr.org/2013/328
89. Mouha, N., Wang, Q., Gu, D., Preneel, B.: Differential and Linear Cryptanalysis Using Mixed-Integer Linear Programming. In: Wu, C., Yung, M., Lin, D. (eds.) Information Security and Cryptology - Inscrypt 2011. LNCS, vol. 7537, pp. 57–76. Springer (2011), https://doi.org/10.1007/978-3-642-34704-7_5
90. Murphy, S.: The Return of the Cryptographic Boomerang. IEEE Trans. Inf. Theory 57(4), 2517–2521 (2011), https://doi.org/10.1109/TIT.2011.2111091
91. Naito, Y., Sasaki, Y., Sugawara, T.: Lightweight Authenticated Encryption Mode Suitable for Threshold Implementation. In: Canteaut, A., Ishai, Y. (eds.) Advances in Cryptology - EUROCRYPT 2020. Lecture Notes in Computer Science, vol. 12106, pp. 705–735. Springer (2020), https://doi.org/10.1007/978-3-030-45724-2_24
92. Nikolic, I.: How to Use Metaheuristics for Design of Symmetric-Key Primitives. In: Takagi, T., Peyrin, T. (eds.) Advances in Cryptology - ASIACRYPT 2017. LNCS, vol. 10626, pp. 369–391. Springer (2017), https://doi.org/10.1007/978-3-319-70700-6_13
93. NIST: Submission requirements and evaluation criteria for the lightweight cryptography standardization process (2018), https://csrc.nist.gov/CSRC/media/Projects/Lightweight-Cryptography/documents/final-lwc-submission-requirements-august2018.pdf
94. NXP Semiconductors: AN12527 - LPC55Sxx PRINCE Real-Time Data Encryption. Application note (2023), https://www.nxp.com/docs/en/application-note/AN12527.pdf
95. Nyberg, K.: Linear Approximation of Block Ciphers. In: Santis, A.D. (ed.) Advances in Cryptology - EUROCRYPT '94. LNCS, vol. 950, pp. 439–444. Springer (1994), https://doi.org/10.1007/BFb0053460

96. Peyrin, T.: Improved Differential Attacks for ECHO and Grøstl. In: Rabin, T. (ed.) Advances in Cryptology - CRYPTO 2010. LNCS, vol. 6223, pp. 370–392. Springer (2010), https://doi.org/10.1007/978-3-642-14623-7_20
97. Qin, L., Dong, X., Wang, X., Jia, K., Liu, Y.: Automated Search Oriented to Key Recovery on Ciphers with Linear Key Schedule Applications to Boomerangs in SKINNY and ForkSkinny. IACR Trans. Symmetric Cryptol. 2021(2), 249–291 (2021), https://doi.org/10.46586/tosc.v2021.i2.249-291
98. Sakamoto, K., Liu, F., Nakano, Y., Kiyomoto, S., Isobe, T.: Rocca: An Efficient AES-based Encryption Scheme for Beyond 5G (Full version). IACR Cryptol. ePrint Arch. p. 116 (2022), https://eprint.iacr.org/2022/116
99. Sasaki, Y., Todo, Y.: New Impossible Differential Search Tool from Design and Cryptanalysis Aspects - Revealing Structural Properties of Several Ciphers. In: Coron, J., Nielsen, J.B. (eds.) Advances in Cryptology - EUROCRYPT 2017. LNCS, vol. 10212, pp. 185–215 (2017), https://doi.org/10.1007/978-3-319-56617-7_7
100. Selçuk, A.A.: On Probability of Success in Linear and Differential Cryptanalysis. J. Cryptol. 21(1), 131–147 (2008), https://doi.org/10.1007/s00145-007-9013-7
101. Shalan, M., Edwards, T.: Building OpenLANE: A 130nm OpenROAD-based Tapeout- Proven Flow : Invited Paper. In: 2020 IEEE/ACM International Conference On Computer Aided Design (ICCAD). pp. 1–6 (2020)
102. Shi, D., Sun, S., Derbez, P., Todo, Y., Sun, B., Hu, L.: Programming the Demirci-Selçuk Meet-in-the-Middle Attack with Constraints. In: Peyrin, T., Galbraith, S.D. (eds.) Advances in Cryptology - ASIACRYPT 2018. LNCS, vol. 11273, pp. 3–34. Springer (2018), https://doi.org/10.1007/978-3-030-03329-3_1
103. Shi, D., Sun, S., Song, L., Hu, L., Yang, Q.: Exploiting Non-full Key Additions: Full-Fledged Automatic Demirci-Selçuk Meet-in-the-Middle Cryptanalysis of SKINNY. In: Hazay, C., Stam, M. (eds.) Advances in Cryptology - EUROCRYPT 2023. LNCS, vol. 14007, pp. 67–97. Springer (2023), https://doi.org/10.1007/978-3-031-30634-1_3
104. Song, L., Yang, Q., Chen, Y., Hu, L., Weng, J.: Probabilistic Extensions: A One-Step Framework for Finding Rectangle Attacks and Beyond. In: Joye, M., Leander, G. (eds.) Advances in Cryptology - EUROCRYPT 2024. LNCS, vol. 14651, pp. 339–367. Springer (2024), https://doi.org/10.1007/978-3-031-58716-0_12
105. Sun, B., Liu, Z., Rijmen, V., Li, R., Cheng, L., Wang, Q., Alkhzaimi, H., Li, C.: Links among Impossible Differential, Integral and Zero Correlation Linear Cryptanalysis. IACR Cryptol. ePrint Arch. p. 181 (2015), http://eprint.iacr.org/2015/181
106. Sun, L., Wang, W., Wang, M.: Accelerating the Search of Differential and Linear Characteristics with the SAT Method. IACR Trans. Symmetric Cryptol. 2021(1), 269–315 (2021), https://doi.org/10.46586/tosc.v2021.i1.269-315
107. Todo, Y.: Structural Evaluation by Generalized Integral Property. In: Oswald, E., Fischlin, M. (eds.) Advances in Cryptology - EUROCRYPT 2015. LNCS, vol. 9056, pp. 287–314. Springer (2015), https://doi.org/10.1007/978-3-662-46800-5_12
108. Todo, Y., Leander, G., Sasaki, Y.: Nonlinear Invariant Attack - Practical Attack on Full SCREAM, iSCREAM, and Midori64. In: Cheon, J.H., Takagi, T. (eds.) Advances in Cryptology - ASIACRYPT 2016. LNCS, vol. 10032, pp. 3–33 (2016), https://doi.org/10.1007/978-3-662-53890-6_1

109. Todo, Y., Morii, M.: Bit-Based Division Property and Application to Simon Family. In: Peyrin, T. (ed.) Fast Software Encryption - FSE 2016. LNCS, vol. 9783, pp. 357–377. Springer (2016), https://doi.org/10.1007/978-3-662-52993-5_18
110. Tribbey, W.: Numerical Recipes: The Art of Scientific Computing (3rd Edition) is written by William H. Press, Saul A. Teukolsky, William T. Vetterling, and Brian P. Flannery, and published by Cambridge University Press, (c) 2007, hardback, ISBN 978-0-521-88068-8, 1235 pp. ACM SIGSOFT Softw. Eng. Notes 35(6), 30–31 (2010), https://doi.org/10.1145/1874391.187410
111. Turan, M.S., McKay, K., Chang, D., Bassham, L., Kang, J., Waller, N., Kelsey, J., Hong, D.: Status Report on the Final Round of the NIST Lightweight Cryptography Standardization Process. NIST IR 8454 (2023), https://doi.org/10.6028/NIST.IR.8454
112. Wagner, D.A.: The Boomerang Attack. In: Knudsen, L.R. (ed.) Fast Software Encryption - FSE '99. LNCS, vol. 1636, pp. 156–170. Springer (1999), https://doi.org/10.1007/3-540-48519-8_12
113. Wang, D., Wang, B., Sun, S.: SAT-aided Automatic Search of Boomerang Distinguishers for ARX Ciphers. IACR Trans. Symmetric Cryptol. 2023(1), 152–191 (2023), https://doi.org/10.46586/tosc.v2023.i1.152-191
114. Wang, J., Huang, T., Wu, S., Liu, Z.: Twinkle: A family of Low-latency Schemes for Authenticated Encryption and Pointer Authentication. IACR Communications in Cryptology 1(2) (2024)
115. Wang, J., Niu, C., Liu, Q., Li, M., Preneel, B., Wang, M.: Cryptanalysis of SPEEDY. In: Simpson, L., Baee, M.A.R. (eds.) Information Security and Privacy - 28th Australasian Conference, ACISP 2023, Brisbane, QLD, Australia, July 5-7, 2023, Proceedings. Lecture Notes in Computer Science, vol. 13915, pp. 124–156. Springer (2023), https://doi.org/10.1007/978-3-031-35486-1_7
116. Wolf, C.: Yosys Open SYnthesis Suite. https://yosyshq.net/yosys/
117. Xiang, Z., Zhang, W., Bao, Z., Lin, D.: Applying MILP Method to Searching Integral Distinguishers Based on Division Property for 6 Lightweight Block Ciphers. In: Cheon, J.H., Takagi, T. (eds.) Advances in Cryptology - ASIACRYPT 2016. LNCS, vol. 10031, pp. 648–678 (2016), https://doi.org/10.1007/978-3-662-53887-6_24
118. Yang, Q., Song, L., Zhang, N., Shi, D., Wang, L., Zhao, J., Hu, L., Weng, J.: Optimizing Rectangle and Boomerang Attacks: A Unified and Generic Framework for Key Recovery. J. Cryptol. 37(2), 19 (2024), https://doi.org/10.1007/s00145-024-09499-1
119. Zhang, L., Wu, R., Zhang, Y., Zheng, Y., Wu, W.: LLLWBC: A New Low-Latency Light-Weight Block Cipher. In: Deng, Y., Yung, M. (eds.) Information Security and Cryptology - Inscrypt 2022. LNCS, vol. 13837, pp. 23–42. Springer (2022), https://doi.org/10.1007/978-3-031-26553-2_2
120. Zhang, Z., Hou, C., Liu, M.: Collision Attacks on Round-Reduced SHA-3 Using Conditional Internal Differentials. In: Hazay, C., Stam, M. (eds.) Advances in Cryptology - EUROCRYPT 2023. LNCS, vol. 14007, pp. 220–251. Springer (2023), https://doi.org/10.1007/978-3-031-30634-1_8
121. Zhang, Z., Hou, C., Liu, M.: Probabilistic Linearization: Internal Differential Collisions in up to 6 Rounds of SHA-3. In: Reyzin, L., Stebila, D. (eds.) Advances in Cryptology - CRYPTO 2024. LNCS, vol. 14923, pp. 241–272. Springer (2024), https://doi.org/10.1007/978-3-031-68385-5_8

Supplementary Materials

A Algorithm for diversity computation between two ciphers

Algorithm 1 Diversity computation of two ciphers C and C'

Inputs:
  $C = S_0, P_0, S_1, P_1, .., P_{n-1}, S_n$
  $C' = S'_0, P'_0, S'_1, P'_1, .., P'_{n-1}, S'_n$
Outputs:
  A value representing the difference between C and C'
$SL \leftarrow S_0, S_1, .., S_n$
$SL' \leftarrow S'_0, S'_1, .., S'_n$
sCounter $\leftarrow [0, ..., 0]$ ▷ initialize the diversity for each subst layer
for each substLayer index i from 0 to n **do**
  for each S-box index j from 0 to 15 **do**
    if $SL[i][j] \neq SL'[i][j]$ **then** sCounter$[i]$ = sCounter$[i]$ + 1
    end if
  end for
  sCounter$[i]$ = sCounter$[i]$/16 ▷ Normalization
end for
$PL \leftarrow P_0, P_1, .., P_{n-1}$
$PL' \leftarrow P'_0, P'_1, .., P'_{n-1}$
pCounter $\leftarrow [0, ..., 0]$ ▷ initialize the diversity for each permutation layer
for each linearLayer index i from 0 to $n - 1$ **do**
  for each row index j from 0 to 63 **do**
    for each col index k from 0 to 63 **do**
      if $PL[i][j][k] \neq PL'[i][j][k]$ **then** pCounter$[i]$ = pCounter$[i]$ + 1
      end if
    end for
  end for
  pCounter$[i] \leftarrow$ pCounter$[i]/(64 \times 64)$ ▷ Normalization
end for
return sum(sCounter) + sum(pCounter)

B uKNIT-BC components

B.1 uKNIT-BC substitution layers and their inverses

The 4-bit S-boxes applied to each nibble of the internal state in uKNIT-BC can be represented by $(D \circ S_{\texttt{MANTIS}} \circ B)(x)$ where $S_{\texttt{MANTIS}}$ is the MANTIS S-box ($S_{\texttt{MANTIS}}[\mathrm{x}]=$ $[\mathtt{c}, \mathtt{a}, \mathtt{d}, \mathtt{3}, \mathtt{e}, \mathtt{b}, \mathtt{f}, \mathtt{7}, \mathtt{8}, \mathtt{9}, \mathtt{1}, \mathtt{5}, \mathtt{0}, \mathtt{2}, \mathtt{4}, \mathtt{6}]$) and D and B are transposition matrices. To represent the S-boxes succinctly, we use cycles. For example, $\begin{bmatrix} 0&0&0&1 \\ 0&0&1&0 \\ 0&1&0&0 \\ 1&0&0&0 \end{bmatrix}$ can be represented as (03)(12). The transposition matrices D and B are given in Table 4.

The inverses of these S-boxes are represented by $(B^{-1} \circ S_{\texttt{MANTIS}} \circ D^{-1})(x)$. B^{-1} and D^{-1} are listed in Table 5.

Table 4: The matrices D (top) and B (bottom) for all the S-boxes in each round.

S-box	Round 0	1	2	3	4	5	6	7	8	9	10	11
0	(021)(3) (0213)	(0)(132) (02)(1)(3)	(0231) (0)(132)	(0321) (0)(123)	(0231) (0)(12)(3)	(021)(3) (0132)	(012)(3) (0)(1)(23)	(03)(1)(2) (02)(1)(3)	(021)(3) (0312)	(0123) (0)(13)(2)	(03)(1)(2) (0321)	(02)(13) (012)(3)
1	(0312) (012)(3)	(032)(1) (0312)	(0132) (0321)	(03)(12) (0)(1)(23)	(0)(1)(2)(3) (0132)	(01)(23) (023)(1)	(03)(12) (0)(132)	(0)(123) (013)(2)	(0231) (0123)	(0321) (03)(1)(2)	(012)(3) (023)(1)	(0132) (023)(1)
2	(023)(1) (013)(2)	(01)(23) (021)(3)	(03)(12) (0231)	(021)(3) (0)(123)	(032)(1) (02)(1)(3)	(0)(123) (01)(23)	(0132) (03)(12)	(0123) (0)(123)	(012)(3) (0)(132)	(02)(1)(3) (0)(1)(2)(3)	(0)(12)(3) (0312)	(03)(1)(2) (0)(1)(23)
3	(0123) (0)(132)	(0)(132) (0213)	(0)(13)(2) (023)(1)	(023)(1) (0)(1)(2)(3)	(03)(1)(2) (0)(12)(3)	(0)(1)(23) (013)(2)	(01)(2)(3) (0321)	(02)(1)(3) (0123)	(03)(1)(2) (0213)	(021)(3) (0)(12)(3)	(03)(12) (0123)	(0132) (03)(1)(2)
4	(032)(1) (0)(1)(23)	(0312) (0213)	(0)(123) (0)(123)	(0)(1)(2)(3) (02)(1)(3)	(0)(13)(2) (02)(1)(3)	(02)(13) (0)(1)(23)	(03)(1)(2) (0132)	(0312) (03)(1)(2)	(031)(2) (0)(1)(23)	(031)(2) (0213)	(0)(132) (021)(3)	(0)(132) (0213)
5	(032)(1) (0231)	(0321) (013)(2)	(021)(3) (03)(12)	(02)(13) (031)(2)	(032)(1) (01)(2)(3)	(031)(2) (03)(12)	(0231) (03)(1)(2)	(02)(13) (0)(123)	(023)(1) (03)(1)(2)	(0123) (01)(2)(3)	(0132) (0)(123)	(0)(123) (031)(2)
6	(0132) (012)(3)	(03)(12) (0321)	(0321) (02)(1)(3)	(01)(23) (013)(2)	(0213) (0)(1)(2)(3)	(021)(3) (032)(1)	(02)(1)(3) (0)(123)	(03)(12) (0)(12)(3)	(012)(3) (031)(2)	(0)(123) (032)(1)	(032)(1) (012)(3)	(0)(13)(2) (02)(1)(3)
7	(032)(1) (0)(123)	(0312) (0)(13)(2)	(02)(1)(3) (0)(1)(23)	(01)(23) (013)(2)	(0)(123) (023)(1)	(0)(12)(3) (0)(123)	(02)(13) (013)(2)	(02)(13) (0123)	(0)(123) (0312)	(031)(2) (0132)	(02)(13) (013)(2)	(0)(12)(3) (0)(13)(2)
8	(0312) (0312)	(02)(1)(3) (02)(13)	(01)(2)(3) (03)(12)	(031)(2) (03)(12)	(0)(132) (0)(12)(3)	(013)(2) (0123)	(0321) (0)(1)(23)	(02)(13) (02)(1)(3)	(023)(1) (012)(3)	(012)(3) (0)(12)(3)	(0)(1)(2)(3) (0321)	(0231) (02)(13)
9	(0)(1)(23) (032)(1)	(0213) (03)(1)(2)	(0321) (0)(13)(2)	(031)(2) (013)(2)	(023)(1) (0231)	(02)(1)(3) (0321)	(01)(23) (01)(2)(3)	(01)(23) (023)(1)	(013)(2) (032)(1)	(02)(1)(3) (031)(2)	(0312) (031)(2)	(03)(12) (0123)
10	(0)(1)(2)(3) (01)(23)	(03)(12) (0)(132)	(0312) (0231)	(012)(3) (03)(12)	(02)(13) (0)(123)	(0213) (0)(1)(23)	(032)(1) (013)(2)	(021)(3) (03)(12)	(0231) (03)(1)(2)	(0231) (0)(12)(3)	(02)(1)(3) (0312)	(012)(3) (0)(1)(23)
11	(0321) (0)(13)(2)	(0231) (032)(1)	(0312) (0)(123)	(012)(3) (0)(132)	(0132) (032)(1)	(03)(12) (0231)	(0)(1)(2)(3) (03)(12)	(0123) (03)(12)	(0)(12)(3) (03)(12)	(0)(13)(2) (023)(1)	(0)(13)(2) (0321)	(013)(2) (0132)
12	(0123) (013)(2)	(02)(13) (0)(132)	(012)(3) (0321)	(02)(13) (0213)	(03)(12) (02)(13)	(0)(1)(23) (0)(132)	(03)(1)(2) (0123)	(01)(2)(3) (02)(1)(3)	(0)(132) (021)(3)	(012)(3) (0123)	(031)(2) (01)(2)(3)	(02)(13) (0)(12)(3)
13	(0)(1)(23) (0)(12)(3)	(031)(2) (0)(12)(3)	(032)(1) (02)(1)(3)	(0)(12)(3) (0312)	(0123) (012)(3)	(0)(132) (032)(1)	(032)(1) (03)(1)(2)	(012)(3) (0)(132)	(0312) (032)(1)	(03)(12) (0231)	(03)(1)(2) (0)(123)	(0312) (02)(13)
14	(0123) (0)(132)	(0123) (0)(123)	(0132) (01)(2)(3)	(0231) (0)(13)(2)	(0)(12)(3) (031)(2)	(0231) (023)(1)	(02)(1)(3) (0)(1)(23)	(0123) (0312)	(0)(1)(23) (0)(13)(2)	(0321) (0321)	(0)(12)(3) (0)(132)	(0)(13)(2) (0231)
15	(02)(13) (0)(1)(23)	(0)(13)(2) (031)(2)	(0132) (0132)	(0)(1)(23) (032)(1)	(0312) (0)(1)(23)	(02)(1)(3) (03)(1)(2)	(0231) (032)(1)	(0321) (0312)	(0)(123) (0123)	(0)(132) (02)(13)	(012)(3) (01)(2)(3)	(0)(132) (01)(23)

Table 5: The matrices D^{-1} (top) and B^{-1} (bottom) for all the inverses of S-boxes in each round. Each inverse of S-box is $B^{-1} \circ S_{\texttt{MANTIS}} \circ D^{-1}$.

S-box	Round 0	1	2	3	4	5	6	7	8	9	10	11
0	(120)(3) (3120)	(0)(231) (20)(1)(3)	(1320) (0)(231)	(1230) (0)(321)	(1320) (0)(21)(3)	(120)(3) (2310)	(210)(3) (0)(1)(32)	(30)(1)(2) (20)(1)(3)	(120)(3) (2130)	(3210) (0)(31)(2)	(30)(1)(2) (1230)	(20)(31) (210)(3)
1	(2130) (210)(3)	(230)(1) (2130)	(2310) (1230)	(30)(21) (0)(1)(32)	(0)(1)(2)(3) (2310)	(10)(32) (320)(1)	(30)(21) (0)(231)	(0)(321) (310)(2)	(1320) (3210)	(1230) (30)(1)(2)	(210)(3) (320)(1)	(2310) (320)(1)
2	(320)(1) (310)(2)	(10)(32) (120)(3)	(30)(21) (1320)	(120)(3) (0)(321)	(230)(1) (20)(1)(3)	(0)(321) (10)(32)	(2310) (30)(21)	(3210) (0)(321)	(210)(3) (0)(231)	(20)(1)(3) (0)(1)(2)(3)	(0)(21)(3) (2130)	(30)(1)(2) (0)(1)(32)
3	(3210) (0)(231)	(0)(231) (3120)	(0)(31)(2) (320)(1)	(320)(1) (0)(1)(2)(3)	(30)(1)(2) (0)(21)(3)	(0)(1)(32) (310)(2)	(10)(2)(3) (1230)	(20)(1)(3) (3210)	(30)(1)(2) (3120)	(120)(3) (0)(21)(3)	(30)(21) (3210)	(2310) (30)(1)(2)
4	(230)(1) (0)(1)(32)	(2130) (3120)	(0)(321) (0)(321)	(0)(1)(2)(3) (20)(1)(3)	(0)(31)(2) (20)(1)(3)	(20)(31) (0)(1)(32)	(30)(1)(2) (2310)	(2130) (30)(1)(2)	(130)(2) (0)(1)(32)	(130)(2) (3120)	(0)(231) (120)(3)	(0)(231) (3120)
5	(230)(1) (1320)	(1230) (310)(2)	(120)(3) (30)(21)	(20)(31) (130)(2)	(230)(1) (10)(2)(3)	(130)(2) (30)(21)	(1320) (30)(1)(2)	(20)(31) (0)(321)	(320)(1) (30)(1)(2)	(3210) (10)(2)(3)	(2310) (0)(321)	(0)(321) (130)(2)
6	(2310) (210)(3)	(30)(21) (1230)	(1230) (20)(1)(3)	(10)(32) (310)(2)	(3120) (0)(1)(2)(3)	(120)(3) (230)(1)	(20)(1)(3) (0)(321)	(30)(21) (0)(21)(3)	(210)(3) (130)(2)	(0)(321) (230)(1)	(230)(1) (210)(3)	(0)(31)(2) (20)(1)(3)
7	(230)(1) (0)(321)	(2130) (0)(31)(2)	(20)(1)(3) (0)(1)(32)	(10)(32) (310)(2)	(0)(321) (320)(1)	(0)(21)(3) (0)(321)	(20)(31) (310)(2)	(20)(31) (3210)	(0)(321) (2130)	(130)(2) (2310)	(20)(31) (310)(2)	(0)(21)(3) (0)(31)(2)
8	(2130) (2130)	(20)(1)(3) (20)(31)	(10)(2)(3) (30)(21)	(130)(2) (30)(21)	(0)(231) (0)(21)(3)	(310)(2) (3210)	(1230) (0)(1)(32)	(20)(31) (20)(1)(3)	(320)(1) (210)(3)	(210)(3) (0)(21)(3)	(0)(1)(2)(3) (1230)	(1320) (20)(31)
9	(0)(1)(32) (230)(1)	(3120) (30)(1)(2)	(1230) (0)(31)(2)	(130)(2) (310)(2)	(320)(1) (1320)	(20)(1)(3) (1230)	(10)(32) (10)(2)(3)	(10)(32) (320)(1)	(310)(2) (230)(1)	(20)(1)(3) (130)(2)	(2130) (130)(2)	(30)(21) (3210)
10	(0)(1)(2)(3) (10)(32)	(30)(21) (0)(231)	(2130) (1320)	(210)(3) (30)(21)	(20)(31) (0)(321)	(3120) (0)(1)(32)	(230)(1) (310)(2)	(120)(3) (30)(21)	(1320) (30)(1)(2)	(1320) (0)(21)(3)	(20)(1)(3) (2130)	(210)(3) (0)(1)(32)
11	(1230) (0)(31)(2)	(1320) (230)(1)	(2130) (0)(321)	(210)(3) (0)(231)	(2310) (230)(1)	(30)(21) (1320)	(0)(1)(2)(3) (30)(21)	(3210) (30)(21)	(0)(21)(3) (30)(21)	(0)(31)(2) (320)(1)	(0)(31)(2) (1230)	(310)(2) (2310)
12	(3210) (310)(2)	(20)(31) (0)(231)	(210)(3) (1230)	(20)(31) (3120)	(30)(21) (20)(31)	(0)(1)(32) (0)(231)	(30)(1)(2) (3210)	(10)(2)(3) (20)(1)(3)	(0)(231) (120)(3)	(210)(3) (3210)	(130)(2) (10)(2)(3)	(20)(31) (0)(21)(3)
13	(0)(1)(32) (0)(21)(3)	(130)(2) (0)(21)(3)	(230)(1) (20)(1)(3)	(0)(21)(3) (2130)	(3210) (210)(3)	(0)(231) (230)(1)	(230)(1) (30)(1)(2)	(210)(3) (0)(231)	(2130) (230)(1)	(30)(21) (1320)	(30)(1)(2) (0)(321)	(2130) (20)(31)
14	(3210) (0)(231)	(3210) (0)(321)	(2310) (10)(2)(3)	(1320) (0)(31)(2)	(0)(21)(3) (130)(2)	(1320) (320)(1)	(20)(1)(3) (0)(1)(32)	(3210) (2130)	(0)(1)(32) (0)(31)(2)	(1230) (1230)	(0)(21)(3) (0)(231)	(0)(31)(2) (1320)
15	(20)(31) (0)(1)(32)	(0)(31)(2) (130)(2)	(2310) (2310)	(0)(1)(32) (230)(1)	(2130) (0)(1)(32)	(20)(1)(3) (30)(1)(2)	(1320) (230)(1)	(1230) (2130)	(0)(321) (3210)	(0)(231) (20)(31)	(210)(3) (10)(2)(3)	(0)(231) (10)(32)

B.2 `uKNIT-BC` linear layers and their inverses

The linear layers L_i of `uKNIT-BC` are very sparse 64×64 binary matrices applied on the entire internal state. Since we have exactly 3 indices in each row having "1" with the rest being "0", we can describe the matrices solely based on these indices. Table 7 and 8 of Appendix B.2 provide the list of these indices.

The inverses of these linear layers are also sparse, we list them as the same style in Tables 9 and 10.

We give here a miniature example of how to read these linear layer tables. The matrix $L_{ex} = \begin{bmatrix} 0 & 1 & 1 & 1 \\ 1 & 0 & 1 & 1 \\ 1 & 1 & 0 & 1 \\ 1 & 1 & 1 & 0 \end{bmatrix}$ can be represented as in Table 6.

Table 6: Example of how we represent the matrix L_{ex} using a table.

Index	L_{ex}		
0	1	2	3
1	0	2	3
2	0	1	3
3	0	1	2

Table 7: The linear layer of `uKNIT-BC` (row index 0 to 31).

Index	L_0	L_1	L_2	L_3	L_4	L_5	L_6	L_7	L_8	L_9	L_{10}
0	0 10 14	3 6 14	0 8 14	0 6 9	3 6 8	3 5 11	3 6 7	7 11 15	5 8 14	4 11 14	1 8 13
1	1 8 15	0 5 15	7 11 15	2 4 10	2 7 10	0 7 8	2 5 13	0 6 9	4 11 12	6 8 60	2 10 12
2	2 9 12	1 7 13	3 5 27	1 7 37	0 5 11	2 6 9	0 4 15	3 10 12	7 9 13	5 9 13	3 11 15
3	3 11 13	2 4 12	2 4 9	3 5 11	1 4 9	1 4 10	1 12 14	1 4 14	6 10 15	7 10 15	0 9 14
4	18 23 25	16 23 30	12 18 21	16 21 24	19 27 28	18 23 30	6 7 10	16 20 24	17 25 31	18 23 31	17 23 26
5	16 22 26	22 27 29	19 23 24	19 23 25	18 21 24	21 26 29	17 22 24	18 23 27	18 21 29	17 24 30	16 24 29
6	19 21 24	17 20 25	17 20 25	18 20 26	16 22 29	17 20 24	18 23 27	17 21 25	16 23 24	19 22 29	22 27 30
7	17 20 27	18 26 31	16 22 26	17 22 27	20 25 30	16 25 31	35 39 47	19 22 26	22 26 30	16 20 28	18 20 31
8	35 36 42	38 42 46	39 42 46	35 39 43	35 41 44	36 40 47	32 36 41	34 39 43	39 40 46	39 41 46	33 43 47
9	32 38 47	32 39 44	36 43 44	35 39 46	32 43 47	39 43 45	33 40 44	33 36 40	38 42 45	36 42 44	37 41 45
10	37 41 45	34 37 41	38 40 45	33 41 44	33 40 45	38 42 44	37 43 45	35 37 41	37 41 47	37 40 45	34 36 40
11	33 40 44	33 43 45	37 41 47	36 40 47	34 42 46	37 41 46	16 20 25	32 38 42	36 43 44	34 39 41	35 39 46
12	55 58 62	52 57 62	48 56 60	50 54 62	51 52 61	53 57 61	53 56 63	53 59 61	49 56 62	55 57 62	53 59 61
13	49 56 61	48 55 56	49 52 61	52 58 60	54 58 60	51 52 56	54 58 61	52 58 60	50 57 60	48 53 58	50 58 62
14	50 52 57	49 59 63	50 54 58	49 53 63	48 56 63	48 59 60	55 57 60	54 57 63	51 59 61	51 59 63	48 54 63
15	51 53 63	50 53 60	55 59 63	51 55 61	49 53 59	49 55 63	52 59 62	55 56 62	48 58 63	12 49 54	51 55 56
16	23 25 30	19 27 29	12 21 28	23 25 30	16 22 26	16 22 31	21 26 31	23 27 29	17 20 31	18 25 31	18 20 25
17	21 24 28	18 21 31	23 24 30	20 26 29	21 24 31	18 23 27	20 25 30	22 26 30	18 21 27	19 27 29	23 26 28
18	22 26 29	20 25 28	20 25 29	22 27 28	19 23 28	19 26 29	23 27 29	20 24 31	19 26 30	16 21 28	16 21 29
19	20 27 31	16 23 24	22 26 31	21 24 31	17 25 30	20 24 28	22 24 28	21 25 28	23 24 28	17 26 30	19 27 30
20	32 38 43	35 42 46	34 40 45	8 42 45	34 37 46	32 40 47	35 39 42	32 38 46	34 41 47	32 36 42	36 40 44
21	36 42 46	32 39 40	35 41 47	8 34 42	35 36 44	34 42 44	33 38 44	35 37 47	35 42 45	38 43 47	32 41 45
22	33 39 44	33 36 45	32 42 46	32 40 47	32 38 47	35 43 45	34 43 45	33 36 45	32 40 46	35 38 43	33 38 47
23	34 41 45	37 41 47	33 43 44	33 38 44	33 39 45	33 41 46	36 41 46	34 39 44	33 43 44	33 37 40	35 39 42
24	49 54 61	49 54 63	51 55 63	52 56 58	48 55 63	49 55 58	50 54 58	48 54 57	53 58 63	53 58 61	55 56 60
25	52 57 60	50 53 58	49 52 57	49 53 59	50 58 60	52 56 62	49 52 59	49 53 59	52 56 62	49 54 56	50 52 62
26	48 58 62	55 56 61	54 58 62	48 51 55	53 59 62	48 54 60	51 55 57	50 55 56	55 57 60	50 57 62	48 54 57
27	51 53 59	51 57 62	51 59 63	50 54 57	51 52 57	50 57 61	48 53 56	51 52 58	54 59 61	51 52 63	49 59 61
28	7 11 13	0 5 8	0 6 14	1 7 12	2 7 14	5 11 12	3 6 10	6 9 13	2 8 14	3 6 8	4 11 15
29	4 8 15	3 6 9	4 9 13	0 6 13	1 4 13	6 9 14	1 8 12	1 4 8	3 10 15	0 7 10	6 9 14
30	6 10 14	1 7 11	3 5 10	3 5 15	3 6 12	4 10 13	0 4 11	3 5 12	0 9 13	1 5 9	5 10 12
31	5 9 12	2 4 10	1 7 15	2 4 14	0 5 15	7 8 15	2 5 9	2 11 15	1 11 12	2 4 11	7 8 13

Table 8: The linear layer of `uKNIT-BC` (row index 32 to 63).

Index	L_0	L_1	L_2	L_3	L_4	L_5	L_6	L_7	L_8	L_9	L_{10}
32	38 43 47	33 36 43	33 36 43	34 42 45	35 36 41	33 37 46	39 42 47	34 43 44	32 39 46	33 37 45	39 42 46
33	34 37 45	34 41 47	35 37 47	33 38 41	33 39 40	35 39 45	32 41 46	35 41 47	34 37 47	35 38 47	32 37 45
34	33 39 40	35 38 46	34 38 45	39 43 46	34 37 42	34 38 44	34 37 45	32 42 46	33 36 44	34 39 46	33 38 43
35	35 42 46	39 40 44	32 39 46	32 36 47	32 38 43	32 36 47	33 38 40	33 40 45	35 38 45	32 36 44	34 40 44
36	50 57 60	49 54 59	48 53 56	53 59 63	52 57 61	48 54 59	50 54 61	48 54 63	48 53 58	48 58 61	50 52 58
37	53 59 63	51 52 62	52 57 61	48 55 61	48 55 56	51 56 62	49 52 62	50 55 62	50 55 57	51 52 59	49 53 61
38	48 55 62	53 58 60	50 58 62	54 57 62	49 59 62	50 53 61	48 53 63	51 52 60	51 54 59	50 55 62	51 56 60
39	49 54 56	48 56 61	48 53 60	52 56 60	50 54 60	55 58 63	51 55 60	49 53 61	49 52 56	12 54 56	54 57 63
40	2 5 9	6 9 14	1 11 15	0 9 13	2 10 14	2 9 14	19 21 26	3 5 10	2 5 14	1 5 13	2 5 10
41	0 6 10	5 8 15	5 10 27	1 12 37	0 11 15	3 11 12	5 9 13	2 7 15	1 4 12	22 27 29	3 4 11
42	3 7 11	4 10 12	2 9 13	16 24 31	1 9 13	0 8 15	4 11 15	4 8 14	3 6 15	2 4 14	0 6 9
43	1 4 8	7 11 13	0 6 8	2 10 14	3 8 12	1 10 13	8 12 14	0 9 13	0 7 13	3 6 60	1 7 8
44	17 27 31	17 25 28	19 24 30	3 11 15	17 20 30	19 21 29	17 24 28	17 25 28	17 20 25	23 25 31	19 22 30
45	19 24 28	18 21 26	12 18 28	18 26 29	18 24 31	17 24 28	19 26 31	16 24 31	21 27 29	20 21 28	17 26 28
46	18 25 30	23 24 30	17 25 29	17 27 28	22 26 29	16 22 25	18 27 29	19 26 30	16 24 28	24 26 30	16 21 24
47	16 26 29	19 22 29	16 26 31	19 25 30	19 23 27	23 27 30	16 25 30	18 27 29	19 22 30	0 7 15	20 25 31
48	48 55 58	50 58 60	53 56 60	56 58 60	55 56 63	54 59 60	48 56 63	50 56 62	48 53 63	50 55 57	48 57 63
49	51 59 63	48 55 61	49 57 61	49 59 63	51 57 61	49 58 63	50 58 61	48 57 63	49 52 62	12 49 56	52 58 62
50	50 52 60	54 59 63	50 54 62	48 51 61	49 53 62	50 53 57	49 59 62	51 58 60	50 55 60	52 59 63	49 53 59
51	54 56 61	51 52 57	51 55 59	50 57 62	50 54 58	51 52 62	51 57 60	49 59 61	51 54 61	48 53 61	51 55 60
52	3 7 13	2 10 12	3 10 27	5 11 15	4 9 13	0 7 15	3 7 10	0 6 13	0 7 9	1 9 13	2 5 12
53	1 4 15	0 8 15	2 4 13	7 12 37	6 8 12	1 4 13	0 11 15	1 8 14	3 6 10	2 11 14	1 7 13
54	2 5 12	1 11 13	1 7 11	4 10 14	5 11 15	3 5 12	2 9 13	2 7 11	1 4 11	0 10 15	3 4 15
55	0 6 14	3 9 14	6 8 14	6 9 13	7 10 14	2 6 14	1 8 14	5 10 12	2 5 8	3 8 60	0 6 14
56	17 20 31	19 22 27	16 22 31	18 20 29	17 20 25	17 20 28	17 22 28	17 21 28	19 22 26	19 22 27	21 24 29
57	19 21 28	21 26 31	18 21 28	17 22 28	16 26 29	19 21 26	18 23 29	19 22 30	20 25 31	18 23 25	17 23 28
58	18 23 30	17 20 28	17 20 29	16 21 31	18 21 31	22 25 31	16 20 30	18 23 29	16 23 28	17 24 26	19 22 27
59	16 22 29	16 24 30	19 23 30	19 23 30	23 27 28	18 27 30	19 21 31	16 20 31	18 27 29	16 20 21	18 25 31
60	39 40 44	36 43 45	34 38 40	8 34 45	36 41 44	32 36 40	32 36 46	39 43 44	35 38 42	32 42 44	38 43 47
61	34 37 41	35 38 42	32 39 42	35 43 46	39 40 45	33 37 41	38 40 44	37 41 47	34 37 41	34 41 46	34 36 44
62	32 43 47	34 37 47	35 37 41	38 41 44	38 43 47	34 38 42	34 37 43	38 42 46	33 36 43	33 40 45	35 42 46
63	35 36 46	32 40 44	33 36 44	32 36 40	37 42 46	35 39 43	35 42 47	36 40 45	32 39 40	35 43 47	32 37 41

Table 9: The inverses of linear layers of `uKNIT-BC` (row index 0 to 31).

Index	L_0	L_1	L_2	L_3	L_4	L_5	L_6	L_7	L_8	L_9	L_{10}
0	0 41 55	1 28 53	0 28 43	0 29 40	2 31 41	1 42 52	2 30 53	1 43 52	30 43 52	29 47 54	3 42 55
1	1 43 53	2 30 54	31 40 54	2 28 41	3 29 42	3 43 53	3 29 55	3 29 53	31 41 54	30 40 52	0 43 53
2	2 40 54	3 31 52	3 42 53	1 31 43	1 28 40	2 40 55	1 31 54	31 41 54	28 40 55	31 42 53	1 40 52
3	3 42 52	0 29 55	2 30 52	3 30 44	0 30 43	0 41 54	0 28 52	2 30 40	29 42 53	28 43 55	2 41 54
4	29 43 53	3 31 42	3 29 53	1 31 54	3 29 52	3 30 53	2 30 42	3 29 42	1 41 54	0 31 42	28 41 54
5	31 40 54	1 28 41	2 30 41	3 30 52	2 31 54	0 28 54	1 31 41	30 40 55	0 40 55	2 30 40	30 40 52
6	30 41 55	0 29 40	28 43 55	0 29 55	0 30 53	2 29 55	0 4 28	1 28 52	3 42 53	1 28 43	29 42 55
7	28 42 52	2 30 43	1 31 54	2 28 53	1 28 55	1 31 52	0 4 52	0 41 54	2 43 52	3 29 47	31 43 53
8	1 29 43	28 41 53	0 43 55	20 21 60	0 43 53	1 31 42	29 43 55	29 42 53	0 28 55	1 28 55	0 31 43
9	2 31 40	29 40 55	3 29 42	0 40 55	3 42 52	2 29 40	31 41 54	1 28 43	2 30 52	2 30 52	3 29 42
10	0 30 41	31 42 52	30 41 52	1 43 54	1 40 55	3 30 43	4 28 52	2 40 55	3 29 53	3 29 54	1 30 40
11	3 28 42	30 43 54	1 40 54	3 44 52	2 41 54	0 28 41	30 42 53	0 31 54	1 31 54	0 31 53	2 28 41
12	2 31 54	3 42 52	4 16 45	28 41 53	30 43 53	28 41 54	3 29 43	2 30 55	1 31 41	15 39 49	1 30 52
13	3 28 52	2 43 54	29 42 53	29 40 55	29 42 52	30 43 53	1 41 54	28 43 52	2 30 43	2 40 52	0 31 53
14	0 30 55	0 40 55	0 28 55	31 43 54	28 40 55	29 40 55	3 43 55	3 42 53	0 28 40	0 42 53	3 29 55
15	1 29 53	1 41 53	1 31 40	30 44 52	31 41 54	31 42 52	2 42 53	0 31 41	3 29 42	3 47 54	2 28 54
16	5 47 59	4 19 59	7 47 56	4 42 58	6 16 57	7 16 46	11 47 58	4 45 59	6 46 58	7 18 59	5 18 46
17	7 44 56	6 44 58	6 46 58	7 46 57	19 44 56	6 45 56	5 44 56	6 44 56	4 16 44	5 19 58	4 45 57
18	4 46 58	7 17 45	4 45 57	6 45 56	5 45 58	4 17 59	6 46 57	5 47 58	5 17 59	4 16 57	7 16 59
19	6 45 57	16 47 56	5 44 59	5 47 59	4 18 47	18 44 57	40 45 59	7 46 57	18 47 56	6 17 56	19 44 58
20	7 19 56	6 18 58	6 18 58	6 17 56	7 44 56	6 19 56	11 17 58	4 18 59	16 44 57	7 45 59	7 16 47
21	6 17 57	17 45 57	4 16 57	4 19 58	5 17 58	5 44 57	16 40 59	6 19 56	5 17 45	18 45 59	18 46 56
22	5 18 59	5 47 56	7 19 56	7 18 57	6 16 46	16 46 58	5 19 56	7 17 57	7 47 56	6 41 56	6 44 58
23	4 16 58	4 19 46	5 17 59	5 16 59	18 47 59	4 17 47	6 18 57	5 16 58	6 19 58	4 44 57	4 17 57
24	6 17 45	19 46 59	5 17 44	4 19 42	5 17 45	6 19 45	5 19 44	4 18 45	6 19 46	5 46 58	5 46 56
25	4 16 46	6 18 44	6 18 46	5 16 47	7 19 56	7 46 58	11 17 47	6 19 44	4 44 57	16 44 57	16 47 59
26	5 18 47	7 45 57	7 19 47	6 17 45	16 46 57	5 18 57	16 40 45	7 17 46	7 18 56	19 46 58	4 17 45
27	7 19 44	5 16 56	2 41 52	7 18 46	4 47 59	17 47 59	6 18 46	5 16 47	17 45 59	17 41 56	6 19 58
28	17 45 57	18 44 58	16 45 57	18 46 57	4 18 59	19 45 56	19 44 56	19 44 56	19 46 58	7 18 45	17 45 57
29	18 47 59	5 16 47	18 46 58	17 45 56	6 46 57	5 18 44	18 46 57	16 47 58	5 45 59	6 17 41	5 18 56
30	16 46 58	4 46 59	17 44 59	16 47 59	7 19 44	4 47 59	17 47 58	17 46 57	7 18 47	5 19 46	6 19 44
31	19 44 56	7 17 57	19 47 56	19 42 58	17 45 58	7 16 58	16 45 59	18 45 59	4 16 57	4 16 44	7 47 59

Table 10: The inverses of linear layers of uKNIT-BC (row index 32 to 63).

Index	L_0	L_1	L_2	L_3	L_4	L_5	L_6	L_7	L_8	L_9	L_{10}
32	9 20 62	9 21 63	22 35 61	22 35 63	9 22 35	20 35 60	8 33 60	11 20 34	22 32 63	20 35 60	21 33 63
33	11 22 34	11 22 32	23 32 63	10 23 33	10 23 33	23 32 61	9 21 35	9 22 35	23 34 62	23 32 62	8 22 34
34	23 33 61	10 33 62	20 34 60	21 32 60	11 20 34	21 34 62	22 34 62	8 23 32	20 33 61	11 34 61	10 35 61
35	8 35 63	20 34 61	21 33 62	8 9 61	8 21 32	22 33 63	7 20 63	10 21 33	21 35 60	22 33 63	11 23 62
36	8 21 63	22 32 60	9 32 63	11 35 63	21 32 60	8 35 60	8 23 60	9 22 63	11 34 62	9 20 35	10 20 61
37	10 33 61	10 23 62	11 33 62	2 41 53	20 34 63	11 32 61	10 34 62	10 21 61	10 33 61	10 23 32	9 33 63
38	9 20 32	8 34 61	10 34 60	23 33 62	22 35 62	10 34 62	21 35 61	11 20 62	9 35 60	21 22 33	22 34 60
39	22 34 60	9 21 35	8 35 61	8 9 34	23 33 61	9 33 63	7 20 32	8 23 60	8 32 63	8 11 34	11 23 32
40	11 34 60	21 35 63	10 20 60	11 22 63	10 33 61	8 20 60	9 35 61	9 35 63	8 22 63	10 23 62	10 20 35
41	10 23 61	10 23 33	11 21 62	10 33 62	8 32 60	11 23 61	8 23 33	10 33 61	10 20 61	8 11 61	9 21 63
42	8 21 35	8 20 61	8 22 61	20 21 32	11 34 63	10 21 62	20 32 63	11 34 62	9 21 60	9 20 60	23 32 62
43	20 32 62	11 32 60	9 23 32	8 34 61	9 35 62	9 22 63	10 22 62	8 32 60	11 23 62	21 22 63	8 34 60
44	11 22 60	9 35 63	9 23 63	10 23 62	8 21 60	10 21 34	9 21 61	23 32 60	11 23 34	9 35 60	20 35 61
45	10 23 33	11 22 60	10 20 34	20 32 60	10 23 61	9 22 33	10 22 34	22 35 63	9 21 35	10 32 62	9 21 33
46	21 35 63	8 20 34	8 22 35	9 34 61	11 20 63	11 23 32	23 33 60	20 34 62	8 22 32	8 34 61	11 32 62
47	9 32 62	23 33 62	11 21 33	11 22 35	9 22 62	8 20 35	7 32 63	21 33 61	10 20 33	21 33 63	8 22 60
48	26 38 48	13 39 49	12 36 39	26 37 50	14 24 37	14 26 36	27 38 48	24 36 49	15 36 48	13 36 51	14 26 48
49	13 24 39	14 24 36	13 25 49	14 25 49	15 38 50	15 24 49	25 37 50	25 39 51	12 39 49	15 25 49	27 37 50
50	14 36 50	15 25 48	14 38 50	12 27 51	25 39 51	27 38 50	24 36 49	26 37 48	13 37 50	26 38 48	13 25 36
51	15 27 49	27 37 51	24 27 51	15 26 50	12 27 49	13 37 51	26 39 51	27 38 50	14 38 51	14 27 37	15 38 51
52	14 25 50	12 37 51	13 25 37	13 24 39	12 27 36	13 25 51	15 25 37	13 27 38	25 39 49	27 37 50	25 36 49
53	15 27 37	15 25 38	36 39 48	14 25 36	15 26 50	12 38 50	12 27 38	12 25 39	24 36 48	13 24 51	12 37 50
54	24 39 51	24 36 50	14 26 50	12 27 38	13 39 51	26 36 48	13 24 36	14 24 36	27 38 51	15 25 39	14 26 39
55	12 38 48	13 26 49	15 24 51	15 26 37	24 37 48	15 24 39	14 26 39	15 26 37	26 37 50	12 38 48	15 24 51
56	13 39 51	13 26 39	12 36 48	24 39 48	14 37 48	13 25 37	12 27 48	15 26 48	12 25 39	25 39 49	15 24 38
57	14 25 36	12 27 51	25 37 49	27 38 51	27 36 49	12 27 50	14 26 51	14 24 49	13 26 37	12 26 48	26 39 48
58	12 26 48	25 38 48	14 26 38	13 24 48	13 25 51	24 39 49	13 24 49	13 27 50	15 24 36	13 24 36	13 36 49
59	27 37 49	14 36 50	15 27 51	25 36 49	15 26 38	14 36 48	15 25 50	12 25 51	14 27 38	14 37 50	12 27 50
60	25 36 50	15 38 48	12 39 48	13 39 48	13 25 39	14 26 48	14 39 51	13 38 50	13 26 50	1 43 55	24 38 51
61	13 24 51	26 39 49	13 37 49	15 37 50	12 36 49	12 27 38	13 36 49	12 39 51	14 27 51	24 36 51	12 27 37
62	12 26 38	12 27 37	26 38 50	12 38 51	26 38 50	25 37 51	15 37 50	15 37 48	12 25 49	12 26 38	13 25 49
63	15 37 49	14 24 50	15 24 27	14 36 49	14 24 48	15 39 49	12 38 48	14 36 49	15 24 48	14 27 50	14 39 48

C An alternative representation of uKNIT-BC

In this section, we provide an alternative representation of uKNIT-BC. Since the linear layers in uKNIT-BC are also "bit-permutation equivalence" to that of in MIDORI, we can represent our cipher using MANTIS's substitution and MIDORI's linear layers with 24 additional bit permutation layers (see Figure below). Let

$$\mathbb{S}_{\mathtt{uKNIT-BC}} = S_{\mathtt{uKNIT-BC}} \,||\, S_{\mathtt{uKNIT-BC}} \,||\, \ldots \,||\, S_{\mathtt{uKNIT-BC}}$$

Then uKNIT-BC can be represented by

$$\begin{aligned}
&\mathbb{S}_{\mathtt{uKNIT-BC}} \cdot L_{\mathtt{uKNIT-BC}} \cdot \mathbb{S}_{\mathtt{uKNIT-BC}} \cdot \ldots \cdot \mathbb{S}_{\mathtt{uKNIT-BC}} \\
&= (\mathbb{B}_0 \cdot \mathbb{S}_{\mathtt{MANTIS}} \cdot \mathbb{D}_0)(\mathbb{A}_0 \cdot L_{\mathtt{MIDORI}} \cdot \mathbb{C}_0)(\mathbb{B}_1 \cdot \mathbb{S}_{\mathtt{MANTIS}} \cdot \mathbb{D}_1) \cdot \ldots \cdot (\mathbb{B}_{11} \cdot \mathbb{S}_{\mathtt{MANTIS}} \cdot \mathbb{D}_{11}) \\
&= \mathbb{B}_0^* \cdot \mathbb{S}_{\mathtt{MANTIS}} \cdot \mathbb{B}_1^* \cdot L_{\mathtt{MIDORI}} \cdot \mathbb{B}_2^* \cdot \mathbb{S}_{\mathtt{MANTIS}} \cdot \mathbb{B}_3^* \cdot \ldots \cdot \mathbb{S}_{\mathtt{MANTIS}} \cdot \mathbb{B}_{23}^*
\end{aligned}$$

where $\mathbb{B}_i$ for $i \in \{0..11\}$ and $\mathbb{B}_j^*$ for all $j \in \{0, ..., 23\}$ are 64×64 transposition matrices. The matrices $\mathbb{B}_i$ and $\mathbb{B}_j^*$ can be found in our GitHub.

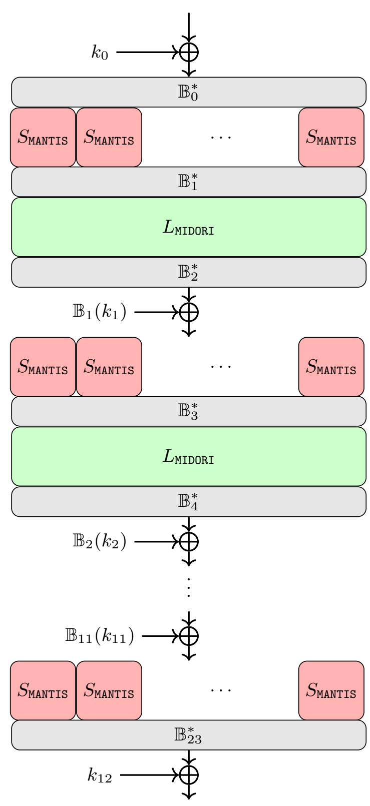

D The matrices of MIDORI and PRINCE

Let $I_4 \in \mathbb{F}_2^{4\times4}$ be the 4×4 identity matrix in and $O_4 \in \mathbb{F}_2^{4\times4}$ be the 4×4 all zero matrix, and let $M_i \in \mathbb{F}_2^{4\times4}$ be a matrix that has zero everywhere except for diagonal entries (j, j) where $j \neq i$. Then, the MixColumns matrices of PRINCE and MIDORI are

$$\tilde{M}^{(0)}_{\texttt{PRINCE}} = \begin{bmatrix} M_0 & M_1 & M_2 & M_3 \\ M_1 & M_2 & M_3 & M_0 \\ M_2 & M_3 & M_0 & M_1 \\ M_3 & M_0 & M_1 & M_2 \end{bmatrix} \tilde{M}^{(1)}_{\texttt{PRINCE}} = \begin{bmatrix} M_1 & M_2 & M_3 & M_0 \\ M_2 & M_3 & M_0 & M_1 \\ M_3 & M_0 & M_1 & M_2 \\ M_0 & M_1 & M_2 & M_3 \end{bmatrix} M_{\texttt{MIDORI}} = \begin{bmatrix} O_4 & I_4 & I_4 & I_4 \\ I_4 & O_4 & I_4 & I_4 \\ I_4 & I_4 & O_4 & I_4 \\ I_4 & I_4 & I_4 & O_4 \end{bmatrix}$$

One may realise that $\tilde{M}^{(0)}_{\texttt{PRINCE}}$ is actually a rotation of $\tilde{M}^{(1)}_{\texttt{PRINCE}}$.

E Security analysis of uKNIT-BC

We provide in this section a large range of state-of-the-art security analysis of uKNIT-BC.

We first introduce a few more notations to facilitate the descriptions of our attacks. The S-boxes and linear layers used in the i^{th}-round uKNIT-BC are denoted by S_i and L_i respectively, where $0 \leq i \leq 11$ (the L_{11} is omitted in uKNIT-BC). For $0 \leq i \leq 10$, the input of the i^{th}-round is x_i, and after the XORing with the round key k_i, it becomes x'_i, i.e., $x'_i = x_i \oplus k_i$. Then, we apply S_i to x'_i to get y_i and apply L_i to y_i to get x_{i+1}. For the last round, i.e., $i = 11$, we have $x_{12} = S_{11}(x_{11}) \oplus k_{12}$.

In differential cryptanalysis, given x_i, x'_i, y_i, their differences are denoted by $\Delta(x_i), \Delta(x'_i)$ and $\Delta(y_i)$, respectively. Given a state $z \in \{x, x', y, k\}$, $z[t]_b$ is the t-th bit of z, while $z[t_0, t_1, t_2, \ldots, t_{n-1}]_b$ are the n bits of z as $z[t_i]_b, 0 \leq t \leq n-1$. Similarly, $z[t]_n$ is the t-th nibble of z, while $z[t_0, t_1, \ldots, t_{n-1}]_n$ are the n nibbles of $z[t_i]_n, 0 \leq i \leq n-1$. When $t_0, \ldots, t_{n-1}$ are consecutive, we also write these n bits and nibbles as $z[t_0 \sim t_{n-1}]_b$ and $z[t_0 \sim t_{n-1}]_n$, respectively. As for the discussions on linear cryptanalysis, the linear masks of a state $z \in \{x, x', y, k\}$ are denoted by $\Gamma(z)$.

E.1 Simple differential cryptanalysis

In this subsection, we analyze the security of uKNIT-BC against differential attacks [27]. Unlike typical ciphers, uKNIT-BC is fully non-aligned as all rounds are very different, so we should check the security of all windows for $\mathcal{W}(i, r)$, $1 \leq r \leq 12$ and $0 \leq i \leq 12 - r$. With our SAT tool, we search for differential characteristics (DCs) for all windows and the results are shown in Table 11 (left).

Even though we do not claim resistance against related-key attacks, we provide in Table 12 the related-key differentials probabilities we found on uKNIT-BC.

Remark. When $r \leq 5$, the differential probabilities of $\mathcal{W}(i, r)$ are higher than the r-round PRINCE ones. However, for $r \geq 6$, the differential probabilities of all r-length windows are lower. This shows that the components of uKNIT-BC are weaker in security than those of PRINCE, but for a higher number of rounds, the freedom to combine different components allowed uKNIT-BC to achieve stronger differential security. Generally speaking, a weaker component goes along with a better latency performance, which helps to explain to some extent why uKNIT-BC is better than PRINCE in both the security and latency criteria.

For 8-length windows, all probabilities are lower than 2^{-64}. We also verified with the quasi-differential technique [21] the best differential characteristic for 8 rounds (see below) and concluded that its success probability 2^{-68} is independent of the key value. As a result, we expect that 8-round uKNIT-BC does not have any useful DCs for key-recovery attack.

Thus, we choose to use a DC of $\mathcal{W}(2, 7)$ to mount a differential key-recovery attack. With an automatic search model that can consider both the distinguisher and the key-recovery process (see below), we check $\mathcal{W}(0 \leq i \leq 1, 11)$ with 7-round DC and 2-round backward and forward propagations. However,

Table 11: Differential probabilities (left) and linear correlations (right), in $-\log_2$, for $\mathcal{W}(i,r)$, $1 \leq r \leq 12, 0 \leq i \leq 12-r$. The last column gives the value for the r-round PRINCE (both v1 and v2) where these r rounds contain $\lfloor (r-2)/2 \rfloor$ forward rounds, $\lceil (r-2)/2 \rceil$ backward rounds and the middle 2 rounds.

r \ i	0	1	2	3	4	5	6	7	8	9	10	11	PRINCE
1	2	2	2	2	2	2	2	2	2	2	2	2	–
2	8	8	6	6	8	8	6	8	8	6	8	–	–
3	14	12	12	12	14	14	12	14	12	12	–	–	–
4	25	23	24	26	30	26	26	24	24	–	–	–	32
5	40	40	39	40	40	39	37	37	–	–	–	–	39
6	49	48	46	46	50	47	49	–	–	–	–	–	44
7	60	58	52	61	60	59	–	–	–	–	–	–	56
8	71	70	68	71	72	–	–	–	–	–	–	–	66
9	81	82	80	82	–	–	–	–	–	–	–	–	74
10	94	87	92	–	–	–	–	–	–	–	–	–	80
11	101	99	–	–	–	–	–	–	–	–	–	–	89
12	113	–	–	–	–	–	–	–	–	–	–	–	99

r \ i	0	1	2	3	4	5	6	7	8	9	10	11	PRINCE
1	1	1	1	1	1	1	1	1	1	1	1	1	–
2	4	4	3	3	4	4	3	4	4	3	4	–	–
3	7	6	6	6	7	6	6	7	6	6	–	–	–
4	13	10	11	13	14	12	12	11	12	–	–	–	16
5	19	18	19	19	19	18	17	17	–	–	–	–	19
6	24	23	22	23	25	23	21	–	–	–	–	–	22
7	29	26	26	30	29	27	–	–	–	–	–	–	27
8	35	34	34	34	34	–	–	–	–	–	–	–	32
9	39	38	37	39	–	–	–	–	–	–	–	–	34
10	45	44	43	–	–	–		–	–	–	–	–	38
11	49	50	–	–	–	–	–	–	–	–	–	–	41
12	55	–	–	–	–	–	–	–	–	–	–	–	49

Table 12: The negative log-2 of probabilities ($-log_2(p)$) of the related-key differentials of uKNIT-BC for $\mathcal{W}(i,r)$ for $1 \leq r \leq 12$ and $0 \leq i \leq 12-r$. The numbers in brackets mean that it is a lower bound.

r \ i	0	1	2	3	4	5	6	7	8	9	10	11
1	0	0	0	0	0	0	0	0	0	0	0	0
2	0	0	0	0	0	0	0	0	0	0	0	–
3	2	2	2	2	2	2	2	2	2	2	–	–
4	6	7	6	6	6	6	6	6	6	–	–	–
5	14	12	14	12	11	13	13	13	–	–	–	–
6	25	21	22	24	19	23	22	–	–	–	–	–
7	(29)	(29)	(29)	(30)	(30)	(31)	–	–	–	–	–	–
8	(32)	(33)	(33)	(32)	(33)	–	–	–	–	–	–	–
9	(35)	(35)	(35)	(35)	–	–	–	–	–	–	–	–
10	(41)	(42)	(41)	–	–	–	–	–	–	–	–	–
11	(45)	(45)	–	–	–	–	–	–	–	–	–	–
12	(49)	–	–	–	–	–	–	–	–	–	–	–

no effective key-recovery attack was detected. We then check $\mathcal{W}(0 \leq i \leq 2, 10)$ with 7-round DC with r_0-round backward propagation and r_2-round forward propagation, where $(r_0, r_2) \in \{(2,1),(1,2)\}$ and manage to detect some useful key-recovery attacks. The best key-recovery attack is depicted in Figure 6 which works for $\mathcal{W}(0,10)$ with 7-round DC, 2-round backward propagation and 1-round forward propagation. The key-recovery process is as follows:

1. A total of 120 key bits (consisting of $k_0[0 \sim 11]_n$, $k_1[0 \sim 2,4,5,7,8,10,11]_n$, and $k_{10}[0,2,3,7 \sim 10,12,15]_n$) are involved in the backward and forward propagations. Thus, we initialize a counter $\mathbb{H}$ with 2^{120} entries.

2. One plaintext structure contains 2^{48} plaintexts. Encrypt plaintexts of s structures and combine them to $s \times 2^{95}$ pairs. Since the ciphertext difference has 7 inactive S-boxes, thus only $s \times 2^{95-28} = 2^{67}$ pairs survive.
3. For each surviving pairs, we guess all 2^{36} values of $\Delta(x_1[0 \sim 2, 4, 5, 7, 8, 10, 11]_n)$. The possible keys of $k_1[0 \sim 2, 4, 5, 7, 8, 10, 11]$ and $k_0[0 \sim 11]$ can be extracted with some table-lookups for the active S-boxes. With $\Delta(x_{10})$ and $\Delta(x_9)$, the 36 bits of $k_{10}[0, 2, 3, 7 \sim 10, 12, 15]$ can be obtained by table-lookups, too.
4. The first 2^{120-a} key candidates with largest occurrence times are selected. k_0 and k_1 are directly related to the master key. Thus, they will be combined with the remaining 44 bits of the master key and be searched exhaustively.

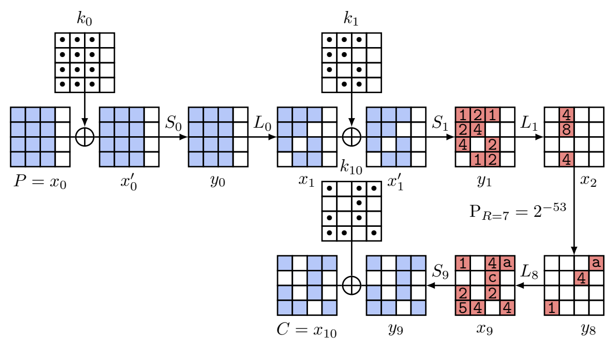

Fig. 6: The differential key-recovery attack on $\mathcal{W}(0, 10)$ based on a DC of $\mathcal{W}(2, 7)$ (red color) whose probability is 2^{-53}.

Complexity. From s structures, $s \times 2^{95}$ pairs can be obtained. The probability they can reach $\Delta(y_1)$ is 2^{-48}, *i.e.*, , $s \times 2^{47}$ pairs will reach $\Delta(y_1)$. According to [100], the number of pairs entering the distinguisher can be computed as

$$N_{pairs} = \frac{(\Phi^{-1}(P_S)\sqrt{S_N + 1} + \Phi^{-1}(1 - 2^{-a}))^2}{pS_N},$$

where P_S is the success probability, Φ is CDF of the standard normal distribution, $p = 2^{-53}$ is the probability of the DC, $S_N = p/2^{-n}$ is the signal-to-noise ratio, and a is the advantage. We set $P_S = 0.95$ and $a = 54$, $N_{pairs} \approx 2^{54.7}$. Thus $2^{7.7}$ structures are needed. The final data complexity is about $2^{55.7}$ and the time complexity is about 2^{110} operations.

Verifying the differential cryptanalysis with quasi-differential Techniques. The classical differential cryptanalysis relies on assumptions such as the hypothesis of stochastic equivalence and round-independence assumptions. In reality, the differential cryptanalysis works under the fixed-key scenario, thus both assumptions might fail. To analyze the differential propagation property under the fixed-key setting, Beyne and Rijmen introduced the quasi-differential framework [21]. In this framework, the quasi-differential basis is chosen to generate the quasi-differential transition matrix.

Definition 4 (Quasi-differential transition matrix [21]). *Let n and m be positive integers and $\mathsf{F} : \mathbb{F}_2^n \to \mathbb{F}_2^m$ a function. The coordinate of the quasi-differential transition matrix D^{F} of F is computed by*

$$D^{\mathsf{F}}_{(v_0,v_1),(u_0,u_1)} = 2^{-n} \sum_{\substack{x \in \mathbb{F}_2^n \\ \mathsf{F}(x)+\mathsf{F}(x+u_1)=v_1}} (-1)^{u^\top x + v^\top \mathsf{F}(x)}. \quad (2)$$

(u_1, v_1) is the difference pair and (v_0, v_1) is the mask pair. The value $D^{\mathsf{F}}_{(v_0,v_1),(u_0,u_1)}$ is called the correlation. When $u_0 = v_0 = 0$, one can find $D^{\mathsf{F}}_{(v_0,v_1),(u_0,u_1)}$ represents the probability of F with the input difference u_1 and output difference v_1.

Let F be an iterative function as $\mathsf{F} = \mathsf{F}_r \circ \cdots \circ \mathsf{F}_1$. When fixing an r-round DC $(u_0, u_1, \ldots, u_r)$ for F, there might be many quasi-differential trails related to this DC, denoted by $((v_0, u_0), (v_1, u_1), \ldots, (v_r, u_r))$. The probability of a DC under the fixed-key setting can be computed as

$$p = \sum_{\omega_r, \omega_{r-2}, \ldots, \omega_0} \prod_{0 \le i < r} D^{\mathsf{F}}_{(\omega_{i+1}, u_{i+1}),(\omega_i, u_i)}.$$

Thus, we can use this formula to check if or how a DC is influenced by the secret keys.

We use the quasi-differential framework to verify the 8-round DC in Figure 7, as this DC for $\mathcal{W}(3, 8)$ is the strongest among all 8-length windows. Since the S-boxes for each position of each round are different in `uKNIT-BC`, we need to generate the corresponding propagation tables according to each S-box S and its input difference u_1 and output difference v_1.

$$Q^S_{v_0,u_0} = 2^{-n} \sum_{\substack{x \in \mathbb{F}_2^n \\ \mathsf{S}(x)+\mathsf{F}(x+u_1)=v_1}} (-1)^{u_0^\top x + v_0^\top \mathsf{S}(x)}.$$

For a linear layer L, the propagation rule for the input/output mask pair (u_0, v_1) is $u_0 = \mathsf{L}^\top v_0$, which is the same as the linear cryptanalysis.

The corresponding automatic search model for masks can be established in a common way. In our case, we focus our attention on the weakest 8 round windows, which is the DC from $winc(3, 8)$ that can be found in Figure 7. We found that there is only one quasi-differential trail with all masks being 0. This shows that the probability of this DC is independent of keys.

E.2 Multiple differential cryptanalysis

Although `uKNIT-BC` is secure against differential attacks built from differential characteristics (Section E.1), we note that $\mathcal{W}(2, 8)$ is the weakest among all

8-length windows, with a differential probability of 2^{-68}. We need to check if there are any differentials with clustering DCs for $\mathcal{W}(2,8)$ whose probability could reach 2^{-64}. With our SAT model, we searched for 100 different DCs whose probabilities are exactly 2^{-68}. The 100 DCs belong to 72 distinct differentials, and all of them belong to 3 similar differential truncated patterns.

Definition 5 (Differential truncated pattern (DTP)). *A differential truncated pattern for* `uKNIT-BC` *is a sequence of bit-strings as*

$$T = (a_i, a_{i+1}, \ldots, a_{i+r}) \in (\mathbb{F}_2^{16})^{r+1}.$$

We say that a DC $(x_i, x_{i+1}, \ldots, x_{i+r})$ *belongs to* T *if*

$$x_i[t]_n = \begin{cases} 0 & \text{if } a_i[t]_b = 0; \\ any & \text{otherwise.} \end{cases}$$

In [41], Canteaut *et al.* applied a multiple differential attack to 10-round `PRINCE`, and later the same attack was applied to 11-round `PRINCEv2` by the designers [39]. In the language of DTP, this attack traces all DCs belonging to some special DTPs where the Hamming weights of all a_i are 4. In this paper, we generalize their attack based on `uKNIT-BC` linear layers.

$\Delta(x_2)$	0000be07000000000		a_2	0000110100000000
	00007d0e00000000			0000110100000000
$\Delta(x_3)$	0000000000000070		a_3	0000000000000010
	00000000000000a0			0000000000000010
$\Delta(x_4)$	0004000001000000		a_4	0001000001000000
	0004000008000000			0001000001000000
$\Delta(x_5)$	0000040480200808		a_5	0000010110100101
	00000808a0a00802	DTP →		0000010110100101
$\Delta(x_6)$	02a4000034040000		a_6	0111000011010000
	0444000024040000			0111000011010000
$\Delta(x_7)$	0000000020400000		a_7	0000000010100000
	0000000080200000			0000000010100000
$\Delta(x_8)$	0000080000000002		a_8	0000010000000001
	0000080000000008			0000010000000001
$\Delta(x_9)$	0004802000082040		a_9	0001101000011010
	000c204000028010			0001101000011010

Fig. 7: Generation of a DTP from a DC of $\mathcal{W}(2,8)$. For convenience, we also give the differences and patterns of $\Delta(y_i)$.

Figure 7 illustrates how to generate a DTP given a DC. By adapting Canteaut *et al.* 's method, we capture all DCs that belong to the DTP. First, for $2 \leq i < 9$, we enumerate all possible $\Delta(y_i)$ that satisfies the active pattern of a_i while $L_i(\Delta(y_i))$ satisfies the pattern a_{i+1}. Denote the Hamming weight of a_i by w_i

and $h_i = \min\{w_i, w_{i+1}\}$, there are 2^{h_i} possible values for $\Delta(y_i)$. Then, we can generate a matrix to describe the propagation of the differences from $\Delta(y_i)$ to $\Delta(x_{i+1})$. Let $M \in \mathbb{F}_2^{h_i \times h_i}$ and the entry at the cross of the u^{th} column and v^{th} row, denoted by $M^{L_i}_{v,u}$, is defined as

$$M^{L_i}_{v,u} = \begin{cases} 1 & u = \sup(\delta_{\Delta(y_i)}) \text{ and } v = \sup(\delta_{\Delta(x_{i+1})}); \\ 0 & \textit{otherwise}. \end{cases}$$

where $\sup(b)$ is the support of a bit vector b and δ_x is a bit unit vector with the entry at x being 1. Thus, $\delta_{\Delta(x_{i+1})} = M_{v,u}\delta_{\Delta(y_i)}$. Then, according to a_i, we can generate all 2^{w_i} possible $\Delta(x_i)$. For all $\Delta(x_i)$ and $\Delta(y_i)$ we can also generate a matrix $M^{S_i} \in \mathbb{F}_2^{w_{i+1} \times w_i}$ with

$$M^{S_i}_{v,u} = \mathrm{P}(\Delta(x_i) \xrightarrow{S_i} \Delta(y_i)) \text{ where } u = \sup(\delta_{\Delta(x_i)}) \text{ and } v = \sup(\delta_{\Delta(y_i)}).$$

Therefore, using the same principles mentioned in [41], the (k, l)-entry of

$$M^{\mathcal{W}(2,8)} = M^{S_9} \times \prod_{8 \geq i \geq 2} (M^{L_i} \times M^{S_i})$$

encodes the probability of the differential where the input difference is represented by the index k of the support for a_2 and the output difference is represented by index l of the support for a_9. With the DTP in Figure 7, we compute $M^{\mathcal{W}(2,8)}$ and the best differential of this DTP has a probability of $2^{-63.3}$. We also found that the other two DTPs and the probability of their respective best differential are also approximately $2^{-63.3}$. These differentials have probabilities larger than but very close to 2^{-64}. Key-recovery attacks based on these differentials would therefore admit extremely high data and time complexities. Considering our security claim, we do not think they will be a threat to `uKNIT-BC`.

Automatic search for differential key-recovery attacks. The complexity of a full key-recovery attack is influenced by both the distinguisher and the key-guessing processes. To search for a good key-recovery-friendly DC, we add the key-guessing part within our search as follows.

1. **Distinguisher.** The SAT model M_d used in the search for the distinguisher is produced.
2. **Backward propagation.** Assume that we add r_0 rounds before the DC, whose input difference is denoted by α. We need to describe the backward propagation of α to the plaintext with probability 1. Thus, we add the following constraints to ensure that:
   - the input and output differences of each S-box are either active or inactive simultaneously
   - for each linear layer, if one output difference bit b_o is active, then all input difference bits that are needed to calculate b_o must be active

   We call this model the backward propagation, denoted by M_b.

3. **Forward propagation.** Similar to the backward propagation, assume we append r_2 rounds to the DC, whose output difference is β. We construct a forward propagation that requires:
   – the input and output differences of each S-box to be either active or inactive simultaneously
   – for each linear layer, if one input difference bit b_i is active, then all output difference bits that are required for calculating b_i must be active

   This model is called forward propagation, denoted by M_f.
4. **Objective function.** To search for a key-recovery-friendly DC, we use two objective functions as follows,

$$\mathcal{A}(M_b) + \mathcal{A}(M_f) \leq O_1, \quad \mathrm{P}(M_d) \leq O_2$$

   where $\mathcal{A}(M_b)$ and $\mathcal{A}(M_f)$ are the number of active S-boxes in the two-end key-guess processes, $\mathrm{P}(M_d)$ is the probability of the DC, and O_1 and O_2 are two positive numbers for the objective functions. In the search, starting from small values, we try all possible combinations of (O_1, O_2), until we find one that returns a solution. Note that this model is rather intuitive in how it searches for good key-recovery attacks based on a DC, but it does not provide a guarantee that the key-recovery attack found is optimal.

E.3 Linear (hull) cryptanalysis

Linear cryptanalysis [87] is another fundamental attack to check the security of a cipher. Akin to the differential attack, we use our SAT models to check for the linear correlations of all possible windows of `uKNIT-BC`. The results for all linear characteristics (LCs) are shown in Table 11 (right). Similar observations are found here, when $r \leq 7$, the correlation of $\mathcal{W}(i,r), 0 \leq i \leq 12-r$ can be larger than those of `PRINCE`. While for $r \geq 8$, the correlations of all $\mathcal{W}(i,r)$ will be smaller than `PRINCE`, which again shows the effectiveness of `uKNIT` strategy – weaker components can be combined to design ciphers that have strong security without sacrificing the latency.

We use a model to search for good linear key-recovery attacks similarly to the differential key-recovery process. The best attack with a single LC works for $\mathcal{W}(0,10)$ consisting of a distinguisher of correlation 2^{-30} for $\mathcal{W}(2,7)$ and a 2-round backward propagation involving 96-bit keys and 1-round forward propagation involving 24-bit keys. Since the squared correlation of its distinguisher is significantly smaller than the 7-round DC we used in Section E.1, we believe the linear attacks based on this LC cannot be stronger than the differential attack.

To examine how much `uKNIT-BC` suffers from the linear hull effect, we use a similar method from Appendix E.2. The main target is still $\mathcal{W}(2,8)$ as it is in the middle which is the most crucial chunk in a possible key-recovery attack. We searched for 100 LCs for $\mathcal{W}(2,8)$ whose correlation is exactly 2^{-34}. These LCs belong to 7 different linear truncated patterns (LTPs). The LTPs share a similar definition with DTPs but it treats linear masks rather than the differences. Also, when clustering LCs, we use the squared correlations to build the matrix M^{S_i}

to avoid the cancellations of positive and negative correlations. Technically, we consider the expected linear potential of a linear hull.

Definition 6 (Expected linear potential (ELP) [95]). *Let $\Gamma(x_i)$ and $\Gamma(x_{i+r})$ be the input and output masks of an r-round key-alternating cipher (note that* `uKNIT-BC` *is key-alternating). The expected linear potential is defined as*

$$\mathrm{ELP}(\Gamma(x_i), \Gamma(x_{i+r})) = \sum_{\Gamma(x_{i+1}),\ldots,\Gamma(x_{i+r-1})} \mathrm{C}^2((\Gamma(x_i), \Gamma(x_{i+1}), \ldots, \Gamma(x_{i+r})))$$

where $\mathrm{C}(\Gamma(x_i), \Gamma(x_{i+1}), \ldots, \Gamma(x_{i+r}))$ *is the correlation of a LC.*

Among the 7 LTPs, the ELP of the best linear hull for $\mathcal{W}(2,8)$ we find is $2^{-62.4}$, denoted by

$$(\mathtt{0,0,0,0,b,4,0,e,0,0,0,0,0,0,0,0}) \xrightarrow{\mathcal{W}(2,8)} (\mathtt{0,2,0,4,2,0,2,0,0,0,0,1,8,0,0,0})$$

The data complexity of linear cryptanalysis based on the ELP should be proportional to $\mathcal{O}(\mathrm{ELP}^{-1})$. Thus, the 8-round linear hulls should be hard to use in the key-recovery attack considering our data limitation of 2^{-47} chosen-plaintexts.

E.4 Impossible differential cryptanalysis

Impossible differential (ID) cryptanalysis was proposed independently by Knudsen [76] and Biham *et al.* [24], remaining one of the most powerful attacks on block ciphers. The automatic search methods for ID distinguishers were developed from the DC searches [99,45]. By implementing these automatic models with our SAT solvers, we detected the following two impossible truncated differentials over $\mathcal{W}(3,7)$. Denote one active S-box by 1 and inactive S-box by 0, the 2 impossible differentials are

$$(0,0,0,0,0,0,0,0,0,0,0,0,0,0,0,1) \overset{7R}{\not\rightarrow} (1,0,0,0,0,0,0,0,0,0,0,0,0,0,0,0) \quad (3)$$

$$(0,0,0,0,0,0,0,0,0,0,0,0,0,0,0,1) \overset{7R}{\not\rightarrow} (0,0,0,1,0,0,0,0,0,0,0,0,0,0,0,0)$$

We use the first impossible differentials (Equation (3)) in a key-recovery attack on $\mathcal{W}(1,11)$. Two rounds are added before the distinguisher and one round after. The key-recovery attack process is shown in Figure 8. The ID of $\mathcal{W}(3,7)$ is from $\Delta(x_3)$ to $\Delta(y_9)$. $\Delta(x_3)$ propagates backward to the plaintext $\Delta(x_1)$ with probability 1 and $\Delta(y_9)$ propagates forward to the ciphertext $\Delta(x_{11})$ with probability 1. The active cells are shown in Figure 8. The key-recovery process is as follows.

1. Initialize a table $\mathbb{H}$ with the 92-bit $k_1[1 \sim 15]_n, k_2[8 \sim 11]_n, k_{11}[7,10,11,13]_n$ as the index and 0 for all the values.
2. As shown in Figure 8, one plaintext structure contains 2^{60} plaintexts, yielding a total of 2^{119} pairs. Encrypt all plaintexts of one structure, combine them into pairs with a hash table. Since there are 10 inactive cells in the ciphertext side, $2^{119-40} = 2^{79}$ pairs survive. For 2^t structures, there are 2^{t+79} pairs.

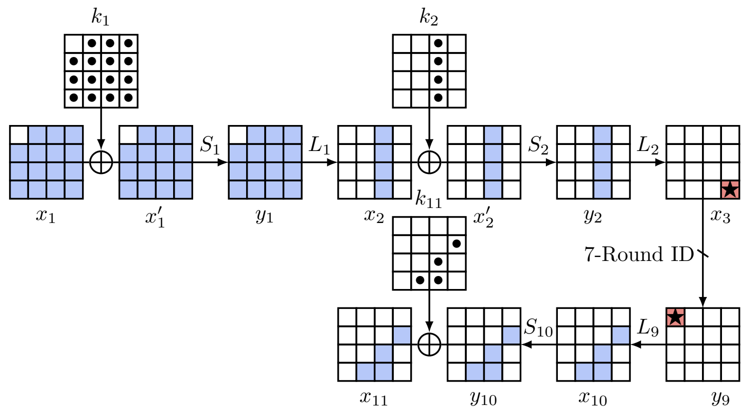

Fig. 8: The key-recovery process for $\mathcal{W}(1, 10)$ based on the second ID of $\mathcal{W}(3, 7)$ (Equation (3)).

3. For each pair, we guess the 2^{16} possibilities of $\Delta(x_2)$ differences and extract the 60-bit $k_1[1 \sim 15]_n$ and 16-bit $k_2[8 \sim 11]_n$ with some look-up tables. At the side of the ciphertexts, 16-bit $k_{11}[7, 10, 11, 13]_n$ can also be extracted with table look-ups.
4. On average, a wrong pair can reach the input and output differences of the ID with a probability of $2^{-56-12} = 2^{-68}$. Thus, with 2^{t+79} pairs, the probability that one wrong key cannot be excluded by all pairs is $(1 - 2^{-68})^{2^{t+79}} = (1 - 2^{-68})^{2^{68} \times 2^{-68} \times 2^{t+79}} \approx e^{-2^{t+11}}$. As we want the number of remaining wrong keys to be less than 1, we have

$$2^{92} \times e^{-2^{t+11}} < 1,$$

which means $t \geq -5.0$. In other words, we only need 2^{55} plaintexts and process $2^{55 \times 2 - 1 - 40} = 2^{69}$ pairs.

Complexity. The data complexity is 2^{55} chosen plaintexts. The time complexity is dominated by processing each pair and updating $\mathbb{H}$ for labelling those impossible keys. For each pair, on average there are $2^{92-68} = 2^{24}$ keys that can pass the filters. Thus, we need to access $\mathbb{H}$ 2^{24} times for each pair. Since $\mathbb{H}$ is a large table, we regard each access to $\mathbb{H}$ as one encryption. The time complexity is eventually $2^{69+24} = 2^{93}$ encryptions. The memory complexity is dominated by $\mathbb{H}$, which is 2^{92} bits that is equivalent to 2^{86} 64-bit blocks.

E.5 Zero-correlation cryptanalysis

Zero-correlation (ZC) attacks are an extension of linear cryptanalysis based on linear hull with exact zero correlation (ZC linear hull) [33,32,34]. The automatic search methods are similar to those for ID, which was first proposed in [45].

With our SAT tools, we detected the following two ZC linear hulls over $\mathcal{W}(3,7)$. Denote one active S-box by 1 and inactive S-box by 0, the 2 ZC linear hulls are as follows,

$$(0,0,0,0,0,0,0,0,0,0,0,0,0,0,0,1) \overset{7R}{\not\to} (1,0,0,0,0,0,0,0,0,0,0,0,0,0,0,0)$$

$$(0,0,0,0,0,0,0,0,0,0,0,0,0,0,0,1) \overset{7R}{\not\to} (0,0,0,1,0,0,0,0,0,0,0,0,0,0,0,0)$$

They are the same as the above two IDs, which is not surprising as all matrices of `uKNIT-BC` satisfy $M = (M^T)^{-1}$. For SPN ciphers, the ZC attacks are usually weaker than ID attacks. Thus, we believe the ZC attacks will not be a threat to `uKNIT-BC`.

E.6 Integral attacks

The integral attacks [77] were first known as *Square attack* as it was proposed for attacking the block cipher `SQUARE` [47], and it was also studied under different names such as *saturation attack* [85] or *multiset attacks* [28]. Nowadays, the most effective way to search for integral properties is the division property method and its automatic search tools [107,109,117,36,70,22].

By modeling the 2-subset bit-based division property [109] with SAT solvers and setting the input division vector as all one but zero at one bit, the longest zero-sum property we have detected is for 7 rounds of `uKNIT-BC`. We did not detect any zero-sum properties for all $\mathcal{W}(i,8)$, $0 \le i \le 4$. We also considered the round keys using the monomial prediction [70,67] to search for possible one-sum properties, but found nothing for windows of length 8.

From the relationship between the zero-correlation linear hulls and the integral properties [105,31], we derive a better integral distinguisher with less data, i.e.,

$$\overline{\{60,61,62,63\}} \xrightarrow{\mathcal{W}(3,7)} \{0,1,2,3\},\ \overline{\{60,61,62,63\}} \xrightarrow{\mathcal{W}(3,7)} \{12,13,14,15\}$$

With a 7-round integral distinguisher, we believe integral attacks will not threaten the security of the 12-round `uKNIT-BC`, as adding forward propagation rounds are more difficult than the differential and linear cases.

E.7 Demirci-Selçuk meet-in-the-middle attack

The Demirci-Selçuk Meet-in-the-Middle (DS-MitM) attack was proposed by Demirci and Selçuk as a new attack on `AES` [49] in 2008 [52]. Later, this attack was significantly enhanced by Dunkelman *et al.* [59] and eventually became the current best attack on `AES-128` thanks to Derbez *et al.* [55]. Several tools have been proposed to search for DS-MitM attacks for different ciphers. Some are designed with general-purpose programming languages such as [53,54], others are built upon the automatic search tools such as [102,103]. We mainly implemented the methods in [102] to search for DS-MitM attacks on `uKNIT-BC`.

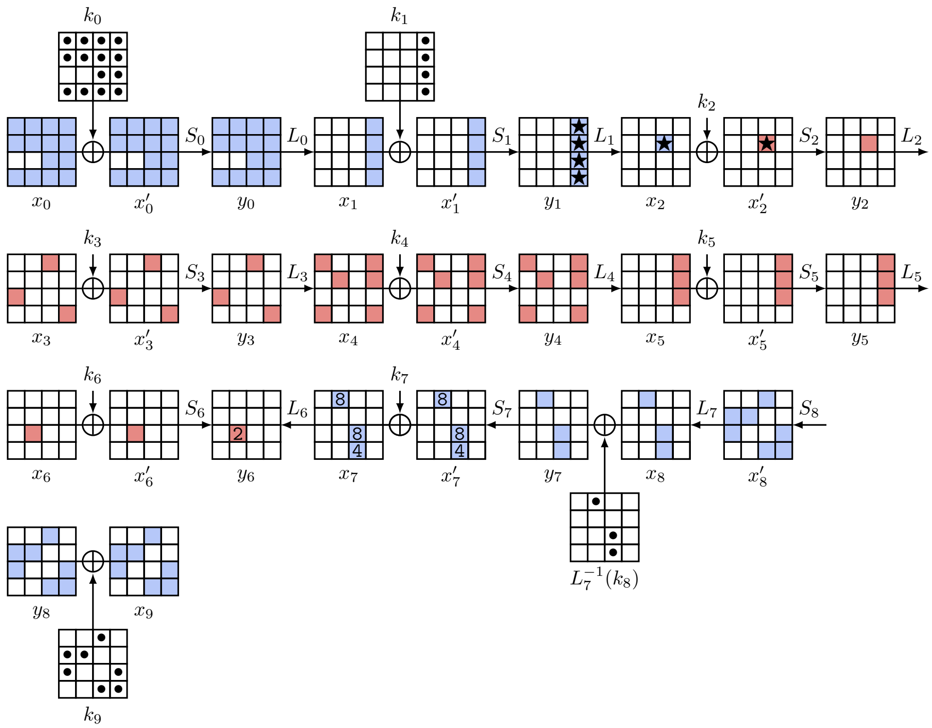

Fig. 9: The DS-MITM attack process for $\mathcal{W}(0,9)$. The distinguisher is applied to $\mathcal{W}(2,5)$ and labeled in red, while the online phase is labeled in blue.

As shown in Figure 9, the best attack we detect covers $\mathcal{W}(0,9)$ with a distinguisher on $\mathcal{W}(2,5)$. Both the backward and forward propagations in the key-recovery process cover 2 rounds. Before we introduce this attack, we will have to give the definition of δ-set [52] in our context, which is a core notion in DS-MitM attacks.

Definition 7 **(δ-set for `uKNIT-BC`).** *A δ-set of size 2^b is a set of internal states such that b bits of the states take up all their possible values while other bits remain constant.*

The distinguisher in this attack covers from x'_2 to y_6. We choose a 2^4-size δ-set for x'_2 such that $x'_2[9]_n$ takes up all 16 possible values. Suppose that the vectorial Boolean function that sends $x'_2[9]_n$ to $y_6[6]_n$ is f, then we have the following observations.

Observation 1 *Suppose that the 16 elements in the δ-set are $X_0, X_1, \ldots, X_{15}$. The total number of possible 60-bit ordered sequence*

$$f(X_0) \oplus f(X_1), f(X_0) \oplus f(X_2), \ldots, f(X_0) \oplus f(X_{15}) \tag{4}$$

is fully determined by the 56-bit parameters,

$$x_2'[9]_n,\ x_3'[2,8,15]_n,\ x_4'[0,3,5,12,13,15]_n,\ x_5'[12\sim 14]_n,\ x_6'[6]_n \qquad (5)$$

where these parameters correspond to one element of the δ-set.

With the *differential enumeration technique* [59,55], the number of parameter bits in Equation (5) can be reduced to 32 bits.

Observation 2 (Differential enumeration technique [59,55]) *Suppose that we have a truncated differential $\Delta(x_2') \to \Delta(y_6)$ where $\Delta(x_2')[9]_n = \bigstar$ (any value except* 0*) and $\Delta(y_2)[6]_n = \mathtt{2}$. The 56-bit parameters can be determined by the following 36-bit differences,*

$$\Delta(x_2)[9]_n, \Delta(y_2)[9]_n, \Delta(y_3)[2,8,15]_n, \Delta(x_5)[12\sim 14], \Delta(x_6)[6]_n.$$

As we have 2^{60} possibilities of Equation 4 in the uniformly random situation, Observations 1 and 2 can be used as a distinguisher. The key-recovery attack process is described as follows.

Offline phase. We compute 2^{32} 60-bit sequences of Equation 4 and store them into a hash table $\mathbb{H}$.

Online phase. In the online phase, we find one right pair that satisfies the truncated differential in Observation 2 and recover the corresponding keys. Then, we use the keys to compute the sequence in Equation 4.

1. As shown in Figure 9, we propagate $\Delta(x_2')$ backward to $\Delta(x_0)$, and propagate $\Delta(y_6)$ forward to $\Delta(x_9)$. By doing so, we constructed a plaintext structure containing 2^{56} plaintexts, yielding 2^{111} pairs. Since the ciphertext difference has 9 inactive nibbles, $2^{111-36} = 2^{75}$ pairs will survive.
2. For each pair,
   - $\Delta(x_0)$ reaches $\Delta(x_2)$ (with $\Delta(x_2)$ being any non-zero difference) with a probability of 2^{-52};
   - $\Delta(x_9)$ propagates to $\Delta(y_6) = 2$ is with a probability of 2^{-28}.

   In total, the probability to obtain a right pair is $2^{-52-28} = 2^{-80}$. Therefore, the number of structures required to get a right pair is $2^{80-75} = 2^5$.
3. For each of these 2^{80} right pair candidates, at the plaintext side, we guess all possible 2^{16} $\Delta(x_1)$ and 2^4 $\Delta(x_2)$, then extract on average one candidate of $k_0[0,1,3\sim 5,7\sim 15]_n$ and $k_1[12\sim 14]_n$. At the ciphertext side, we enumerate all possible 2^{12} $\Delta(y_7)[4,10,11]_n$, and we can extract on average one $L_7^{-1}(k_8)[4,10,11]_n$ and $k_9[1,2,5,8,14,15]_n$.
4. Suppose that we select $x_2'[9]_n = k_2[9]_n$, then we can get the δ-set at x_2. Decrypting them to x_0 with the keys we obtain, we get all 16 plaintexts for the δ-set. Encrypt the 16 plaintexts to ciphertexts. Using the guessed k_8 and k_9 bits to decrypt these 16 ciphertexts to y_6, compute the sequence of Equation (4).

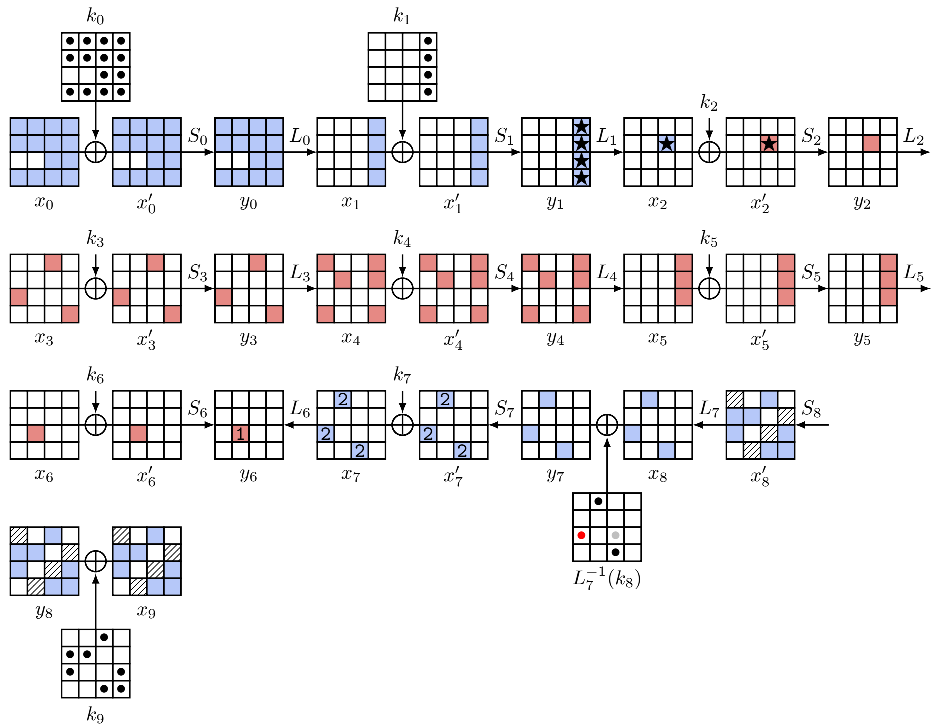

Fig. 10: The second DS-MitM key-recovery on $\mathcal{W}(0, 9)$.

5. Check if the calculated sequence is in $\mathbb{H}$ built in the offline phase. Since the number of possibilities of Equation (4) is 2^{56} (note that 4 bits have been determined by the truncated differential), only $2^{80-(56-36)} = 2^{60}$ pairs can survive. For each surviving pair, we have on average 15 values for $k_0[0, 1, 3 \sim 5, 7 \sim 15]_n$, $k_1[12 \sim 14]_n$, $L_7^{-1}(k_8)[4, 10, 11]_n$ and $k_9[1, 2, 5, 8, 14, 15]_n$ according to the guessed $\Delta(x_2)$, or equivalently, we have about 2^{62} key candidates with its corresponding plaintext, ciphertext and intermediate pairs.
6. To further determine the keys, we can play the DS-MitM with a slightly modified distinguisher shown in Figure 10. As the probability that a pair of the 2^{60} being a right pair is 2^{-44}, with 2^{44} surviving pairs, we can find a right pair for the second DS-MitM attack. So the same key candidates with the first attack except that $L_7^{-1}(k_8)[10]_n$ is replaced with $L_7^{-1}(k_8)[2]_n$ can be recovered. The filtering effect is 2^{-20} again. Thus only $2^{62-20+2} = 2^{44}$ key candidates survives. The time complexity of the second attack has been negligible compared to the first one. We can repeat this process several times, until we recover the only one key candidates.
7. Finally, we can exhaustively search the unknown 56 bits of k_0 and k_1, and use the 60-bit values of k_8, k_9, as well as the internal keys derived from the right pairs as filters, Finally, we expect only correct key.

Complexity. The complexities are all dominated by the first attack. The data complexity basically consists in encrypting the 2^{61} plaintexts. The memory complexity represents the storage of the 2^{36} 60-bit sequences, which is 2^{40} bits or 2^{34} 64-bit blocks. The time complexity of the offline phase is to computing all sequences, which is $2^{36+4} = 2^{40}$ 5-round encryptions. For the online phase, the time complexity is dominated by processing all 2^{80} pairs. For each pair, we need to guess 15 $\Delta(x_2)$, and the remaining time complexity is dominated by partially encrypting the δ-set, which is $2^{80+4+4} = 2^{88}$ 4-round encryptions, approximately, 2^{87} 9-round encryptions.

E.8 Boomerang and rectangle attacks

The boomerang attack was proposed in 1999 as a variant of differential cryptanalysis [112]. In this attack, we first throw a plaintext pair (p_0, p_1) with $p_0 \oplus p_1 = \alpha$ and obtain their corresponding ciphertexts (c_0, c_1). Then, we choose c_2 and c_3 such that $c_0 \oplus c_2 = \beta$ and $c_1 \oplus c_3 = \beta$, and decrypt c_2, c_3 to get corresponding p_2, p_3. We observe if $p_2 + p_3 = \alpha$. If so, we say that the boomerang returns and (p_0, p_1, p_2, p_3) is called a right quartet. The boomerang attack is an adaptively-chosen-ciphertext attack, so in many cases, we prefer its chosen-plaintext version, called rectangle attack [74,25]. The rectangle attack generates plaintext quartets (p_0, p_1, p_2, p_3) satisfying $p_0 \oplus p_1 = \alpha, p_2 \oplus p_3 = \alpha$ and observe after encryption if $c_0 \oplus c_2 = \beta, c_1 \oplus c_3 = \beta$. If so, (p_0, p_1, p_2, p_3) is called a right quartet. We apply the rectangle attack to `uKNIT-BC` in this subsection.

For a random permutation with block size n, a right quartet appears with a probability of 2^{-2n}. To estimate the right quartet probability for a block cipher E, classically we usually divide the cipher into 2 parts as $E = E_1 \circ E_0$. We then find a good differential for E_0 with the input difference α whose probability is p, and a good differential for E_1 with the output difference β whose probability is q (in practice, we find these differentials first and then determine α and β afterwards). The probability of obtaining a right quartet is then estimated as $2^{-n}p^2q^2$. Therefore, only when $p^2q^2 > 2^{-n}$, then we will have a rectangle distinguisher. According to Table 11, the best rectangle attack on `uKNIT-BC` can only reach 6 rounds.

Such an estimation heavily relies on the assumption that E_0 the E_1 are independent, which is not always true in practice [90]. Several refinements have been proposed to mitigate such independence problems [60,61,43]. The boomerang connectivity table (BCT) is one of the latest technique among them [43].

Definition 8 (Boomerang connectivity table (BCT) [43]). *For an n-bit S-box, denoted by S, its* BCT *is a 2-dimensional $2^n \times 2^n$ table, with the entry* $\mathrm{BCT}(\delta, \delta')$ *being*

$$\mathrm{BCT}(\delta, \delta') = \#\{x \in \mathbb{F}_2^n : S^{-1}(S(x) \oplus \delta') \oplus S^{-1}(S(x \oplus \delta) \oplus \delta') = \delta\}$$

The cipher is decomposed into three parts, $E = E_2 \circ E_1 \circ E_0$ and in the simple BCT attack, E_1 is only one substitution layer. We first find a good differential of E_0, say $\alpha \to \alpha'$ and a good differential of E_2, say $\beta' \to \beta$. For

$E_1 = S_0||S_1||\cdots||S_{15}$ where S_i are the 16 S-boxes, we have the following computation

$$\begin{aligned}&\mathrm{P}(E_1^{-1}(E_1(x)\oplus\beta)\oplus E_1^{-1}(E_1(x\oplus\alpha')\oplus\beta)=\alpha')\\&\quad=\prod_{0\le i<16}\mathrm{P}\left(S_i^{-1}(S_i(x[i]_n)\oplus\beta[i]_n)\oplus S_i^{-1}(S_i(x[i]_n\oplus\alpha'[i]_n)\oplus\beta[i]_n)=\alpha'[i]_n\right)\end{aligned} \tag{6}$$

For each S-box, the right side of the equation is computed using its BCT. Denote the probability of E_1 calculated from Equation (6) by r, then the probability of obtaining a right quartet of E is estimated to be $2^{-n}p^2q^2r$. When $p^2q^2r > 2^{-n}$, then we have a rectangle distinguisher.

We constructed a SAT model for the rectangle distinguisher incorporating the BCT. Our targets are the windows with length 7. For $\mathcal{W}(i,7)$, a differential search model covers $\mathcal{W}(i,3)$ as E_0 and $\mathcal{W}(i+3,3)$ without the first S-box layer as E_2. The middle S-box layer is described using the BCT. The objective function is then to maximize p^2q^2r.

For windows with length 8, the best rectangle distinguisher detected by us has an estimated probability $2^{-64}\times 2^{-77} = 2^{-141}$ for $\mathcal{W}(1,8)$. The best rectangle distinguisher we found for 7-round window is one for $\mathcal{W}(2,7)$ with probability of $2^{-64}\times 2^{-51} = 2^{-116}$. Both rectangle distinguishers are illustrated in Figure 11. As stated in [104,118], the data complexity for a rectangle attack is

$$D = \frac{\sqrt{s}2^{\frac{n}{2}+1}}{\sqrt{p}},$$

where s is the number of right quartets, n is the block length and p is the boomerang probability (rather than the rectangle probability). Thus, both rectangle distinguishers cannot work within the data limitation of 2^{-47} chosen-plaintexts even we consider $s = 1$.

E.9 (Higher-order) differential-linear attacks

Similar to the boomerang attacks, resistance against the plain differential and linear cryptanalysis does not necessarily lead to resistance against their variants or combinations. Differential-linear (DL) cryptanalysis, proposed by Langford and Hellman in 1994 [79], combines the differential and linear attacks. For a cipher E, let $C = E(P)$ and $C' = E(P')$. Given a difference-mask pair (δ,λ), the correlation of the DL distinguisher is

$$\mathrm{C}(\delta,\lambda) = 2^{-n}\sum_{x\in\mathbb{F}_2^n}(-1)^{\lambda\cdot(E(x)\oplus E(x\oplus\Delta))}$$

Similar to the case of linear cryptanalysis, if the correlation is not 0, we have an opportunity to distinguish the cipher from a random permutation.

The classical method to estimate the correlation is to divide the cipher into two parts as $E = E_1\circ E_0$. If we have a DC for E_0, say $\delta\to\delta'$, with a probability

$\Delta(x_1)$	0000092820240000	2^{-12}	Upper Diff.
	0000042180880000		
$\Delta(x_2)$	0000000000000041	2^{-4}	
	0000000000000088		
$\Delta(x_3)$	0000000009000000	2^{-3}	
	0000000002000000		
$\Delta(x_4)$	0000010040000002	2^{-6}	
	0000010040000008		
$\Delta(x_5)$	0024214041010010	2^{-3}	BCT
	000000000228c119		
$\Delta(x_6)$	0023000000000000	2^{-4}	Lower Diff.
	008a000000000000		
$\Delta(x_7)$	0000000000100000	2^{-2}	
	0000000000100000		
$\Delta(x_8)$	0080000080000008	2^{-6}	
	0010000020000002		
Boom. Pro. $= 2^{77}$ (expl. 2^{-14})			

$\Delta(x_2)$	0000000018400000	2^{-6}	Upper Diff.
	0000000048100000		
$\Delta(x_3)$	0000000080000000	2^{-2}	
	0000000010000000		
$\Delta(x_4)$	00c0000000000004	2^{-4}	
	0050000000000002		
$\Delta(x_5)$	3000002002602a00	2^{-1}	BCT
	a3c0804100000000		
$\Delta(x_6)$	6100000000000000	2^{-5}	Lower Diff.
	1300000000000000		
$\Delta(x_7)$	8000000000000000	2^{-2}	
	2000000000000000		
$\Delta(x_8)$	0000000100400200	2^{-6}	
	0000000800800400		
Boom. Pro. $= 2^{-51}$ (expl. 2^{-10})			

Fig. 11: The upper and lower DCs and connectivity of the rectangle distinguishers for $\mathcal{W}(1,8)$ (left) and $\mathcal{W}(2,7)$ (right). the expl. values are the sum of the experimental probability of the 3 rounds with the BCT round in the middle.

p, and a LC for E_1 say $\lambda' \to \lambda$, with a correlation q. The correlation can be estimated as pq^2 [79]. However, such an estimation relies on many assumptions such as E_0 and E_1 being independent. To overcome this assumption, Dunkelman *et al.* introduced the differential-linear connectivity table (DLCT) to connect the differential and linear parts [9]. The DLCT is defined as follows,

Definition 9 (Differential-linear connectivity table (DLCT) [9]). *For an n-bit S-box denoted by S, its* DLCT *is a 2-dimensional $2^n \times 2^n$ table, with entry* $\mathrm{DLCT}(\delta, \lambda)$ *being*

$$\mathrm{DLCT}(\delta, \lambda) = \sum_{x \in \mathbb{F}_2^n} (-1)^{\lambda \cdot (S(x) \oplus S(x \oplus \delta))}$$

With the DLCT, a cipher is decomposed into three parts, say $E = E_2 \circ E_1 \circ E_0$, where E_1 is an S-box layer. We then construct a SAT model to search for the DL distinguishers for `uKNIT-BC`. In the SAT model, we model E_0 and E_2 to search for DC and LC respectively and for E_1, we model the DLCT for each S-box. With this method, the best DL distinguisher we could find has a correlation of 2^{-25} for $\mathcal{W}(2,7)$. With 2^{28} messages under 100 randomly-chosen keys, we verified the correlation of the middle 4 rounds (from `0004000001000000` to `2100000000000000`). The average experimental correlation is about 2^{-11}. Thus the correlation for the full 7-round DL distinguisher is about $c = 2^{-8-11-2\times2} = 2^{-23}$, which is potential to use in a key-recovery attack. After propagating the input difference (resp. output mask) backwards (resp. forwards) 1 round, we obtain a key-recovery process illustrated in Figure 12.

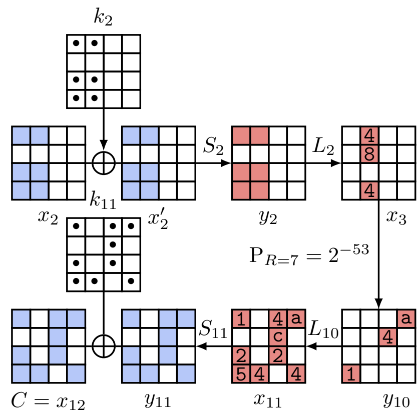

Fig. 12: The key-recovery process for $\mathcal{W}(1,9)$ based on the 7-round DL distinguisher of $\mathcal{W}(2,7)$ in Figure 13 (left).

According to [100], the number of pairs we need for the key-recovery attack is computed as

$$D_{pairs} = \frac{(\Phi^{-1}(1-2^{-a+1}) + \Phi^{-1}(P_S))^2}{|c|^2},$$

where Φ is the CDF of the standard normal distribution, a is the advantage, P_S is the success probability, and c is the DL correlation. We set the success probability as 0.95, then

$$D_{pairs} = (\Phi^{-1}(1-2^{-a+1}) + 1.65)^2 \times 2^{46}.$$

We will use the structure for the key-recovery attack. Each structure has 2^{40} plaintexts and will generate 2^{79} pairs, among which 2^{39} pairs will meet $\Delta(x_2)$. Thus, the number of structure we need is

$$s = D_{pairs} 2^{-39},$$

thus the data complexity is $D = s \times 2^{40}$.

The key-recovery process is as follows:

Offline phase: For all 2^{28} values of $k_9[1,4,7,10,11,13,14]_n$ and 2^{28} $C[1,4,7,10,11,13,14]_n$, precompute a table $\mathbb{H}$ containing the corresponding parity with the mask $\Gamma(y_8)$.

Online phase:

1. Initialize a counter with 68-bit index;
2. Prepare $s \times 2^{40}$ plaintexts where the 2^{40} plaintexts are from the structure of x_1 in Figure 12, s is the number of structures;
3. Ask for the corresponding $s \times 2^{40}$ ciphertexts;
4. For each of the 2^{40} values of $k_1[0 \sim 3, 4 \sim 7, 9 \sim 11]_n$:
   (a) Partially encrypt $s \times 2^{40}$ plaintexts and combine them to pairs and choose those that can meet $\Delta(x_2)$; (we will get $s \times 2^{39}$ pairs)

(b) For all pairs, get the corresponding ciphertext pairs, access $\mathbb{H}$ for this pair to see if the parity of the two ciphertexts agree or disagree.
(c) If the two ciphertexts' parity agree, increase by 1 the counter with index $(k_1[0 \sim 3, 4 \sim 7, 9 \sim 11]_n, k_9[1, 4, 7, 10, 11, 13, 14]_n)$; otherwise, decrease it by 1.

5. Select the first 2^{68-a} candidates, combine them together with the remaining key bits and do the exhaustive search.

Time complexity. The time complexity is roundly

$$T = D + 2^{40} \times 2^{39} \times s + 2^{128-a} \approx \max\{D, 2^{40} \times 2^{39} \times s, 2^{128-a}\}.$$

When $a = 54$, $D_{pairs} \approx 2^{52.6}$, the time complexity is $2^{92.6}$ operations, and the data complexity is $2^{53.6}$ chosen plaintexts. operations.

However, for 8 rounds, the best DL distinguisher we detect is with correlation of 2^{-35}, as shown in Figure 13 (left). We experimental verified the middle three rounds for this distinguisher (from `e000000000d00700` to `0000000000008041`) with 2^{26} messages, and the correlation for this three rounds (without the last diffusion layer) is about $2^{-9.83}$. Thus, the whole correlation of this 8-round DL approximation is about $c \approx 2^{-6-9.83-16} \approx 2^{-31.83}$. Considering that the data complexity of a DL attack is $\mathcal{O}(1/c^2)$ where c is the DL correlation, we believe that this 8-round DL attacks would not be a threat to `uKNIT`, under the data limitation of 2^{-47} chosen-plaintexts we set.

Higher-order differential cryptanalysis. Higher-order differential-linear (HDL) cryptanalysis was first proposed by Biham *et al.* to study possible combined attacks [26]. In [69], the authors used the HATF technique inspired by the ATF methods [83] to give a practical estimation process of the HDL bias. This attack strategy can be effective against some low-degree permutation-based ciphers, but considering that `uKNIT-BC` is a block cipher with degree-3 S-boxes (all S-boxes are bit-permutation equivalence of the `MANTIS` S-box), we believe `uKNIT-BC` resists HDL attacks.

E.10 Invariant attack

Invariant attacks study the structural properties of a cipher where a partition of the plaintext space into a set S or its complement is preserved. In [80], Leander *et al.* introduced the invariant subspaces and in [108] Todo *et al.* presented the nonlinear invariants. Beierle *et al.* studied how to choose the constants to resist invariant-type attacks in [13]. Later, in [19] Beyne showed that the invariant attacks can be effectively explained by the eigenvectors of correlation matrices [46]. As discussed in [38, Chapter 9], the invariant attacks mainly provide threats to lightweight ciphers with a simple key schedule, *e.g.*, the identical round keys with different constants XORed (like `PRINCE`) or two round keys are used alternatively (like `MIDORI`). For a cipher with a relatively complicated key schedule, variant attacks are much more difficult to be found. With our key schedule based on the gSTK, we believe that invariant attacks are not a threat to the security of `uKNIT-BC`.

$\Delta(x_3)$	0000000000260000	2^4	Diff.
	0000000000120000		
$\Delta(x_4)$	00c0000000000000	2^2	
	00b0000000000000		
$\Delta(x_5)$	e000000000d00700	2^7	
	5000000000e00100		
$\Delta(x_6)$	90b10d800150060e	2^0	DLCT
	0000210488022024		
$\Delta(x_7)$	0000000000004048	2^3	Linear
	0000000000008041		
$\Delta(x_8)$	0000000000004000	2^1	
	0000000000008000		
$\Delta(x_9)$	0001000008008000	2^3	
	0008000002004000		
$\Delta(x_{10})$	0000064041000000	2^4	
	00000a3021000000		
DL Cor. $= 2^{-35}$ (expl. $2^{-31.83}$)			

$\Delta(x_2)$	0000910600000000	2^6	Diff.
	0000930300000000		
$\Delta(x_3)$	0000000000000090	2^2	
	00000000000000a0		
$\Delta(x_4)$	0004000001000000	2^4	
	0004000008000000		
$\Delta(x_5)$	0000040480200808	2^1	DLCT
	6a60000004420000		
$\Delta(x_6)$	3010000000000000	2^2	Linear
	1020000000000000		
$\Delta(x_7)$	8800000000000000	2^2	
	2100000000000000		
$\Delta(x_8)$	8000000100000000	2^2	
	9000000500000000		
DL Cor. $= 2^{-25}$ (expl. 2^{-23})			

Fig. 13: The DC and LC and connectivity part of the DL distinguishers for $\mathcal{W}(3,8)$ (left) and $\mathcal{W}(2,7)$ (right).

E.11 Slide attacks and internal differential attacks

The slide attack and its variants [29,30,62,64] explore the symmetry of different round functions. While the internal differential attacks [96,56,121,120] uses the symmetry between a part of the round function and the other part. `uKNIT-BC` enjoys a highly non-aligned property where (almost) all S-boxes and linear layers are different so it has an inherent strong resistance against both attacks.

F Application to PRF: XoP with uKNIT-BC

One of the benefits of uKNIT is not only providing very competitive minimum latency, but also a wider range of area-latency trade-offs. As demonstrated in the last two rows of Table 2, uKNIT can provide $\sim 10\%$ lower latency that PRINCEv2, but, interestingly, for the same latency as PRINCEv2 is requires only $\sim 80\%$ of the area. This leads to a very interesting trade-off: consider a user that can dedicate the same latency and area as PRINCEv2 for low latency applications but requires a PRF rather than a block cipher, *e.g.,* using the CounTeR (CTR) mode. It is well known that using PRINCEv2 in the CTR mode is insecure as it only offers 32 bits of security. On the other hand, consider the single-permutation Sum of Permutation (XoP) construction given by:

$$E_K(0\|M) \oplus E_K(1\|M).$$

It was given in [68] and its security was proven in [50], where it was shown to have a PRF security bound $O(q/2^n)$, where $q < 2^{n-1}$ is the number of queries and n is the block size. Note that the construction consists of two calls to the block cipher with the same key. Thus, it requires implementing the main SPN twice, while the key schedule only once. This leads us to conclude that for roughly $1.33\times$ area as PRINCEv2 we can double the PRF security. This is an extra level of security optimization, on top of optimizing the primitive itself. Note that since PRINCEv2 does not have a key schedule per se (the round keys are just copies of the master key), the same does not apply to prince. At $1.65ns$, XoP-uKNIT-BC would need $\approx 37551.59\mu m^2$, while XoP-PRINCEv2 would need $\approx 55128.24\mu m^2$.

Note that Orthros and Gleeok128 are both PRFs based on other variants of XoP, where the internal block ciphers are pruned by reducing their number of rounds compared to a secure PRP version. uKNIT has lower latency than both of them without this trade-off and is transformed into a PRF using the XoP construction above. However, the former PRFs operate on 128 bits.

G Rotations for the AES variant

Table 13: Byte-permutations for the AES variant searched by our genetic search algorithm. Note that the convention we use to represent the position follows that of the one in [49] (i.e. column-first).

Rd \ Pos.	0	1	2	3	4	5	6	7	8	9	10	11	12	13	14	15
1	13	5	8	11	6	2	14	15	9	4	10	1	7	3	0	12
2	6	9	15	2	8	7	1	12	11	4	14	0	13	3	5	10
3	8	5	0	15	4	9	3	13	7	10	12	1	11	14	6	2
4	11	0	4	8	6	14	13	9	12	10	3	1	2	7	15	5
5	7	3	6	0	13	12	2	10	15	1	11	9	14	4	5	8
6	15	11	4	6	2	1	10	7	13	14	8	3	0	9	12	5

H Power consumption and area at different frequencies

Table 14: Power consumption and area at different frequencies.

Power consumption (in mW) using TSMC 65nm

Frequency	675 MHz	606 MHz	500 MHz	250 MHz	10 MHz
PRINCEv2	Infeasible	17.60	7.49	3.02	0.43
uKNIT-BC (SL)	13.73	8.02	4.92	2.22	0.34
Gain	∞	54.4%	34.3%	26.4%	20.9%
uKNIT-BC	18.15	9.83	6.08	2.76	0.50
Gain	∞	44.1%	18.8%	8.6%	−16.3%

Power consumption (in mW) using FDSOI 28nm 1.1V

Frequency	1.07 GHz	1 GHz	961 MHz	500 MHz	250 MHz	10 MHz
PRINCEv2	Infeasible	Infeasible	15.47	3.41	1.75	0.18
uKNIT-BC (SL)	13.95	7.19	6.07	2.58	1.33	0.14
Gain	∞	∞	60.8%	24.3%	24.0%	22.2%
uKNIT-BC	14.39	8.39	6.72	2.93	1.53	0.21
Gain	∞	∞	56.6%	14.1%	12.6%	−16.6%

Area (in μm^2) using FDSOI 28nm 1.1V

Frequency	1.07 GHz	1 GHz	961 MHz	10-500 MHz
PRINCEv2	Infeasible	Infeasible	9968.42	4777.51
uKNIT-BC (SL)	8015.40	4750.10	4297.06	3744.29
uKNIT-BC	10939.79	7635.64	6905.32	6078.71